EXPERIMENTAL AND COMPUTATIONAL STUDIES OF FLUID STRUCTURE INTERACTION OF TSUNAMI BORE ON COASTAL BRIDGES

IMAN MAZINANI

FACULTY OF ENGINEERING
UNIVERSITY OF MALAYA
KUALA LUMPUR

2021

EXPERIMENTAL AND COMPUTATIONAL STUDIES OF FLUID STRUCTURE INTERACTION OF TSUNAMI BORE ON COASTAL BRIDGES

IMAN MAZINANI

THESIS SUBMITTED IN FULFILMENT OF THE REQUIREMENTS FOR THE DEGREE OF DOCTOR OF PHILOSOPHY

FACULTY OF ENGINEERING
UNIVERSITY OF MALAYA
KUALA LUMPUR

2021

UNIVERSITY OF MALAYA

ORIGINAL LITERARY WORK DECLARATION

Name of Candidate: Iman Mazinani

Matric No: KHA110075

Name of Degree:

Title of Thesis ("this Work"):

EXPERIMENTAL AND COMPUTATIONAL STUDIES OF FLUID STRUCTURE INTERACTION OF TSUNAMI BORE ON COSTAL BRIDGES

Field of Study: Civil Engineering

I do solemnly and sincerely declare that:

(1) I am the sole author/writer of this Work;
(2) This Work is original;
(3) Any use of any work in which copyright exists was done by way of fair dealing and for permitted purposes and any excerpt or extract from, or reference to or reproduction of any copyright work has been disclosed expressly and sufficiently and the title of the Work and its authorship have been acknowledged in this Work;
(4) I do not have any actual knowledge nor do I ought reasonably to know that the making of this work constitutes an infringement of any copyright work;
(5) I hereby assign all and every rights in the copyright to this Work to the University of Malaya ("UM"), who henceforth shall be owner of the copyright in this Work and that any reproduction or use in any form or by any means whatsoever is prohibited without the written consent of UM having been first had and obtained;
(6) I am fully aware that if in the course of making this Work I have infringed any copyright whether intentionally or otherwise, I may be subject to legal action or any other action as may be determined by UM.

Candidate's Signature　　　　　Date:15.05.2021

Subscribed and solemnly declared before,

Witness's Signature　　　　　Date:

Name:

Designation:

EXPERIMENTAL AND COMPUTATIONAL STUDIES OF FLUID STRUCTURE INTERACTION OF TSUNAMI BORE ON COASTAL BRIDGES

ABSTRACT

To understand the potential effect of the tsunami forces on coastal bridges due to tsunami bore, a series of experimental tests were conducted, and results were compared to those calculated with a fluid-structure interaction (FSI) analysis. Various wave heights and shallow water were utilized in the experiments and computational process. Nine types of 1:40 scale concrete bridge models were placed in a mild beach profile to a 24 m × 1.5 m × 2 m wave flume for the experimental investigation. An Arbitrary Lagrange Euler (ALE) formulation was developed for the propagation of tsunami solitary and bore waves by an FSI package of LS-DYNA using a high-performance computing (HPC) system. The results showed that the fully coupled FSI models could plausibly capture the tsunami wave forces for all ranges of wave heights and shallow depths. It was identified that after ~1.4 s, the wave elevation could potentially reach it's maximum (here, 0.35-0.4 m), which was in good agreement with the results calculated by the Weigel model. Likewise, the Bore height increased with an increase in the wave height, reaching ~0.22 m at a wave height of 0.38 m. The horizontal force reached 180 N after 7.3 seconds and then gradually decreased approaching zero after 8 seconds. The effects of the overturning moment, horizontal force, uplift, and impact force on the pier and deck of the bridge were evaluated. The presence of girders, on a model of a bridge deck with girders, is studied by making a direct comparison by changing the number of girders on the model. It appears that the girders have a significant influence on the uplift and overturning moment. Increasing the number of girders on bridge models significantly increased uplift and overturning moments. However, this variation depended on wave conditions and shallow water.

The effect of four different baffle plates on the mitigation of tsunami force is investigated. The result indicated the full baffle plate reduced horizontal and uplift force up to 40 %.

Keyword: Coastal bridge; tsunami; fluid-structure interaction; Arbitrary Lagrange Euler.

‘

KAJIAN EKSPERIMENAL DAN PENGIRAAN INTERAKSI STRUKTUR BENDALIR TSUNAMI TERHADAP JENIS PANTAI

ABSTRAK

Untuk memahami kesan pengaruh daya tsunami pada jambatan pantai akibat jara tsunami, satu siri eksperimen dilakukan, dan hasilnya dibandingkan dengan yang dihitung dengan analisis interaksi bendalir-struktur (FSI). Berbagai ketinggian gelombang dan perairan cetek digunakan dalam eksperimen dan proses pengiraan. Sembilan jenis model jambatan konkrit berskala 1:40 dengan profil pantai ringan berbanding flum gelombang 24 m × 1.5 m × 2 m untuk penyelidikan eksperimen. Formulasi Arbitrary Lagrange Euler (ALE) dibina dengan pakej FSI LS-DYNA menggunakan sistem pengkomputeran berprestasi tinggi (HPC) untuk mewakili penyebaran gelombang tsunami dan jara gelombang. Hasil kajian menunjukkan bahawa model FSI yang digabungkan sepenuhnya dapat menangkap kekuatan gelombang tsunami untuk semua jarak ketinggian gelombang dan kedalaman cetek. Telah dikenal pasti bahawa setelah ~ 1.4 s, ketinggian gelombang berpotensi mencapai maksimum (di sini, 0.35-0.4 m), yang sesuai dengan hasil yang dikira oleh model Weigel. Begitu juga, ketinggian jara meningkat dengan peningkatan ketinggian gelombang, mencapai ~ 0.22 m pada ketinggian gelombang 0.38 m. Daya mendatar mencapai 180 N selepas 7.3 saat dan kemudian secara beransur-ansur menurun mendekati sifar setelah 8 saat. Kesan momen terbalikan, daya mendatar, angkat naik, dan daya hentaman pada tambangan dan geladak jambatan yang dinilai. Kehadiran,galang-galang pada model geladak jambatan dengan galang, dikaji secara-perbandingan langsung dengan mengubah jumlah galang pada model tersebut. Nampaknya galang-galang mempunyai pengaruh yang bererti terhadap angkat naik dan momen terbalikan. Meningkatkan bilangan galang-galang pada model jambatan menaikkan angkat naik dan momen terbalikan dengan ketara. Walau bagaimanapun, variasi ini bergantung pada keadaan gelombang dan perairan cetek.

Kesan empat plat sesekat yang berbeza terhadap pengurangan kekuatan tsunami disiasat. Hasilnya menunjukkan plat sesekat penuh mengurangkan daya mendatar dan angkat naik sehingga 40%.

Kata kunci: Jambatan pantai; tsunami; interaksi struktur-bendalir; Arbitrary Lagrange Euler.

ACKNOWLEDGEMENTS

First and foremost, I would like to extend my sincere gratitude to my supervisor, Prof. Dr. Zubaidah Binti Ismail, for introducing me to this exciting field of science and for her dedicated help, advice, inspiration, encouragement and continuous support throughout my Ph.D. Her enthusiasm, integral view on research and her mission for providing high-quality work has made a deep impression on me. I would also like to extend a special thankyou to my co-supervisor, Prof. Dr. Ahmad Mustafa Hashim, for her continuous support, guidance, cooperation, encouragement and for going out of his way to facilitate all the requirements. My sincere thanks also goes to Almarhum Dr. Ramlee for his inspiration, support and guidance. I am also very thankful to Meisam Gordan for his assistance and support.

I would like to thank all my friends and all staff in the Department of Civil Engineering, University of Malaya. They have always been very supportive and made the entire process of my study at the University so much easier.

I would also like to say a heartfelt thank you to my lovely parents, Elham and Arvin for always believing in me and encouraging me to follow my dreams.

Finally, I would also like to thank my beloved wife, Dr. Marjan Mansourvar, and my daughter, Anika Mazinani. Thank you for your unwavering support, and especially I cannot thank you enough for encouraging me throughout this experience. I love you both and I appreciate everything that you have done for me.

TABLE OF CONTENTS

LIST OF FIGURES

LIST OF TABLES

LIST OF SYMBOLS AND ABBREVIATIONS

a	Amplitude of wave (m)
b	Width of wall (m)
β	Constant in Tait's equation of state
c	Speed of sound in water (m/s)
C_0	Reference speed of sound in water at the reference density (m/s)
c_i	Speed of sound in water at particle i (m/s)
c_w	Wave celerity near wall (m/s)
c	Constant
g	gravitational acceleration
K	number of the front in water water at the depth of the current wave-generator
L_m	Wavelength in deep-water conditions (m)
L	Dimension
m	Mass (kg)
np	Total number of particles in simulation
nb	Number of boundary particles in simulation
Pk	Fluid pressure (Pa)
ρ	Fluid density
P	Fluid pressure at transducer *k* (Pa)
Pa	Pressure in star region of Riemann Solver
Q	Overtopping rate (m^3/s/m)
Qa	Dimensionless overtopping rate (m^3/s/m)
Rc	Free-board clearance (m)
R	Dimensionless wave runup (m)
rij	Distance between two particles and (m)

$\underline{r}$	Distance vector between two particles and (m)
s	Slope of beach (m/m)
S	Wave board stroke (m)
t	Time (s)
t_f	Stroke duration (s)
T	Wave period (s)
U	Wave period at toe of wall (s)
u	Velocity (m/s)
Ua	Velocity vector (m/s)
W	Smoothing kernel function
hgid	Hourglass ID
ihq	Hourglass control type
qm	Hourglass coefficient
ibq	Bulk viscosity type
q1	Quadratic bulk viscosity coefficient
qb	Hourglass coefficient for shell bending
vdc	Viscous damping coefficient
Qw	Hourglass coefficient for shell warping
ro	Mass density
E	Young's modulus
Pr	Poisson's ratio
mid	Material identification
den	Material density
pc	Pressure cutoff
mu	Dynamic viscosity coefficient

LIST OF APPENDICES

CHAPTER 1: INTRODUCTION

1.1 Background

Hundreds of thousands of humans have died in the recent two giant tsunami tragedies. The Indian Ocean tsunami on December 26, 2004 was among the heaviest natural tragedies in human history with human losses exceeding 300,000 and resulting in extensive damage to buildings and infrastructure, far beyond the 186 bridges affected by the tsunami on Sumatra Island. The tragedy of the Great Eastern Japan Tsunami on March 11, 2011 recorded 15,883 deaths with more than 300 bridges experiencing significant destruction. Similar to the tsunami disaster, on August 29, 2005 in the United States, Hurricane Katrina caused substantial destruction on the Gulf Coast, where more than 1,800 people died, many buildings were destroyed and 45 bridges suffered damage. It can be concluded that the vital role of a bridge in high tsunami hazard zone is a reminder to the international scientific community to deeply evaluate, simulate and finally estimate tsunami load induced on coastal bridges. A safe design structure for predicting the tsunami load influence on coastal structures requires careful consideration.

Most of the usual systems and/or methods used for mitigation of tsunami effect on bridges such as opening methods reduce the resistance of bridge structures against other loads such as gravity and seismic load. Some, such as spring and vegetation, are very difficult and costly to install to existing bridges. Although there have been several theoretical studies carried out on the systems and methods for mitigating the effects of tsunami force, there are found to be unsatisfactory due to the difficulty in installation and implementation such that they contain certain drawbacks that made them not to become widely used.

1.2 Objective of research

This study was based on investigating the fluid structure interaction of tsunami and bridges. The main objective of this research is to evaluate tsunami forces on bridges experimentally and numerically. The effect of various bridge configurations is assessed, and tsunami force mitigating applied with the utilization of the baffle plate. The specific objectives of this study are as follows:

a) To experimentally evaluate a tsunami load on bridge models and record the forces on various bridge model configurations in terms of bridge type and girder beams.
b) To numerically simulate the experimental tests on bridge modes with an Arbitrary Lagrange Euler (ALE) formulation in various configurations, shallow waters and wave height.
c) To evaluate experimentally and computationally simulate the tsunami mitigation on a bridge with the utilization of the baffle plate.

The results of this study help engineers to better understand the complete response of a bridge in a tsunami load in order to design future bridges more safely or to mitigate the tsunami effect on existing bridges by applying counter-measures like installing baffle plates.

1.3 Problem Description

Hundreds of bridges were washed away or heavily damaged by tsunami waves during the two tragic tsunamis that devastated the west coast of Sumatra Island, Indonesia, in 2004 and North East Japan in 2011. This has demonstrated that the present design code does not contribute an adequate resistance for bridges in the tsunami forces. In this research, in order to understand the tsunami force on a coastal bridge due to tsunami bore, the experimental tests in a wave flume and a fluid structure interaction (FSI) analysis were carried out.

Due to the complication of the wave-structure interaction, wave propagation onshore, and theoretical approach, the evaluation of tsunami forces cannot be simply applied to a complete bridge structure. Consequently, the experimental test was performed to analyze the flow characteristics of tsunami bore around the complete pier-deck bridges and to estimate tsunami forces on bridges.

Most previous research focused on evaluating the tsunami load on a bridge deck or applied a very small scale bridge model. However, for evaluating the tsunami load on a bridge and to assess the complete response of a bridge in various beach slope, combination of superstructure and substructure in a real situation involving the complicity of the structure and tsunami flow should be applied.

Photos and videos that captured the Indian Ocean Tsunami in 2004 and the 2011 Japan Tsunami showed solitary tsunami waves breaking in offshore, along with an extremely turbulent tsunami-induced bore propagating towards onshore with significantly higher velocity. Consequently, the outcomes of this current experimental and numerical study are highly relevant in the evaluation of tsunami bore forces on the coast, over sea or river bridges.

The tsunami induced forces on the coastal bridge has three components i.e. a vertical, a horizontal and overturning moment. In the typical wave forces, the vertical force component is always larger than the horizontal component. Due to these forces, an overturning moment is also acting on the deck. Structural failure occurs if any of these loads exceeds the structural capacity. However, in the tsunami wave induced force, this scenario depends on some factors such as shallow water, wave height and bore velocity. In this research, we will consider these factors on tsunami forces.

This study not only aims to evaluate the effect of tsunami bore force to three various bridge models, but also to evaluate the application of the baffle plate as a mitigation device in bridges.

The study highlighted strategies to mitigate the effect of the tsunami on bridges. Previous literature reviews show that the investigation on tsunami loads mainly focused on the effect of tsunami on deck.

The main point of interest in this research is the tsunami loading influence on a complete bridge in the variety of configurations, bed slope, wave heights and shallow water. The behaviour of a complete bridge on tsunami force is different from in the case of only applying a deck.

In view of shortcomings of current methods, it is desirous to provide a system and method for mitigating the effects of coastal wave. Accordingly, the present research provides a system for mitigating the effects of tsunami force on coastal bridges. This research is therefore aimed to increase the integrity of new and existing bridges against tsunami attack with respect to structural behaviour at lower cost.

1.4 Scope

This study includes six main aspects. The scope of research is as follows:

a) A rigid platform with adjustable piers and rigid bed for presenting the various beach slope profile.
b) Five different wave height i.e. 0.38 m, 0.34 m, 0.30 m, 0.26 m, 0.22m created by wave generator and two shallow water applied in the 24m*2m*1.5 wave flume.
c) Three types of bridge models with 1/40 scale applied consisted of Box Girder Bridge, Steel Girder Bridge and Box Beam Bridge with various girder beam i.e. three to six.
d) Bridge models are placed on a bed slope and various shallow water subjected to tsunami bore acting to a longitudinal axis of the models.

e) One six axial load cells connected to the base plate and four axial load cells installed to deck and piers to measure the tsunami forces. Optitrack is used to evaluate the displacement of the structure during the tsunami attack.

f) Solitary wave and bore heights that were obtained in the experiment evaluated by Wiegel (1980) and Fukui et al. (1963) methods, respectively.

g) An Arbitrary Lagrange Euler formulation for the propagation of tsunami solitary and bore waves by an FSI package of LS-DYNA on high-performance computing (HPC) system to evaluate the experimental results.

h) Evaluate the baffle plate as a countermeasure device in the tsunami force on bridges.

1.5 Contribution

The significant contributions of this research are as follows:

a) As a first ever study, this research provides an insight into the tsunami flow characteristics around a realistic bridge model in a shallow water that consists of various complete pier-deck bridge configurations.

b) Evaluate the effect of various bridge geometry characteristics on tsunami forces, including Box Girder Bridge, steel girder bridge and Box Beam Bridge with variety of beams i.e. three to six.

c) It reveals the importance of employing a complete pier-deck model to estimate the bore force on the bridge pier with limited deck height which obstructs the flow.

d) Applied an Arbitrary Lagrange Euler (ALE) formulation to create waves with wave generator, and also the propagation of tsunami solitary and bore waves by an FSI package of LS-DYNA in 1:1 scale of experiments.

e) The effect of baffle plate in the four types of configuration applied in bridges due to mitigating tsunami forces on bridges which has not yet been investigated in research is evaluated.

1.6 Outline of the thesis

This thesis includes five parts. The first chapter presents a brief introduction to the tsunami and importance of evaluation of tsunami on the bridge structure and summarizes the objective, contribution and brief review of this research. Chapter 2 provides the review of literature on experimental and numerical research on the tsunami effect on bridges and mitigation system as tsunami force countermeasures. Chapter 3 presents the methodology of this study consisting of instruments t applied in the experiment, experimental modelling, numerical and simulation modelling. Chapter 4 shows the significant contribution and findings as well as result analysis and discussion. This chapter presented an analysis of experimental results, the FSI modelling and analysis and comparison of experimental and numerical result. Chapter 5 presented the conclusion and summary of contribution of this thesis and recommendation for future study.

CHAPTER 2: LITERATURE REVIEW

2.1 Introduction

Previous studies on effect of tsunami load on bridges in variety condition i.e. bridge model, wave height, shallow water and beach slop are reviewed in this chapter.

The main objectives of the literature review are to: (i) provide a background on the concepts of tsunami waves, bores and tsunami forces on coastal bridge, (ii) provide a starting point for the interpretation of the results presented in this research, (iii) provide a background on the tsunami mitigation system on coastal bridges, (iv) demonstrate the novelty of the this research with respect to similar studies performed using tsunami induced force on coastal bridge and FSI method.

2.1 Tsunami wave and bore

Tsunamis are waves that are mainly created by submarine earthquakes when vertical deformations of the seafloor occur. In the epicentre, the wavelengths are huge and wave heights are quite small in comparison with ocean depths. However, when these types of wave move towards a coastline somewhere in the shallow water the height reduces quickly, and the wave energy is concentrated by refraction, which, accompanied by shoaling and local resonance effects, leads to considerably increased wave amplitudes (Hammack 1973). Figure 2. 1 shows the creation mechanism of a tsunami wave.

When a tsunami wave is transferred to the shoreline with high velocity it breaks somewhere, and the shallow still water level is nearly equivalent to the occurring wave height. It then runs up the shoreline like a hydraulic bore (Nistor et al. 2005). These types of huge waves subsequently attack the coastline at the locations, displaying a significant hazard to humans, property and the environment.

Hundreds of thousands of people have died in tsunami disasters and many structures and infrastructures have been destroyed. Table 2. 1 indicates the major tsunamis over the last 130 years. Two huge tsunami disasters have occurred in recent years, including the giant Indian Ocean tsunami induced by of the M 9.1 earthquake that occurred on December 26, 2004 (USGS 2007). The tsunami was among the heaviest natural catastrophes in human history with human losses exceeding 300,000 and causing devastating damage to buildings and infrastructure leaving more than 1.5 million people homeless (Ghobarah et al. 2006). In this tsunami, from among the 186 bridges affected by the tsunami on Sumatra Island, 81 of them were totally washed away or heavily damaged (Unjoh and Endoh 2006).

On March 11, 2011, the Great Eastern Japan Earthquake with a 9-moment magnitude caused a catastrophic tsunami along the eastern part of Japan (Simons et al. 2011) and even effected U.S. west coast (Allan et al. 2012) . The Japanese National Police Agency Headquarters reported 15,883 deaths during this disaster on 12 September 2012. Kosa (2012), reported that during this tsunami more than 300 bridges suffered serious damage, and losses included 9 national roads, 14 prefectural roads and 101 railroads. Figure 2.2 indicates the types of bridge washed away in this tsunami (Kosa 2012).

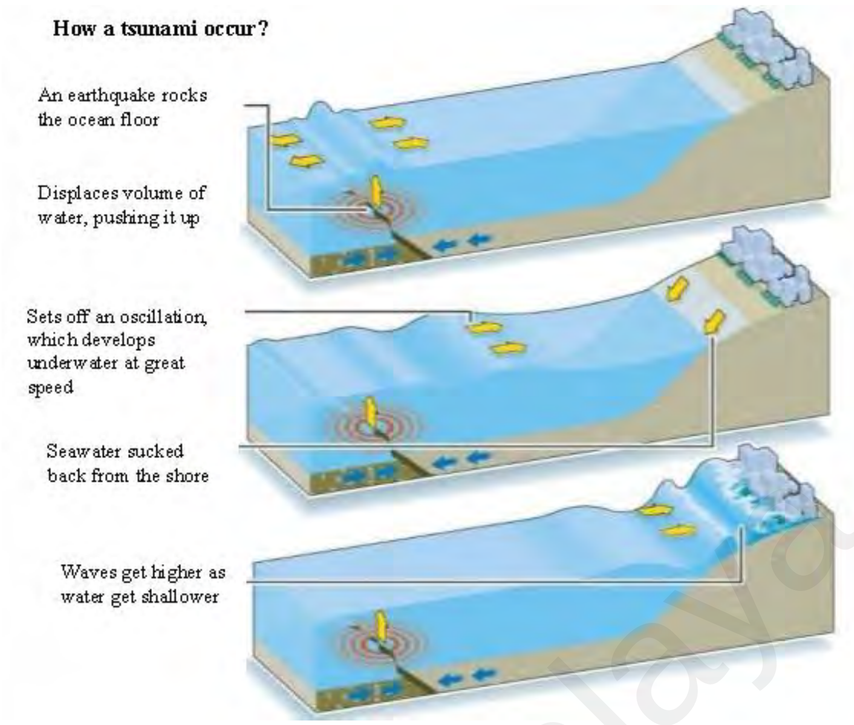

Figure 2. 1: Tsunami creation mechanism

A similar experience to the tsunami water waves occurred on August 29, 2005 in the United States when Hurricane Katrina made landfall on the Gulf Coast. The storm surge flooded New Orleans and more than 1,800 people died (Graumann et al. 2006). Hurricane Katrina generated significant deterioration of the infrastructure with 45 bridges suffering damage in Mississippi, Alabama, and also Louisiana, as reported by Padgett et al. (2008). The majority of the damaged bridges by Hurricane Katrina were due to destruction by storm surge-induced forces. Most of the destruction was on the superstructures. Typically, the bridge decks were unseated and drifted away.

The massive loss of human lives during these enormous catastrophes by tsunamis is a reminder to the international scientific community that there is a dire need to identify and simulate the tsunami mechanism, propagation and structural inundation procedures. It can be concluded that the main objectives of future research are to mitigate the tsunami influence on coastal structures, to predict the structural behaviour, as well as design safe structures.

During 2004 Indian Ocean Tsunami photos and video captured in Indian Ocean Tsunami demonstrated tsunami waves breaking offshore, occurred by a highly turbulent tsunami bore propagating onshore with significantly high velocity Nouri (2008). The broken tsunami waves in the form of a hydraulic bore also reported by Takahashi et al. (2011) during Japan tsunami 2011 , Chilian Tsunami in 1960 Cox and Mink (1963) and Nihonkai-Chubu earthquake tsunami in the 1983 Yeh (1991).

A bridge structure performs a vital role in enabling people to perform activities related to their daily needs and development. A damaged bridge needs to be repaired expeditiously, as it can cause disruption to critical national humanitarian systems, which causes delays to the rescue operations and recovery progress that include repairing and improving the affected areas.

Table 2. 1: Tsunami history from 1883 in the world

Name of tsunami	Date	Earthquake Magnitude	Location	Maximum Tsunami height	Number of human loss
Krakatoa, Sunda Strait,Latter (1981)	Aug 27, 1883	-	Sunda strait ,indonesia	37	36,000
Meiji Sanriku, Japan,Nakao (2009)	June 15, 1896	8.5	Iwate, japan	38.2	22,000
Messina, Italy Tinti and Giuliani (1983)	Dec 28, 1908	7.1	Messina, italy	12	70,000
Kanto, Japan Aida (1970)	Sep 1, 1923	7.8	Kanto, japan	12	150
Grand Banks Fine et al. (2005)	Nov 18, 1929	7.2	South of Newfoundland	13	28
Sanriku earthquake Shuto (1993)	Mar 3, 1933	8.4	Sanriku coast of northeastern Honshu, Japan	23	3060
Tonankai, Japan Tanioka and Satake (2001)	Dec 7 1944	8	Shima Peninsula in Japan	8	1223
Aleutian Islands López and Okal (2006)	April 1, 1946	7.8	Aleutian islands	30	165
Nankaidō, Japan Aida (1981)	Dec 21 1946	8	Nankaido, japan	6	1443
Severo-Kurilsk Kaistrenko and Sedaeva (2001)	Nov 5, 1952	9	Kuril islands, russia	18	2,336
Chilean Earthquake Liu et al. (1995)	May 22, 1960	9.5	Cost of South Central of Chile	25	6000
Good Friday Earthquake Grantz et al. (1964)	Mar 27, 1964	9.2	Alaska, USA	23	128

Table 2.1: Tsunami history from 1883 in the world (continue)

Name of tsunami	Date	Earthquake Magnitude	Location	Maximum Tsunami height	Number of human loss
Moro Gulf Wiegel (1980)	Aug 16, 1976	7.9	Moro gulf, mindanao, philippines	5	5000
Tumaco Tsunami Soloviev and Kim (1997)	Dec 12, 1979	7.9	Along the Pacific Coast of Ecuador	5	259
Sea of Japan Pelinovsky et al. (1985)	May 26, 1983	7.7	Around 100 km west of the coast of Noshiro in Akita Prefecture, Japan	14	100
Okushiri, Hokkaido Shuto and Matsutomi (1995)	July 12, 1993	7.8	Okushiri islands, japan	31.7	201
Papua New Guinea Tappin et al. (2002)	July 17 1998	7.1	North coast region of Papua New Guinea	15	2200
Indian Ocean Goff et al. (2006)	Dec 26, 2004	9.1	Sumatra, indonesia	30	230000
South of Java Island Lavigne et al. (2007)	July 17, 2006	7.7	South of Pangandaran, Indonesia	8.6	668
Solomon Islands Fisher et al. (2007)	Apr 24, 2007	8.1	South of Ghizo Island, the Solomon Islands	9	52
Samoa Okal et al. (2010)	Sep 29, 2009	8	South of Samoa Islands	14	123
Chile Verdugo et al. (2011)	Feb 27, 2010	8.8	Maule region, Chile	28.3	521
Pacific coast of Japan Mimura et al. (2011)	Mar 11, 2011	9	The northeastern coast of Japan	15	15,776
Sulawesi earthquake and tsunami ANSS (2018)	Sep. 28, 2018	6.1	the Anak Krakatau volcano	7	4,340

2.2 Tsunami load and building codes

Most of the current building codes have not been designed to withstand the conditions presented by tsunamis. Some of them are being planned to include the effects of tsunamis, such as ASCE for 2016 (Chock 2012).

Table 2.2: Classification of the standard building code equations considered by FEMA646 and CCH

Loads	FEMA646,2007	CCH, 2007	
Hydrostatic	$F_h = p_c A_w = \frac{1}{2}\rho_s g b h_{max}^2$	$F_H = \frac{1}{2}\rho g \left\{h + \frac{up^2}{2g}\right\}^2$	This is the cause of fluctuation pressure due to a different water level between opposite
Buoyant	$F_b = \rho_s g V$	$FB = \rho g V$	Uplift due to complete or partial submergence of a structure
Hydrodynamic	$F_d = \frac{1}{2}\rho_s C_d B (hu^2)_{max}$	$F_D = \frac{\rho\, C_d A u^2}{2}$	Caused by the steady flow around a structure
Uplift	$F_u = \frac{1}{2} C_u \rho_s A_f u_v^2$	Not available	Upward wave pressure on the bottom side of floor structures due to quickly increase flood waters
Impulsive	$F_s = 1.5 F_d$	$FS = 4.5\,\rho g h^2$	Due to the leading edge of a surge of water impacting a structure
Debris	$F_i = C_m u_{max}\sqrt{km}$	$F_I = \frac{m dU_d}{dt}$	Due to impact of debris including small boat, shipping containers, automobiles carried in
Retained water	$f_r = \rho_s g h_r$	Not available	Due to additional gravity water retained on the top of elevated

Note: ρ_s= fluid density including sediment, A_w, A_f= wetted area of the bridge, b = width of element, B = breadth of the structure in a plane normal to the direction of flow, C_d = drag coefficient, C_u = uplift coefficient, C_m= added mass coefficient, g = gravitational acceleration constant, F_B = buoyant force acting vertically, p = density of water, h_{max}= maximum water height above the base, g = gravitational acceleration, h_r = maximum potential depth of water retained on an elevated floor, hu^2= momentum flux per unit mass, k = effective stiffness of debris, m = mass of debris, u_{max}= maximum flow velocity, V = volume of water displaced, V = displaced volume of water, h = surge height, C_D = drag coefficient, A = projected area of the body normal to the direction of tsunami flow, U = velocity of flow relative to body, m = mass of the water displaced by the body impacting the structure (slugs), U_b= velocity of the body, t = time (s), $\frac{dU_b}{dt}$ = acceleration.

Studies on the effects of tsunamis on coastal structures, especially bridge structures, are therefore important for the scientific community to gather information upon which the codes can be based. Some studies were conducted by Yeh et al. (2005) to evaluate tsunami loads on structural loads under flooding and wave situations. They examined five building codes; namely, the City and County of Honolulu Building Code (CCH 2000), the 2000 International Building Code (IBC 2000), the 1997 Uniform Building Code (UBC 1997), American Society of Civil Engineers Committee (ASCE 1998), and the Federal Emergency Management Agency Coastal Construction Manual (FEMA55 2000) to evaluate guidelines for the design of buildings subjected to tsunami loading. Yim (2005) also presented that only the Honolulu Building Code (CCH 2000) includes the tsunami loads. Based on the comparison of these codes, Yeh et al. (2005) proposed generalized equations for breaking wave forces, hydrodynamic force, buoyant force, hydrostatic force, surge force, impact force, and design flood velocity. Later the Federal Emergency Management Agency provided FEMA P-646 in June 2008, FEMA646 (2008), which constitute the present guidelines for the design of structures for proposed vertical evacuation from tsunamis and performed tsunami loads on structures. Other building codes, such as the City and County of Honolulu Building Code introduced a specific section in CCH, 2007, Chapter 16, Article 11, with the title of “structural design of buildings and structures subject to tsunamis” in Section 16-11.5 to provide an equation for tsunami loads on structure CCH (2007). Table 1 classifies FEMA646 and CCH for tsunami loads. The ASCE Structural Engineering Institute decided to update ASCE 7 with a section on Tsunami Loads and Effects in 2016 Chock (2012).

2.3 Review of tsunami effects on bridges

Several studies on the effects of the tsunami fluid forces have been conducted on coastal and port structures. Cumberbatch (1960), studied the impact force of waves and proposed a similar solution for the impact of a two dimensional fluid wedge on a flat impermeable wedge.

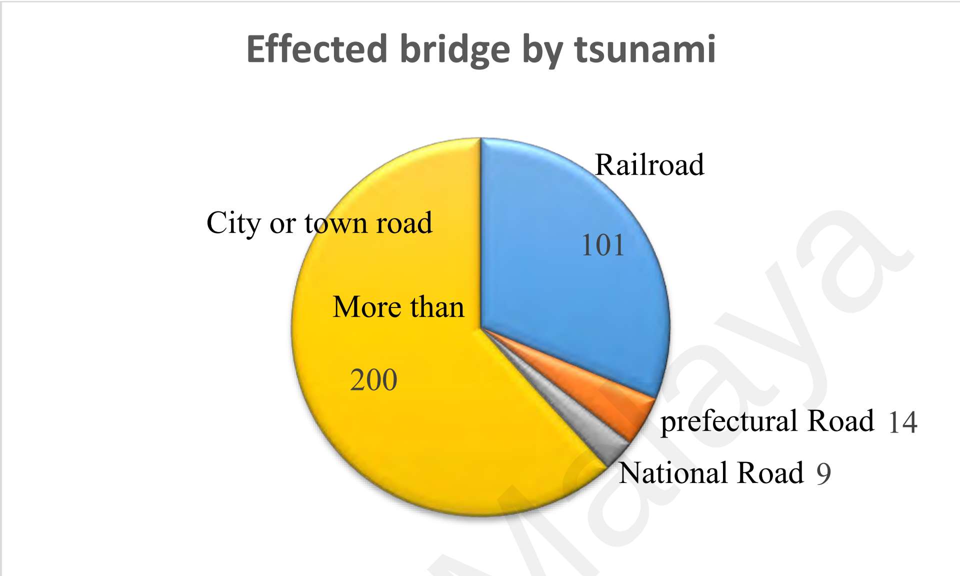

Figure 2.2: Types of bridges washed away Kosa (2012)

Fukui et al. (1963) investigated impulsive and continuous pressures created by tsunami wave loads on a dike with different seabed slopes by reflection of a bore. They indicated that impulsive pressure scales as the fourth power of the incident wave velocity. Cross (1966; Cross (1967) studied the tsunami impact forces acting on vertical walls with a smooth and roughened bottom and proposed a formula for the effect of impact force on a vertical wall. Nakamura and Tsuchiya (1973) investigated the impact of surge propagation on a composite structure over a horizontal bed. They stated that the maximum pressure was only 50% higher than the maximum value of hydrostatic pressure developed in the wall. Continuing research on the effects of tsunami loads on vertical walls, dikes and structures have been conducted by other researchers, such as Tanimoto et al. (1984), Togashi (1986), Ramsden (1996), Matsutomi and Shuto (1994), Asakura et al. (2000), Ikeno et al. (2001), Ikeno and Tanaka (2003) and Ikeno and Tanaka (2003), Arikawa et al. (2005), Kathiresan and Rajendran (2005), Pacheco (2005), Arikawa et al. (2006), Arikawa et al. (2007), Fujima et al. (2009), van de Lindt et al. (2009), Bandara and Dias (2012) Salem H. et al. (2017) Winter et al (2018), Zhu. M. Et al. (2018) and Mazinani et al. (2021).

Surprisingly, numerical and experimental investigations of the effects of tsunamis only began from 2006 through research by Kataoka et al. (2006), and Shoji and Mori (2006b). Although there has been little research on this area, the following are reviews on previous research published as research articles, conference proceedings, report papers and technical notes concerning the effects of tsunamis on bridges. This part includes three sections – numerical and experimental research on bridges against tsunami load, survey reports of affected bridges after tsunami disaster and mitigation of tsunami effects on bridges.

2.4 Numerical and Experimental Research on Bridges against Tsunami Load

This section discusses experimental and numerical research on bridges subject to tsunamis and the challenges. A wave flume (2D or 3D) with various dimensions was employed in the experimental test to study the effect of a tsunami wave on a coastal or inland bridge. There are various approaches to create a tsunami wave, such as wave generation, open gate systems, and draping a block in a flume. The initial experimental tests concerning the effect of the tsunami load on bridges was performed by Kataoka et al. (2006). The authors conducted an experimental study on the wave force action on a girder bridge. They utilized three spans of bridge deck in several scales from 1/18 to 1/108. They applied three wave scenarios as breaking, non-breaking and broken wave. They assessed the drag force and impulsive force in still water and different tsunami wave heights. The results showed that the impulsive load is a function of the wave condition. This agreed with Nouri et al. (2010), and Ikeno et al. (2001). Kataoka et al. (2006) verified the drag force using the formula of Goda (1974) concerning the slowing tsunami force. However, Shoji et al. (2011), showed through an experiment that the tsunami wave pressure computed by Goda (1974) was lower than their experimental results. In the model by Kataoka et al. (2006), the pier bridges were assumed to be very thin, as mentioned by Lau (2009). This resulted in a reduced flow load on the bridge model. Lukkunaprasit and Lau (2011) showed that in the model with complete pier and deck tsunami pressure by a bore was significantly higher than a stand-alone deck or pier.

Shoji and Mori (2006b) carried out an initial experimental study on the effect of the 2004 Sri Lanka Giant Tsunami in the Indian Ocean to evaluate the bridge failure mechanism measured by Shoji and Mori (2006a). The bridge model was assumed to be a box girder shape, fixed on the abutment in the wave flume 6 m long. No pressure sensors were placed on the models to measure the wave pressure. In the experiments, the drag coefficient was assumed to be two for the purpose of calculating the static friction coefficient. They developed the research of Shoji and Moriyama (2008) by adding force measurements. Sugimoto and Unjoh (2007) conducted hydraulic experiments to evaluate the failure mechanism of a bridge. Steel and RC bridges were applied as bridge models in this study. The experiments were carried out in two scenarios: fixed bearing and movable models. The scale of the bridge models was 1/50. The wave flume size was 26 m in length, 1 meter wide and 0.8 m high. Two tsunami heights of 3 m and 5 m with 5 different still water cases from 1 m to 3 m were performed. They found that the concrete bridge maximum drag force was 0.93 times the self-weight and that the maximum lift force was 1.76 times the self-weight. In the steel bridge model, the maximum drag force was 1.46 times the self-weight and the maximum lift force was 1.84 times the self-weight. The results indicated that increasing the tsunami height increases the drag force. In addition, increasing the water level increases the lift force. Shoji et al. (2011) verified this fact. The superstructure of the bridge was washed away when the drag and lift force exceeded a certain threshold value. The superstructure could also be displaced when the uplift did not exceed the threshold value. Sugimoto and Unjoh (2007) neglected the effect of piers on their analysis. In reality, tsunami loads on bridge decks are significantly reduced ((Lau 2009),(Lukkunaprasit and Lau 2011))

Iemura et al. (2007) conducted experiments in a wave flume to study the effect of tsunami waves, debris and breakwaters in front of dry land bridges. The tsunami wave was generated by moving a paddle with certain strokes and durations in a 50 m flume. A three-girder bridge model results in larger force than a five-girder bridge model. They showed that the higher value of force occurred at the highest wave velocity, which was at the initial stage of the wave attack on the bridge. In addition, assuming 0.2 seconds as the impact duration, the results were found to be acceptable for the foreseeing impact force of floating wooden cylinder debris. This value is also recommended by FEMA55 (2006) for reinforced concrete walls. However, the City and County of Honolulu Building Code CCH (2000) proposed impact duration quantities for wood construction as 1 .0 Sec, steel construction as 0 .5 Sec, and reinforced concrete as 0.1 Sec. A low breakwater around 1/3 of the tsunami flow height would not considerably influence the flow velocity. However, a larger breakwater height of around 1/2 of the tsunami flow height starts to be effective in decreasing the flow velocity. van de Lindt et al. (2009) and Tanimoto (1983) studied the effect of a breakwater in reducing the tsunami force. However, the relationship between the breakwater and the tsunami wave height should be considered on a larger scale. They also indicated in their study that in the case of the largest velocity and tsunami force, the drag coefficient is 1.1 for the proposed bridge. Shoji et al. (2011) found that the average value of the drag coefficient in plunging breaker bore was 1.56, and, in the surging breaker bore scenario, it was 1.52 in the bridge models. However, the Hydraulic Engineering Circular No. 18 by Richardson and Davis (2001) and Arneson et al. (2012), suggested a drag coefficient between 2 to 2.2.

Araki et al. (2008) indicated that the characteristics of tsunami behavior on a beam of PC-girder bridges from studies in a two-dimensional wave channel of 40 m long, 0.9 m high and 0.7 m wide. The scale of the model was 1/70. In the experiments, the range of wave height was 2.48 to 12.55 cm. The pressure and total horizontal force and lift forces were measured by 8 pressure sensors and a two-component force recording method utilizing a strain gauge. These were digitized at a time interval of 0.005s and measured by the data acquisition method. The results indicated that the bridge is impacted by a force with significant magnitude and that the highest horizontal force significantly depends on the clearance under the bridge and tsunami height. Additionally, it was found that the amount of lift force was similar to the horizontal force. This is contrary to the research by Shoji et al. (2012) and Kawashima et al. (2011). This difference is due to the lack of laboratory facilities, such as a load cell, in the Araki et al. (2008) research. The effect of entrapped air-bubble size in the impact force was ignored in the experiments. Yim et al. (2004) stated that because of the turbulent characteristics, which are extremely delicate to length scales, researchers cannot properly evaluate using small-scale laboratory models. In addition, to increase the accuracy of measuring the horizontal and vertical force an appropriate load cell should be used instead of a strain gauge.

Shoji and Moriyama (2008) studied the effects of tsunami loads on various structural components of a bridge, such as length of the deck, width of the deck, height of the deck and the height from the bed of a water flume to the deck. The velocity of wave varied from 0.2 m/s to more than 0.9 m/s. In real conditions, the tsunami velocities vary from 2 m/s to 9 m/s. They showed that by increasing the deck width the drag coefficients were reduced proportionately. While the ratio of the drag force of the specific mass of the bridge deck decreased, the height of inundation did not differ significantly. This is because the lateral tsunami load is higher than the drag force on the bridge deck. Another effect of a tsunami on the configuration of a bridge deck is the deck height. It was found that increasing the deck height increased the drag coefficients proportionately. The ratio of drag force increased synchronously by increasing the normalized inundation height. Increasing the height of the deck increases the normalized inundation height due to the deck movement under the abutment. The bridge deck movement caused by increasing the height and weight of the bridge deck only influences the impulsive tsunami load. The experimental study was simplified by using a box shape girder deck that was fixed on the abutments. They also ignored the effect of piers on the bridge. Computational simulation was notably lacking. In addition, the configuration of the bridge and characteristics of the tsunami wave and entrapped air-bubbles in small-scale models was neglected in this research. Takahashi et al. (1985), and Cuomo et al. (2010), applied a good approach for scaling wave impact pressures measured on small scale physical models.

Lukkunaprasit et al. (2008) stated that higher amounts of horizontal pressure at the bottom of the bridge pier could be as high as 4.5 times the hydrostatic pressure for both bridge models. This is in agreement with Kenji Kosa et al. (2010). They also stated that the value of horizontal wave force was higher by 2.6 times compared to the hydrostatic pressure. Nistor et al. (2011) stated that for a 1 m impoundment depth on the circular column section that could develop on bridge piers, the higher value of pressure occurred at 40% of the height of the bore from the bottom of the structure.

Thusyanthan and Martinez (2008) performed experiments on a simple pier and deck bridge at 1:25 scale. The length of the wave tank was 4.5 m and the wave creation mechanism could release heavy forces to the water. They studied the impact of the pressure wave in relation to the pier height and pier width of the bridge. The results indicated that the bottom of the pier in dry conditions experienced the largest amount of impact pressure through a tsunami wave. Lau (2009) indicated that the maximum value of impact pressure occurred at the bottom of the pier bridge with a value of 3.5 to 4.5 times of the hydrostatic pressure. Nouri et al. (2010) indicated that the highest impact pressure occurred at approximately 40% of the surge height. In wet conditions, the highest value occurred at relatively higher above the water level. This is similar to the findings of Hamzah et al. (2001) concerning the effect of tsunamis on barriers.

Araki et al. (2010) investigated the effect of vertical and horizontal components of the tsunami fluid pressure and force in a girder bridge. They applied two hydraulic waves in the experiments; namely, post-breaking and just-breaking wave. The wave flume size was 41 m long and 0.7 m wide. The wave pressure acting on the prototype was measured at four points using pressure gauges. They showed that in the case of the post-breaking wave the vertical and horizontal components of the maximum measured fluid force were smaller than in the case of the just-breaking force. The impact force on the bridge was based on the additional mass to the bridge model due to varying submerged conditions. They noted that in the case of the just-breaking wave the horizontal component of the impact force was not significant. They indicated the direct relationship between the normalized maximum pressure and normalized height of a tsunami wave over the model. The increased normalized height of a tsunami wave decreased the normalized maximum wave pressure. The wave pressure was measured using the method of Tanimoto (1983) and Tanimoto et al. (1983). The results showed that the higher amount of wave pressure exposed on the lower section of the proposed bridge model was higher than the pressure on the upper section of the bridge. This is similar to the findings of Nouri et al. (2010) and Ramsden (1996). Kenji Kosa et al. (2010), performed an experimental test to evaluate tsunami wave force on the bridge deck with a 1/50 scale model. They used a wave flume 41 m long, 0.80 m wide, and 1.25 m high with two wave cases; namely, unbroken and broken wave types. They concluded that in the broken wave the horizontal wave force was higher than the uplift force. This is opposite to the case of the unbroken waveform. However, Araki et al. (2010) stated that in the case of the broken wave, the vertical and horizontal components of the maximum measured fluid force were smaller than in the case of the just-breaking force. The authors also proposed an equation for the estimation of the uplift and horizontal wave force in place of the formula by Goda (1974). In this research, the authors did not apply any pressure sensor to measure the wave pressure on the structure. In addition, piers have no influence in measuring tsunami wave forces on bridge models, as shown by Araki et al. (2010), Iemura et al. (2007), and Sugimoto and Unjoh (2007).

Yoshinori Shigihara and Fujima (2010) presented the numerical analysis to study a horizontal tsunami on three bridges, – Cut River Bridge, Lueng Ie Bridge and Kr. Ritting Bridge – that suffered damage in the 2004 Sumatra tsunami. They applied the method by Koshimura et al. (2009), for the numerical analysis. They also provided a safety factor, which was defined as the ratio of the horizontal tsunami wave force acting on the girder and the resistance of bridge due to the weight. This factor was also used by Bricker et al. (2012), and Sugimoto and Unjoh (2007). Sugimoto and Unjoh (2007) analyzed the Lueng Ie Bridge with a lower tsunami height of 3 m instead of 17.22 m in reality. The authors indicated that the horizontal force was 2784kN and the safety factor was 0.93. The uplift force was 5269kN (1.76 times the self-weight), or the safety factor was 1.76, and, based on the 16 m length of bridge, these two results differed significantly. Some other researchers, like Shoji et al. (2011), used these bridges as case studies to evaluate the drag coefficients. Yoshinori Shigihara and Fujima (2010) neglected the effect of uplift and overturning moment.

Shoji et al. (2011) conducted hydraulic tests to evaluate a tsunami wave load on a bridge deck. The emphasis of this research was the impact of the style of breaker bores on the value of the drag coefficient in addition to the dependence of the variations of the condition of a bridge deck against a tsunami on the variation of horizontal wave load. The model scales were 1/79 and 1/100 of the Lueng Ie Bridge, which was affected by the 2004 Indian Ocean tsunami. The average value of the drag coefficient illustrated was 1.52 in the condition of surging breaker bores, and 1.56 in the condition of plunging bores. Galvin (1968) stated that when the crest separates from the wave and plunges into the free surface plunging bore occurred. The value of the drag coefficient for plunging breaker bores is higher than surging breaker bores. This shows that the horizontal drag force on a bridge deck exposed to plunging breaker bores tends to be slightly higher than when exposed to surging breaker bores. However, Iemura et al. (2007) indicated that for the largest velocity and a tsunami force in their experiments, the drag coefficient is 1.1 for the proposed bridge. Richardson and Richardson and Davis (2001) in Hydraulic Engineering Circular No. 18 and Arneson et al. (2012) suggested a drag coefficient of 2 to 2.2. In the comparison between the induced horizontal wave load and the condition of a bridge deck under wave height, it was discovered that the improvement of induced horizontal wave was notable while the increase of tsunami wave height appears for the lesser still water rate. The higher section of a tsunami wave behaves on a bridge deck rapidly with great energy and the increase of average horizontal wave force is much more vulnerable to the rise of the tsunami wave height in comparison to the condition, while a smaller section of tsunami wave attacks on a bridge deck. This phenomenon might be more significant for plunging breaker bores in comparison with surging breaker bores when plunging breaker bores behave on a bridge deck with great energy before the wave breaks. The effects of uplift and air trapped on the bridge were neglected. They also evaluated the formulae by Goda (1974) and Asakura R et al. (2000). They stated that these methods provide a possibility of calculating the reduced wave pressure on a bridge deck compared to an actual tsunami wave pressure on a bridge deck exposed to breaker bores. Santo and Robertson (2011) also confirmed that the formula by Asakura R et al. (2000) was lower than the actual pressure in the experiments. Araki and Deguchi (2012) stated that the methods of Goda (1974) were based on cases where the wave pressure acts on the seaward side of the horizontal plate. The reason being that two formulae assume the various boundary conditions of a concern model, as compared to the proposed models.

Lukkunaprasit and Lau (2011) carried out an experimental test on the effect of tsunami loads in the case of bore in a stand-alone pier and complete pier and deck. The results showed that in the model with the complete pier and deck, the tsunami pressure by bore was 50% higher than a stand-alone pier. This increase is a result of the blockage of the splashing and topping due to the wave over the proposed piers. Therefore, to evaluate the tsunami load on the pier of a bridge the result of a stand-alone model could not be used, as stated by Nouri et al. (2010), and Árnason (2005). They neglected the effect of other loads introduced by CCH (2000) and FEMA646 (2008), such as uplifts and the overturning moment on the complete pier and deck model, and the stand-alone pier.

Murakami et al. (2012) investigated a bridge damaged in a tsunami by the Tohoku earthquake in 2011. The height of the tsunami bore on the proposed coast was around 2.2 m. Due to the narrow location of the bridge, it reached to 5.5 m at the rear and front of the bridge. The numerical analysis included hydraulic and structural analysis. In the structural analysis, they discussed the mechanism of damage by tsunami action on the proposed bridge. In the experimental section in the hydraulic laboratory, using a 1/50 scale model, they conducted numerical hydraulic analysis using CADMAS-SURF/3D. They stated that the significant difference of pressure between the bottom and the higher section of the bridge plays a vital role when considering the stability of the slab under tsunami conditions. This bridge included five anchor bars in both bearing sections. The results of the analysis showed that during the initial phase the seaside section of the bridge slab lifted up and then the slab floated onto the adjacent highway bridge counter clockwise. Therefore, only the first and second anchors supported the slab while the other anchors could not work as a bearing section. In this study, contrary to the research by Shoji et al. (2011), the horizontal force acting on the bridge slab was found to be lower than the vertical uplift force. Douglass et al. (2006), indicated that in Hurricanes Katrina, the uplift was higher than the horizontal load. It overcame the deck weight and connections and washed away the deck as in three examples of bridges in Florida; the I-10 ramp near Mobile, Alabama; the I-10 Bridge across Escambia Bay, and the U.S. 90 Bridge across Biloxi Bay, Mississippi.

Shoji et al. (2012) determined the horizontal and vertical tsunami wave pressures on the Pacific Coast as a result of the Tohoku earthquake tsunami in 2011, which washed-away nine bridge decks. They used the formerly recommended experimental formulation incorporating the simulated inundation heights for this determination. Initially they performed the tsunami flow simulations at the five impacted locations by applying the finite difference method with the staggered leapfrog approach. They determined the tsunami wave pressures on the nine bridge decks that were washed-away by using the experimental formulae by Shoji et al. (2012) for the simulated data. They obtained the inundation heights at the locations where the nine bridges were washed away. Furthermore, by applying the simulated inundation heights, they determined the horizontal and vertical hydraulic pressures experienced on the bridge decks based on the formulation for the assessment of the relationship of the location of a bridge deck η to an inundation height with the horizontal and vertical wave pressures acting on a bridge deck κ and λ.

Bricker et al. (2012) performed a numerical analysis and survey report to assess the bridge failure during the Great East Japan Tsunami of March 11, 2011. The prototype model was the Utatsu highway bridge in Minamisanriku town. The survey report showed that the deck sections were subjected to a huge amount of lift force and overturning moment. They applied Computational Fluid Dynamics (CFD) to evaluate the effect of the tsunami on the bridge. The investigation explored two scenarios that occurred for the bridge – tsunami surge and smoothly rising water surface. CFD analysis was performed for initial flow speeds of 3 m/s, 5 m/s, 7 m/s, and 9 m/s. Although Kosa (2012), using the rough analytical process of wave velocity and video, showed that the wave velocity at the location around Utatsu Bridge should not exceed 7.0 m/s, with reference to the effect of the debris it is reasonable to assume a wave velocity of 6 m/s around the Utatsu Bridge. Numerical analysis indicated that failure of the bridge deck was due to surge. It was indicated that the air trapped increased the effective gravity load to increase the effect of the lift load and overturning moment. This was proven by Chen et al. (2005), and Patil et al. (2009). Bricker et al. (2012) stated that fluid density significantly increases the lift load and overturning moment. In tsunami action, according to FEMA646 (2008), the water density is assumed to be 1200 kg/m^3. Takahashi et al. (1985), Cuomo et al. (2009) and Xiao, S. C et al. (2019) suggested making an opening in the deck to decrease the effect of the trapped air. Furthermore, for the accuracy of the numerical result, the mesh size should be independent in the CFD analysis, however, in this research, it was not.

Nakao et al. (2012) conducted experiments to investigate the hydrodynamic forces induced by tsunamis applied to five different bridge sections. The hydraulic experiments were conducted using bridge models with trapezoidal, rectangular, inverted trapezoidal, hexagonal, and mixed rectangular/semicircular cross-sectional geometries. The results indicated that a rectangular section model experienced the highest horizontal hydrodynamic force. Modified rectangular and trapezoidal models were subjected to low lift forces. The results also showed that applying baffle plates to the girder bridge reduced the lift force although they did not significantly affect the horizontal force. The models in this paper were not scaled and were only geometrically shaped to assume the bridge models. Fuchs and Hager (2012) stated that hydraulic models were different from the prototype scale and were affected by model effects; in addition, the measuring data may be affected by scale effects like surface tension or viscosity. Hughes (1993) recommended a scale family method to determine the model effects. This method was utilized by Heller et al. (2008) for landslide-generated impulse waves.

2.5 Survey Report on The Affected Bridge and Failure Mechanisms

Survey report and damage investigation on the bridges subject to the tsunami wave load in the affected area was another challenging issue in this research. Figure 2.3 displays a washed-away concrete girder bridge during the Japan tsunami. This section reviews, evaluates and quantitatively analyzes the damage data for the bridge structures due to the tsunami wave load. After the Sumatra Islands tsunami of 2004 in the Banda Aceh region, Unjoh (2006) performed a damage investigation on bridges affected by the tsunami wave. The author found that the bridges with shear keys sustained less or no damage than bridges without any shear key. However, the research of Murakami et al. (2012), and Bricker et al. (2012), showed that even bridges that had shear keys also experienced wash out and heavy damage.

Figure 2.3: Washed away bridges (a) deck panels lifted from piers and deposited nearby in Utasu-Ohashi bridge (b) failed pier in Tutanigawa bridge Kosa (2012)

Based on the data collected in Sri Lanka by Shoji and Mori (2006a) on bridges affected by the tsunami in 2004, Shoji and Moriyama (2007) categorized the damage of the subject bridges into three categories. This included washed-out, movement of a deck, severe damage of an abutment due to scour and erosion of soil embankment, and damage of handrails upon a deck. The damage of bridges was related to the observed inundation depth and tsunami wave height. The relation of those values with the fragility of the subject bridges, that is the fragility curve, was clarified. The fragility curve, which was first introduced by Shuto (1993), was applied. The derived fragility curves indicated that simple spanned bridges without suitable shear keys between the deck and its supporting piers, or abutments are fragile against a tsunami. This is also reported by Unjoh (2006), and Unjoh and Endoh (2006). Shoji and Moriyama (2007) concluded that when the inundation depth reaches around 10 m the failure mode of a bridge structure might be due to the flow induced by a tsunami wave. On the other hand, for inundation heights of more than 10 m, the failure mode of the bridge might be due to the impulsive pressure induced by the tsunami wave. H. Kasano et al. (2012) carried out a survey on the bridges affected by the tsunami wave in the Tohoku area. They studied the structural feature of both the affected and the preserved bridge subject to the tsunami wave. They found that the fall-off prevention devices could not prevent the bridge deck from being washed out. Kosa (2012) also studied this type of device. The weight of the bridge deck plays a vital role in the destruction of the bridge. This is also stated by Douglass et al. (2006), and Chen et al. (2009). Kosa (2012) stated that 300 bridges suffered from the tsunami caused by the 2011 Great East Earthquake in Japan. A survey carried out on Utatsu Bridge revealed a wave velocity of 6 m/s. Ten spans of the Utatsu Bridge experienced movement. The deck devices to prevent the bridge from being displaced and washed out, such as steel brackets, RC blocks and anchor bolts, suffered serious damaged. This is similar to the findings of H. Kasano et al. (2012), and Bricker et al. (2012). The velocity findings were compared with other methods, such as those by Jaffe and Gelfenbuam (2007), and Tsutsumi et al. (2000). The ratio of the superstructure of the bridge resistance to the horizontal wave force (drag force), referred to as β, between the Sumatra Earthquake 2004 and Tohoku Region in the 2011 Great East in Japan were determined. Especially for damage ranked as Class A, similar degrees of damage to the affected bridges due to the tsunami wave give similar damage ranking β.

2.6 Mitigation of tsunami effects on bridges

There are several available methods for mitigation and damping of the tsunami force on bridges. These techniques may be classified into two sections, i.e. physical protection before the bridge and additional protection installed in the bridge. Figure 2.4, classified the tsunami mitigation approach on bridges.

2.6.1 Physical protection before bridges

To reduce the tsunami wave impact before reaching the bridge, Sato et al. (2003), stated that Tsunami breakwaters and seawalls are major structural countermeasures to mitigate the tsunami effect in structures. Tsunami breakwaters and seawalls are massive constructions and the maintenance of these structures is very costly. Additionally, these kinds of structure are not friendly to the landscape, the daily lifestyle of people or the environment. Shuto (1987), Dahdouh-Guebas et al. (2005) and Kathiresan and Rajendran (2005) suggested that vegetation can play a vital function in decreasing the intensity of tsunami waves and mitigating the catastrophic amount of the wave. Shuto (1987) evaluated the performance of coastal forests against tsunami waves by applying statistical analysis to gauge the physical damage experienced by various types of pine trees in Japan. Latief et al. (1999) proved experimentally the mitigating effect of a variety of mangroves to withstand the tsunami hit due to the hydraulic resistance. The results indicated that this type of vegetation performed efficiently as protection against tsunami waves. Tanaka et al. (2007), studied the effect of six types of coastal vegetation to reduce the drag force by tsunami waves with a field survey and data analysis. The results showed the effect of vegetation in reducing the tsunami force on the structure and the gaps between the vegetation were assumed to be effective for trapping broken branches and decreasing the tsunami flow velocity. Noarayanan et al. (2012) stated that the bending of vegetation has an important effect on the wave before it reaches the coastline. Pradono et al. (2008) performed an experimental study on mitigation of the tsunami force on a bridge by mangrove vegetation and breakwaters to reduce the force in a bridge model. The results indicated that tightly populated and flexible mangroves and breakwater front models considerably reduced the tsunami forces. The efficiency of the flexible mangrove and breakwater decreased with the increasing tsunami flow depth.

2.6.2 Additional Protection for Bridges

There is very little research done on the damping of the tsunami effects on bridges. However, there are some studies concerning the damping of hurricane wave forces that can be applied to bridges in the tsunami-hazard zone.

Parvin and Ma (2001) presented experiments to utilize a combination of helical springs and fluid dampers to create an energy dissipation and an isolation device for bridges subject to seismic load, which may reduce tsunami induced effects on bridges. In the proposed model, they generated vertical springs at the bearing points of the supports and the bridge, and horizontal springs in the abutments and the bridge decks. In addition, nonlinear fluid dampers were added near the springs. The results showed that in terms of vertical direction, the bridge with spring supports was considerably more flexible. It was concluded that the response of acceleration in an isolated damped bridge model, specifically at the mid-span, was decreased by up to 75% compared to the non-isolated models. Consequently, the inertia forces caused by the acceleration response in the bridge structure decreased, which is the aim of a structural design. In addition, because of the flexibility of the spring bearings the damage due to the deflection gap between the span and the bearing was reduced. The flexibility of the model produced a higher amplitude displacement response than the models without springs. This function may dampen the lateral load of a tsunami wave in the bridges.

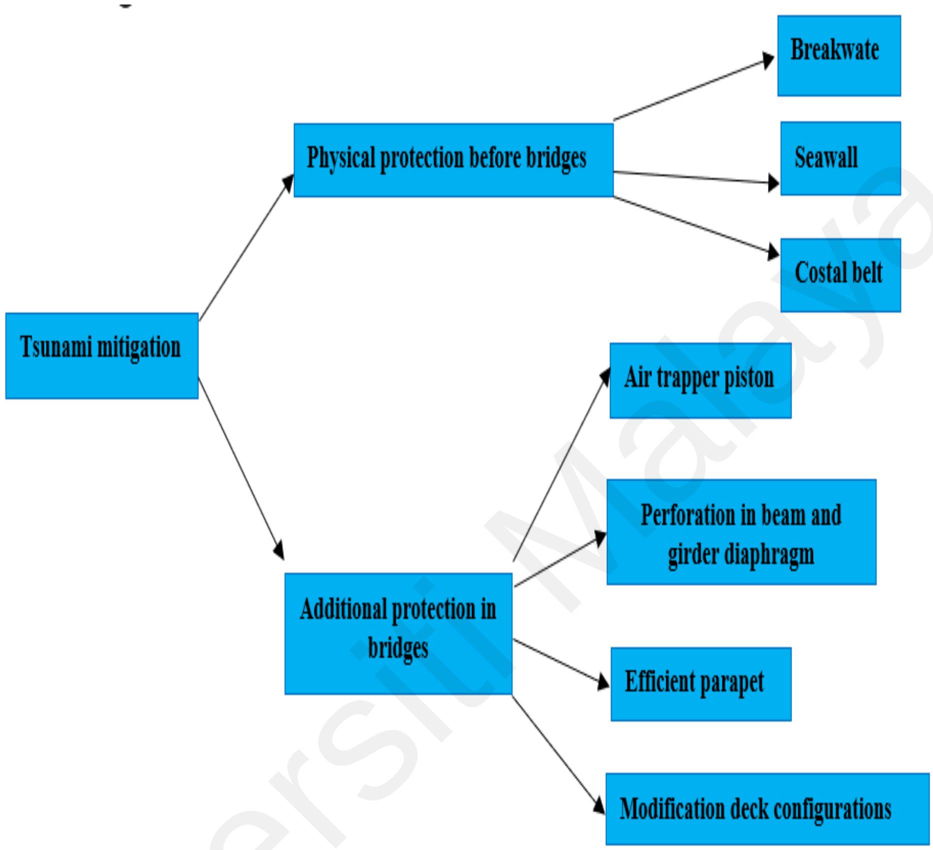

Figure 2.4: Summary of tsunami mitigation approach.

Schumacher et al. (2008), and, later, Bradner et al. (2010) Fang. Q et al. (2019) presented results of experiments on a large-scale model of a highway bridge superstructure subjected to the wave force of Hurricane Katrina. Two different bridge connections, i.e. rigid and flexible, with a spring placed horizontally between the bridge deck and the support, were used. The results indicated that the model with a flexible connection produced greater forces. This is contrary to the anticipated result of the flexible supports, which should produce lower forces. The results are shown in Figure 5. Henry (2011) presented two techniques for damping a wave load. In the first method, the deck support allowed horizontal and rotational movement, and, in the second model, venting holes were drilled in the girder diaphragms. The results showed that only the second method was effective and decreased the uplift force significantly. Takahashi et al. (1985) and Cuomo et al. (2009) indicated the effect of openings in the deck slab to reduce the uplift force. In addition, Klenzendorf (2007), Klenzendorf et al. (2010), and Lau et al. (2010) indicated in their experiments the effect of perforation in the parapet to decrease the horizontal load by wave action.

Iemura et al. (2005) presented three approaches as countermeasures to the effect of the tsunami on bridges. First, preventing the bridge from being washed away by limiting the movement of the deck and strengthening the piers. Second, reducing the drag force through modification of the bridge configuration on the deck and pier of the bridge, i.e. rounding the sharp edges of the deck so the parapet does not obstruct the flow during a tsunami wave. Third, reducing the impact force of debris by adding flexible devices to absorb and reduce the impact force of the debris.

Lukkunaprasit et al. (2008), and Lau et al. (2010) conducted experimental studies on the effect of perforated parapets on horizontal tsunami loads. Chung et al. (2003), and Liu and Chung (2003) indicated the possibility of applying perforations in beams. The experiments were carried out on a bridge model with 1/100 single scale columns and six I-girder decks with parapets. The wave flume length was 40 m with 1 m ×1 m cross section. They evaluated two types of parapet bridges; namely, solid and 60% perforated using a 1/100 scale bridge. The results showed that bridges with perforated parapets reduced the horizontal force by 17%. In addition, they stated that perforated parapets also significantly increased the time-history of the horizontal force. This is due to the smaller energy input to the bridge.

Klenzendorf (2007), and Klenzendorf et al. (2010), in their experiments on the effect of different parapets, stated that the T 101 parapet introduced by TxDOT (2005) had a better hydraulic performance than a solid parapet. This indicated that perforation decreased the horizontal effect of the tsunami wave. Triatmadja and Nurhasanah (2012) stated that the effect of openings is to decrease the tsunami horizontal loads. Triatmadja and Nurhasanah (2012), and Lau et al. (2010) indicated that the force reduction on a structure by openings is not linearly related to the percentage of the opening. Cuomo et al. (2009), stated that openings decreased the intensity of the impact pressure wave loads around coastal structures. Due to a contractive tendency of the wave surface, the characteristic of interaction of the tsunami wave and bore with the costal structure is affected by the shape and material of the structure Peregrine (1995).

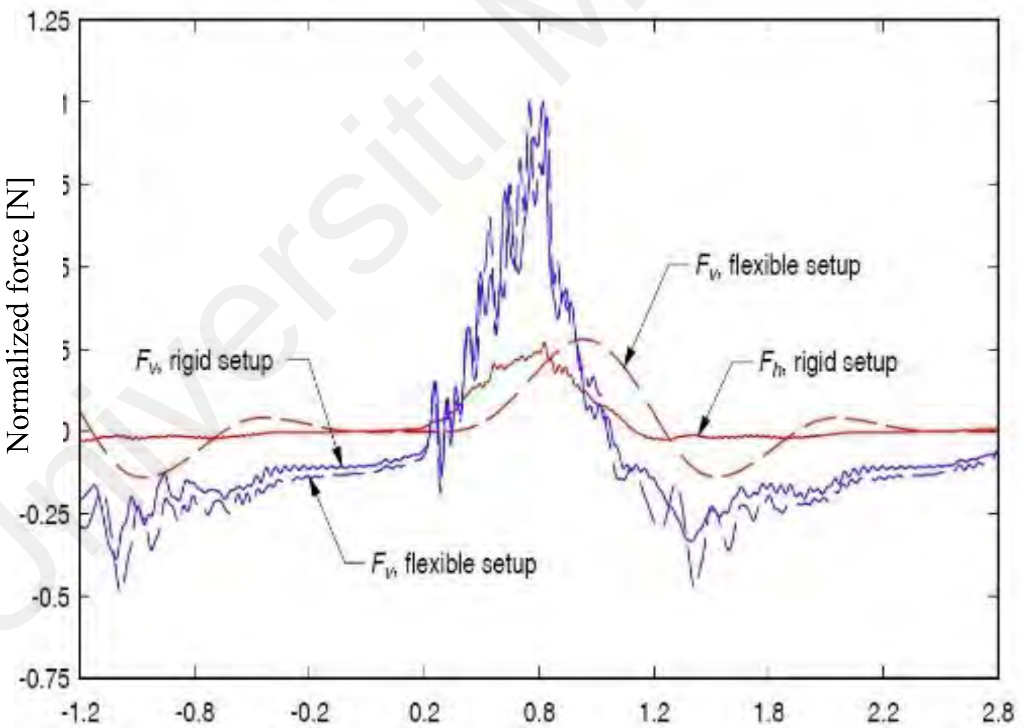

Figure 2.5: Comparison of Vertical (blue) and Horizontal (red) Forces With rigid and flexible connection Bradner et al. (2010)

Considering the wave forces involves the appropriate representation of the characteristics of the real fluid element Sarpkaya et al. (1981; Zienkiewicz and Bettess (1978).

Evaluating drag, uplift, impact forces and inertia requires accurate illustration of the fluid kinematics and dynamics mechanism and the coupling procedure between the appropriate motion of the fluid as well as the force on the models.

This can be determined in large physical models, where all the forces are scaled geometrically, facilitating extrapolation of the measured results to the prototype scale. This might be achieved with moderate to large-scale prototype models. Table 2.3 summarized the researches on tsunami effect on bridges.

Table 2.3: Research into tsunami effect on bridges

source	Methods							Wave Co			Mea. Fac.					B.M.C			L.D		Advantage	Disadvantage	Remarks
	Com. Sim.	Num. Meth	Soft.	Exp.	Mod. Sc.	Field Sur.	Sur. Meth.	Broken	Unbr.	just Br.	scale effect	Hori. load	Ver. load	Over Mo.	Drag Co.	S.T.B	D.B	Com. Br.	Eff. Pier	Eff. Deck			
S. C. Yim (2005)	Y	CSD, CFD,FSI	ANSYS, LS-DYNA, Star-CD	Y	N	N	N	N	N	N	N	Y	Y	N	N	N	N	N	N	Y	Brief discussion on tsunami effect on costal bridge	Lack of discussion on experimental and numerical works	Physical experimental facilities and comprehensive experimental studies in FSI and hydraulic loads.
Kataoka et al. (2006)	N	N	N	Y	1/18 to 1/108	N	N	Y	Y	Y	N	Y	Y	N	N	Y	N	Y	N	Y	Primary study in tsunami effect on bridge	Very thin piers assumed , no numerical result, and Froude number were not measured	Carried out the experiments to study the wave force action on cases breaking, non-breaking and broken on girder bridge
G Shoji and Mori (2006b)	N	N	N	Y	N	N	N	N	Y	N	N	Y	N	N	N	Y	N	N	N	Y	Initial study on effect of tsunami on bridge	Simplify the models as a box shape girder, and no pressure sensor	Initial study on effect of tsunami on bridge by the experimental test for evaluating bridge failure mechanism
Unjoh (2006)	N	N	N	N	N	Y	Dam. Inv.	Y	Y	Y	N	N	N	N	N	N	N	Y	Y	Y	Survet report after 2 months of tsunami on effected bridges	The author didn't evaluate his founding with experimental test	Damage investigation on bridges effected by the Sumatra islands tsunami
Shoji and Moriyama (2007)	N	N	N	N	N	Y	Frag. Eva.	N	N	N	N	N	N	N	N	Y	N	N	N	N	Research the wide variety of the failure bridge in tsunami	Neglect the structural characteristic of bridge in the tsunami	Fragility analysis of a bridge structure affected by the tsunami wave load
Sugimoto and Unjoh (2007)	N	N	N	Y	1/50, 1/25	N	N	N	Y	N	Y	Y	Y	N	N	Y	N	N	N	Y	Study on effect of uplift and drag force, on concrete and steel bridge, with the scale effect	Omit the effect of piers, the piles beneath the abutments, no numerical analysis.	Study with the hydraulic experiments to evaluate the failure mechanism of bridge Indian Ocean Tsunami

Table 2.3: Research into tsunami effect on bridges (continue)

source	Methods							Wave Co			Mea. Fac.					B.M.C			L.D		Advantage	Disadvantage	Remarks
	Com. Sim.	Num. Meth	Soft.	Exp.	Mod. Sc.	Field Sur.	Sur. Meth.	Broken	Unbr.	just Br.	scale effect	Hori. load	Ver. load	Over Mo.	Drag Co.	S.T.B	D.B	Com. Br.	Eff. Pier	Eff. Deck			
Iemura et al. (2007)	N	N	N	Y	1/77	N	N	N	N	N	N	Y	Y	N	Y	N	Y	Y	N	Y	Provide the experiments in a wave flume to study tsunami wave, debris and breakwaters in front on dry land bridges	Very thin piers in the models, no pressure sensor for impact load, lack of laboratory facility	Experiments in wave flume to study effect tsunami wave, debris and breakwaters in front on dry land bridges
Susumu Araki, Itoh, and Deguchi (2008)	N	N	N	Y	1/70	N	N	N	Y	N	N	Y	Y	N	N	N	Y	N	N	Y	Investigation in relation of impact force and the maximum in-line force	Lack of laboratory, no effect on piers	Experimental study on tsunami characteristics on beam of PC-girder bridges.
Shoji and Moriyama (2008)	N	N	N	Y	N. Ava.	N	N	N	Y	N	N	Y	Y	N	Y	Y	N	N	N	Y	Study on the variant of the deck height bridge on tsunami wave	Not applicable in the reality. Neglect the effect of piers.	Hydraulic experience of tsunami load effect on a bridge decks
Lukkunaprasit, Lau, Ruangrassamee, and Ohmachi (2008)	N	N	N	Y	1/100	N	N	Y	N	N	Y	Y	N	N	N	N	Y	Y	Y	Y	Used the complete pier and deck for experiments	Lack of validation of experimental result with computational simulation and applied a small scale.	Experimental study on the effectiveness of perforations in the girders and parapets of bridges in tsunami
Thusyanthan and Martinez (2008)	Y	N	N	Y	1/25	N	N	Y	N	N	Y	Y	N	N	N	Y	Y	Y	Y	Y	Measuring scale and use pier and deck in experiments	Small wave tank, lack of computer simulation, the bridge case study not exist	Study on impact pressure on bridge pier and deck
Lau et al. (2010)	N	N	N	Y	1/100	N	N	Y	N	N	Y	Y	N	N	N	N	Y	Y	Y	Y	Study to mitigation of tsunami effect on bridge	Neglect the effect perforation parapet on the uplift, overturning moment	Study on the effect of perforated 60% parapets on horizontal tsunami loads by experimental test
S. Araki, IshiN, and Deguchi (2010)	N	N	N	Y	N. Ava.	N	N	Y	N	Y	N	Y	Y	Y	N	Y	N	N	N	Y	Comparison of wave force between two cases of post-breaking and just-breaking on bridge	Neglect the scale effect and pier effect also lack of computational simulation	Investigate the effect of vertical and horizontal components of the Tsunami fluid pressure and force in a girder bridge

Table 2.3: Research into tsunami effect on bridges (continue)

source	Methods							Wave Co			Mea. Fac.					B.M.C			L.D		Advantage	Disadvantage	Remarks
	Com. Sim.	Num. Meth	Soft.	Exp.	Mod. Sc.	Field Sur.	Sur. Meth.	Broken	Unbr.	just Br.	scale effect	Hori. load	Ver. load	Over Mo.	Drag Co.	S.T.B	D.B	Com. Br.	Eff. Pier	Eff. Deck			
Kenji Kosa et al. (2010)	N	N	N	Y	1/50	N	N	Y	Y	N	N	Y	Y	N	N	Y	Y	N	N	Y	Comparison of horizontal and uplift force in the broken and unbroken wave, proposed an estimation equation	Omitted the effect of piers, lack of computational simulation	Experimental test to evaluate tsunami wave force on bridge in two case of broken and un-broken wave.
YOSHINRI SHIGIHARA and FUJIMA (2010)	N	N	N	N	N	Y	Koshimura	Y	N	N	N	Y	N	N	N	Y	N	Y	N	Y	Discussed on safety factor of effected bridge	Neglect the effect of uplift and overturning moment	Presented the numerical analysis to study the horizontal tsunami on three effected bridges by tsunami
Shoji et al. (2011)	N	N	N	Y	1/79 , 1/100	N	N	Y	N	N	N	Y	Y	N	Y	Y	N	N	N	Y	Applied the variations of the condition of a bridge deck against a tsunami bore on the variation of horizontal wave load	Omitted the effect of piers on experiments and lack of computational simulation	Study in the impact force in a case of breaker bores on the value of the drag coefficient in addition to the dependency
Panitan Lukkunaprasit and Lau (2011)	N	N	N	Y	1/100	N	N	Y	N	N	Y	Y	N	N	N	N	Y	Y	Y	Y	Evaluation of tsunami bore on the pier of the bridge and the effect of peers on tsunami load	Neglect the effect of tsunami bore on torsion, shear and overturning moment on piers, lack of numerical simulation	Experimental study on effect of the tsunami load in case of bore in a stand-alone pier and pier with deck
Murakami, Sakamoto, and Nnaka (2012)	Y	VOF	CADMAS-SURF/3D	N	1/50	N	N	N	N		Y	Y	Y	N	N	N	Y	N	N	Y	Consideration of horizontal and uplift forces, validate the numerical result with experimental results.	Lack of comparison to other researcher result	Investigate on a damaged bridge in tsunami by Tohoku earthquake in 2011
Shoji et al. (2012)	N	N	N	N	N	Y	S.L.F	Y	N	N	N	Y	Y	Y	N	Y	Y	N	N	Y	Survey report to find the inundation height	Omitted the evaluation result with experimental test	Determined the horizontal and vertical tsunami wave pressures by the formerly recommended experimental formulation with the simulated inundation heights.

Table 2.3: Research into tsunami effect on bridges (continue)

source	Methods							Wave Co			Mea. Fac.					B.M.C			L.D		Advantage	Disadvantage	Remarks
	Com. Sim.	Num. Meth	Soft.	Exp.	Mod. Sc.	Field Sur.	Sur. Meth.	Broken	Unbr.	just Br.	scale effect	Hori. load	Ver. load	Over Mo.	Drag Co.	S.T.B	D.B	Com. Br.	Eff. Pier	Eff. Deck			
BRICKER, KAWASHIMA, and NAKAYAMA (2012)	Y	CFD	Open FOAM	N	1	Y	N	Y	N	N	Y	Y	Y	N	N	Y	N	N	N	Y	Simulate the bridge in real size and variety of wave velocity	The mesh grid was not independence, omitted the effect of pier in the Utatsu highway	Computational fluid dynamics (CFD) methods to evaluate the effect of tsunami on the bridge in japan tsunami
Nakao, Nzaka, IzuN, and Kobayashi (2012)	N	N	N	Y	1/150	N	N	N	N	N	N	Y	Y	N	N	N	Y	N	N	Y	Used various configurations against tsunami attack	Neglect from scale of models, short length of the flume, of the models wasn't applicable in reality	Investigated on tsunami induced hydrodynamic forces applied to five various bridge sections
H. KasaN, J. Oka, J. Sakurai, N. Kodama, and T. Yoda (2012)	N	N	N	N	N	Y	N	Y	Y	Y	N	Y	Y	N	N	Y	Y	Y	Y	Y	Survey report on concrete and steel bridge also evaluated Fall-off prevention devices	Limited field of survey, this study can develop to the whole affected	Survey report to the bridges effect by tsunami wave in the Tohoku area and appropriate structural feature that mitigates the effect of the tsunami on the bridge
Kosa (2012)	N	N	N	N	N	Y	D.M.F.G.E	Y	N	N	N	Y	N	N	N	Y	Y	Y	N	Y	Field survey and calculate the velocity by the Google Earth's distance measurer	Lack of numerical analysis to evaluate Survey report result	Evaluation tsunami velocity in Utatsu Bridge and comparison of β ratio (ratio of superstructure of bridge resistance to the horizontal wave force) in effect bridges
Salem H. et al (2017)	Y	AEM	Open FOAM	N		Y	N	Y	Y	Y	Y	Y	Y	N	N	Y	N	N	Y	Y	The full scale of wave flume simulation, various wave condition	Lack of experimental and validation	The study of bridge strengthening showed that the collapse water speed could be increased based on the condition of the jacket

Table 2.3: Research into tsunami effect on bridges (continue)

source	Methods							Wave Co			Mea. Fac.					B.M.C			L.D		Advantage	Disadvantage	Remarks
	Com. Sim.	Num. Meth	Soft.	Exp.	Mod. Sc.	Field Sur.	Sur. Meth.	Broken	Unbr.	just Br.	scale effect	Hori. load	Ver. load	Over Mo.	Drag Co.	S.T.B	D.B	Com. Br.	Eff. Pier	Eff. Deck			
Xiao, S. C., (2019)	Y	Y	Open FOAM N	N	N	Y		Y	N	N	N	Y	N	N	N	Y	Y	Y	N	Y	Air trap evaluation and Air relief opening application	Small scale	Air relief opening could effectively reduce the vertical wave forces on bridge decks
Fang (2019)	Y	Y	N	N	N	Y		Y	N	N	N	Y	N	N	N	Y	Y	Y	N	Y	A full-bridge specimen, including superstructure, substructure, and neighboring segments, has applied	Lack of evaluation method with the experimental result	Assessment of wave overtopping and pressure distribution.
Moideen (2019)	Y	CFD	N	N	N	Y		Y	N	N	N	Y	N	N	N	Y	Y	Y	N	Y	A parametric study for increasing wave heights, girders spacing, and depth for varying airgaps is investigated	Lack of validation method with the experiments	Numerical evaluation of solitary wave on bridge models
Mazinani I. et al. (2021)	Y	FSI	LS Dyna	N	N	Y		Y		N	N	Y	N	N	N	Y	Y	Y	N	Y	Evaluation of various wave heights and water depths on tsunami forces	A limited type of bridge models	Investigation on the effect of wave height of tsunami force and full-scale numerical modeling

Abbreviation, the wave Condition in the experiments: Wave Co., measuring factor in the experiments: Mea. Fac., bridge model condition in the experiments: B.M.C, load evaluation in the bridge model: L.D, Tsunami effect on bridge. Computer Simulation: Com. Sim., Numerical method: Num. Meth, Software: Sof., Experimental: Exp., Model Scale: Model Scale. Survey report: Filed Sur. Survey method: Sur. Meth. Broken: Br., Unbroken: Unbr. Horizontal load: Hor. Load, Vertical Load: Ver. Load, Overturning moment: Over. Mo. Drag Coefficient: Drag Co. Still water bed: S.T.B, Dry bed: D.B, Complete Bridge: Com. Br., Effect of pier: Eff. Pier, Effect of deck: Eff. Deck. Not available. Ava, Damage investigation: Dam. Inv. Fragility evaluation: Frag. Eva. , Method: Meth, staggered leap frog: S.L.F, Distance measuring function of Google Earth for : D.M.F.G.E

2.7 Conclusion

After the two recent huge tsunami disasters – Sumatra Island in 2004 and North East Japan in 2011 – numerical and experimental investigations of the effects of tsunami loads on structures and the mitigation of tsunami disasters have created a new research impetus in civil, coastal and mechanical engineering. The investigation of bridge structures on the effects of tsunamis only started from 2004 onwards. Unfortunately, there are limited studies on the effects of tsunamis on bridges. However, due to the high risk of tsunamis on the coastline and the importance of bridges to deliver the emergency and recovery services to the injured and affected people this field of research should be quickly developed. Regardless of the international building codes with improved structural systems and tsunami warning mechanisms, the recent tsunami in North East Japan in 2011 caused extraordinary destruction with thousands of fatalities and more than $300 billion in economic losses. This kind of disaster indicates the significance of research on the effect of tsunamis on structures, and, especially, for important structures, such as bridges. The challenge is to design a bridge that is able to withstand the impact of such a disaster in a scientific and economical manner. However, theoretical and experimental approaches to evaluate the tsunami wave load and tsunami mitigation in various cases of tsunami waves on bridges cannot be applied simply due to the complexities of wave propagation along the shores and coastlines coupled with fluid-structure interactions. This paper categorizes the tsunami wave into four types of solitary wave that may act on a bridge: breaking, non-breaking, just breaking and a combination of these cases. The location of the prototype bridge in experiments is categorized into the dry bed (inland) and seabed (coastal) bridges. In addition, some of the major challenging effects of tsunamis on bridges that are described are based on the literature. The discussion is based on the comparison of international building codes, and the tsunami force on structures including breaking wave forces, hydrodynamic force, buoyant force, hydrostatic force, surge force, impact force, and design flood velocity. The effects of tsunamis were analyzed and classified, and challenging mitigation techniques have been proposed. The experimental values of drag coefficients were discussed and compared with the values suggested by the international building codes. The survey indicated that although there have been several academic and industrial investigations of tsunami effects on bridges, there are no comprehensive studies yet that cover all cases of tsunami waves and possible bridge locations with complete pier and deck models. All of the previous studies only focused on the effects of tsunamis on girder bridges while other types of bridge were surprisingly omitted. The effect of tsunamis on the piers of bridges and roll-on-roll-off pier configurations in tsunami loads was also excluded. The mitigation approach concerning the effect of tsunamis on bridges was analyzed and classified. According to the type of mitigation function, it was categorized as physical protection before bridges and additional protection in bridges. Discussion on some of the protection methods to mitigate tsunami forces on bridges has been presented.

Finally, investigation guidelines associated with the rapidly expanding tsunami research in the field of bridge structure are opening new areas of study with the possibility for innovation. Developing the aforementioned knowledge gaps can mitigate the effect of tsunamis and save human lives and property. Table 2 classified the previous research on tsunami acting on bridges.

CHAPTER 3: MATERIAL AND METHODS

This study includes experiments in the Coastal & Offshore Laboratory of University Technology Petronas and computational and numerical modelling with a supercomputer to validate the experimental study.

3.1 Experimental Procedure

A wave flume was used to obtain the time histories of tsunami bore forces on a bridge model over still water subjected to tsunami loading. The experimental study was carried out in the Coastal & Offshore Laboratory of University Technology Petronas (UTP).

In the first phase, the bridge models were used to evaluate and determine the scaling considerations for formulating the experimental process. Therefore, bridge models were designed and manufactured to represent a bridge prototype. The bed slope was designed and was constructed in the flume. The model was installed in bed slope in the flume. The data after calibration of the instrument were recorded. For obtaining the appropriate and accurate result, calibration was performed in the experiment. Data loggers recorded signals from instruments i.e. load cells, velocity-meters and Optitrack. In addition, to ensure the appropriate functioning of all instruments during the experiments, recalibration was performed. The signal processing was carried out to generate the demanded outcome regarding time histories of forces on bridges.

3.1.1 Model-Prototype Relation

Generally, physical models in hydraulic engineering are utilized to evaluate the fluid flow experienced under operated laboratory circumstances. Appropriate modelling to generate modelling relationships in hydraulic similitude between the prototype and physical model should be applied. The prototype is the full-sized purpose model. A perquisite for comprehensive similarity is achieved when the model is geometrically equivalent to prototype. Similitude is conducted by utilizing dimensional evaluation to assure that specific dimension details are equivalent in the behavior of both the prototype and model.

The Froude number in the hydraulic flow states the relation between influence of internal and gravity forces as illustrated in Equation 3. 1,

$$\sqrt{\frac{inertial\ force}{gravity\ force}} = \sqrt{\frac{\rho L^2 V^2}{\rho L^3 g}} = \frac{V}{\sqrt{gL}} \tag{3.1}$$

where ρ is fluid density, L is length, V is velocity and g is the gravitational acceleration. In the scenario of tsunami wave, Hughes (1993) and Lau (2009) stated that where inertial and gravitational forces are dominant the Froude number of the model and prototype should be equivalent. On the other hand, regarding the high Reynolds number of tsunami flow that is higher that $1 * 10^4$ in the laboratory and field observed (Chanson et al. 2002), the flow is considered turbulent. Consequently, the viscous forces considered independent of Reynolds number and the effects of flow, viscosity in the bridge models might be ignored (Lau, 2009). The similitude ratio between model and prototype that applied with Chanson et al. (2002), Robertson et al. (2008) and Lau (2009) in this research utilized with 1:40 linear scale and illustrated in Table 3.1.

Table 3.1: Similitude ratio for Model and prototype

Characteristic	Dimension	Scale
Length	L	1:40
Area	L^2	$A_r= L^2 =1:1600$
Volume	L^3	$V_r= L^3 =1:64000$
Flow	L^3/T	$Q_r=L_r^{5/2}=1:10120$
Time	T	$T_r=L_r^{1/2}=1:6.33$
Velocity	L/T	$V_r=L_r/T_r=1:6.33$
Force	F	$F_r= L^3=1: 64000$
Pressure	F/L^2	$P_r=L_r=1:40$

Abbreviation, A_r: area scale, V_r: Volume scale, Q_r: Flow scale, L_r: Length scale, T_r: Time scale, F_r : Force scale, P_r :Pressure scale.

3.1.2 Wave Flume and Wave Generation System

A wave flume with a pedal wave generator was used to create a solitary wave in the flume with wave break at the platform in shallow water. The experimental process was carried out in the Coastal & Offshore Laboratory of University Technology Petronas (UTP).

3.1.2.1 Wave flume

A flume with dimension 24m long, 150cm wide and 200cm deep was used for the experimental study. Bottom and both sides of the wave flume were constructed by utilizing the reinforced concrete. To enable observations from the sides, the sidewalls of the tank is made of six Plexiglas panels embedded in the wall of the flume. Figure 3.1 illustrates the entire structure of the wave tank in UTP laboratory.

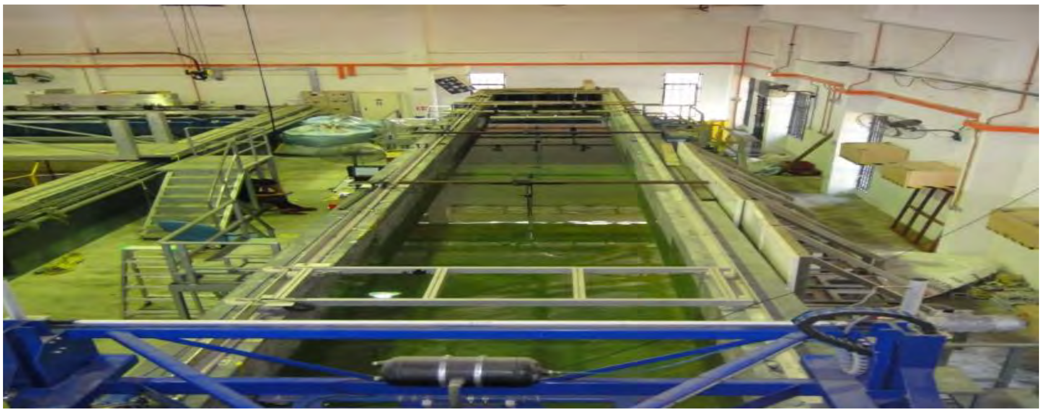

Figure 3.1: UTP wave flume

3.1.2.2 Wave generator

The wave generator on the right side of the flume is a wave paddle type that is driven by an electric motor and controlled by a computer. The wave generator was designed and fabricated by Edinburgh Design Ltd, UK. The computer controls the wave heights and initial water depths. The computer automatically performs calculations and determines the necessary force to push the wave-making board by utilizing ocean and wave software supplied by Edinburgh Design Limited. The wave paddle as illustrated in Figure 3.2 was manufactured from anti-corrosive materials, which is prepared to absorb re-reflected waves.

Figure 3.2: Wave generator

To produce the desired solitary wave height in the wave flume, signals coded should process with WAVE computation software in varying water depth. This function focuses the energy of the wave-set by manipulating the starting phases of each front and create a solitary wave. The start phases of all the fronts in a wave can be set such that the fronts will have an equal phase at a particular time and location in the tank, which can be used for special effects and tank demonstrations. The start phase of each front obtains from Equation 3. 2;

$$(k\ (x \cos\theta + y \sin\theta) - 2\pi ft + \phi) \bmod 2\pi \tag{3.2}$$

where k is the number of the front in water at the depth of the current wave-generator and θ is the angle of the front, x is the X coordinate of the focused event, y is the Y co-ordinate of the focused event, time of the focused event is ft and phase of the focused event is ϕ.

With a constant volume of water, different paddle speeds of the wave generator generate different wave heights for the same water volume. The single solitary wave was formed after the wave generator in the location of H1 (refer to Figure 3.16) as illustrated in Figure 3.3a. Then the solitary wave moved towards the bridge. On reaching the first slope, the wave changed to almost a vertical wave and broke in the second slope in the still water as a breaking wave. Then the solitary wave changes to a bore in the shallow water. This turbulent bore moved forward and attacked the bridge.

Figure 3.3a shows a tsunami bore in the flume. The bore then flowed over the platform and contacted the wave absorber at the end of the flume as illustrated in Figure 3.16.

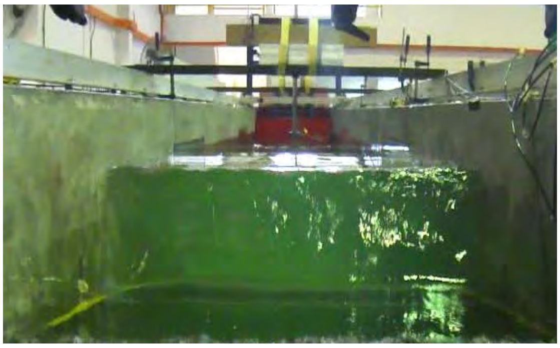

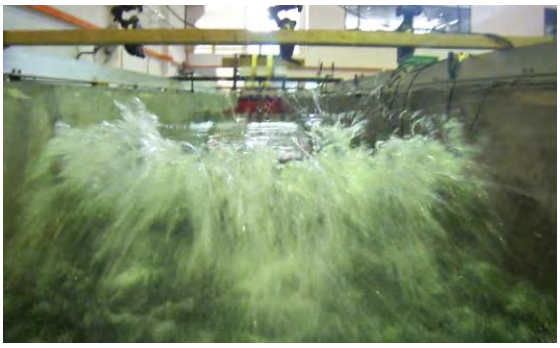

(a) (b)

Figure 3.3: Solitary tsunami wave in the flume, (a) Tsunami wave in the UTP flume 0.4 second before breaking, (b) Broken tsunami wave.

3.1.2.3 Wave Absorber

The wave absorber device improves the accuracy of the experimental test in the flume due to minimizing wave reflections to the bridge model. The wave absorber utilized at the end of wave flume absorbs the remaining turbulence bore energy from the incident bore produced by the wave generator. The wave absorber is fabricated from absorbent material that absorbs about 90% of incident wave energy. Figure 3.4 shows the wave absorber in the flume to avoid any reflection on reading.

Figure 3.4: Wave absorber at the end of wave flume

3.1.3 Target Bridge Prototype

The first bridge model, Model A is an approximate laboratory model of the approach bridge of the Second Penang Bridge that is indicated in Figure 3.5: Second Penang Bridge. This bridge is the Box Girder Bridge type and reinforced concrete that is typically employed in Southeast Asia and around India Ocean. The bridge deck is mounted on damping rubber bearing. The approach span of the bridge is 55 m, the deck width is 14.5 m, and 3.5 m is the height of the deck. Other types of bridges have the same width and span of this bridge. The expected tsunami wave height in and around Indian Ocean is 4-20 meters.

Figure 3.5: Second Penang Bridge

3.1.3.1 Bridge Models

Four types of scale bridge models including superstructure and piers were tested in the experiments and numerical procedure. The superstructure and pier models were all constructed from reinforce concrete and included Box Girder Bridge (Model A), Spread Box Beam Bridge (Model B), Steel Girder Box Bridge (Model C), Box Beam Bridge (Model D). Model F is the Box Girder Bridge that is combined with baffle plate to reduce tsunami wave. The deck and piers of Model B, C, and D are constructed from reinforced concrete and girders from steel. All models are constructed from scale 1:40. All models are constructed with similar span, width of deck and deck height from still water and ground levels. Models consist of two piers with 1.375 distances. The details of bridge models are described in the following section. A stainless plate with 135 mm diameter (similar to the diameter of load cell) in Models is connected to the bar of piers before casting to pre-form a rigid connection between piers and 6 axis load cell. The plate is illustrated in Figure 3.6. The base plate includes two steel plates with 0.18 m length and 0.18 width that hinged at one side and on the other side 3 long bolts with 0.30 m length and 10 mm diameter cross the base plate to create a flat level according to the angle of platform. The angle of the base plate is adjusted with bolts on top and bottom of base plate as indicated in Figure 3.6.

Figure 3.6: Plate and base plate in set up

(a) Model A

The model A is 1/40 scaled and includes pier and deck of the approach bridge of the Second Penang Bridge. This bridge is the Box Girder Bridge type. The deck and box girder of the bridge model was constructed of reinforced concrete. The span is ls = 1.375 m, the deck width is 0.36 m and total height is 0.273 m (refer to Figure 3.7). As illustrated in Figure 3.6, the piers are bolted to the superstructure on top and to the base plate at the bottom. This plate connects to the 6 axis load cell with 3 bolts.

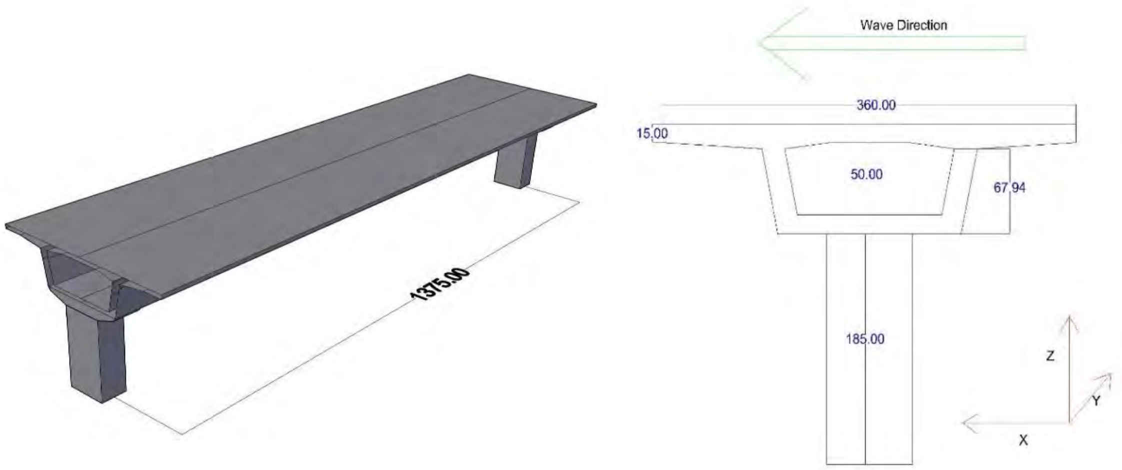

Figure 3.7: Bridge model dimensions

As illustrated in Figure 3.7, the piers are bolted to the superstructure on top and to the load cell at the bottom.

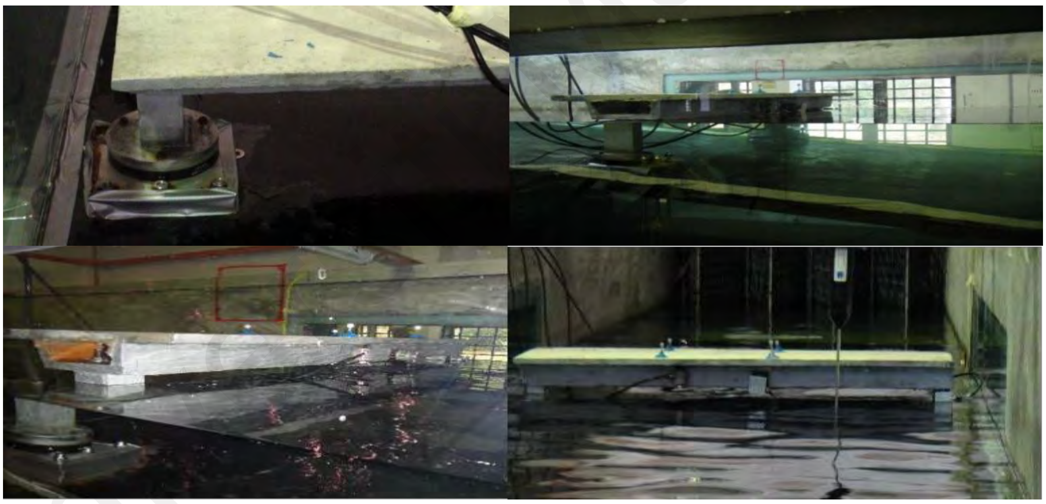

Figure 3.8: Model dimensions and location in the flume

(b) Model B

The model B was a model of a typical steel plate girder bridge with a concrete deck. The dimensions of the model scale to 1:40 as given in Figure 8. In this model, 3 to 6 girder beams are applied. The distance of the girder to the edge of the deck is kept constant in a variety of Girder Bridges. The distance between girders in three girders (Model B3) is 144.10 mm, in four girders (Model B4) is 95.0 mm, in the model with five girders (Model

5B) is 70.45 mm and in 6 girders (Model 6B) is 55.72 mm as indicated in Figure 3.9. All beams are fixed with two bolts with 90 cm distance from each other and 20 cm distance from edge as shown in the Figure 3.18.

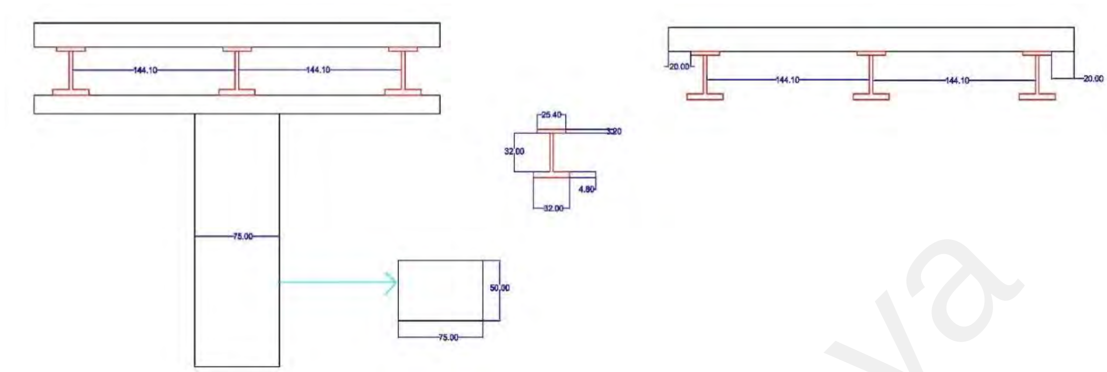

Model B3

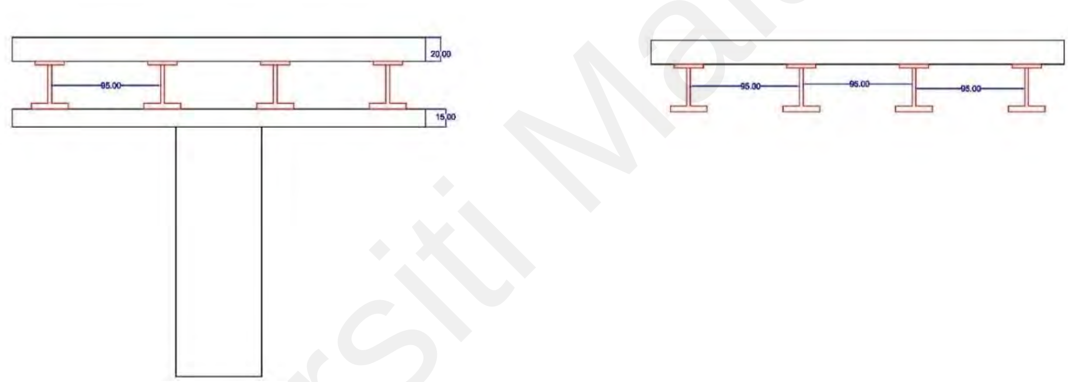

Model B4

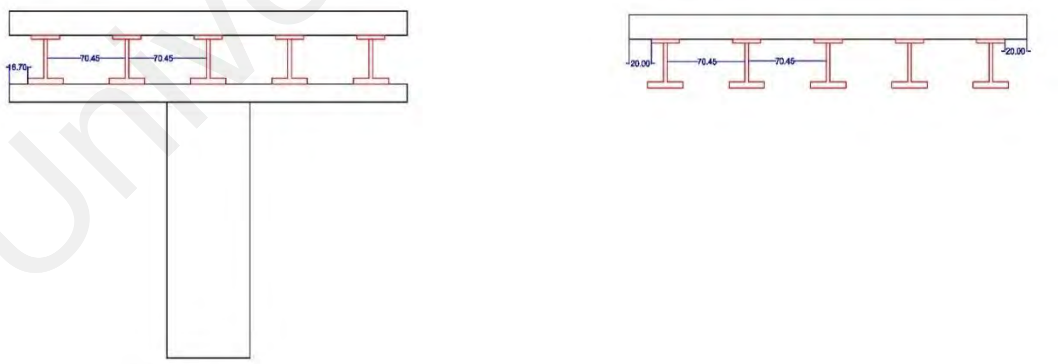

Model B5

Figure 3.9: Gird bridge dimension in Model B3-B6

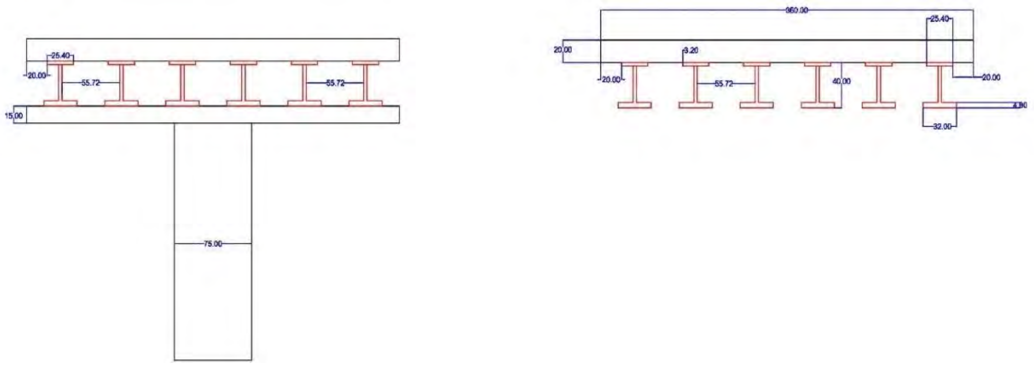

Model B6

Figure 3.9: Gird bridge dimension in Model B3-B6 (continue)

The deck in this research, being identical to Bridge Model B, meant that only the girders needed to be changed on the Model B to create model Bridge Model C. The same comment is applicable to Model D and E. All concrete decks and piers are casted in the wooden mould.

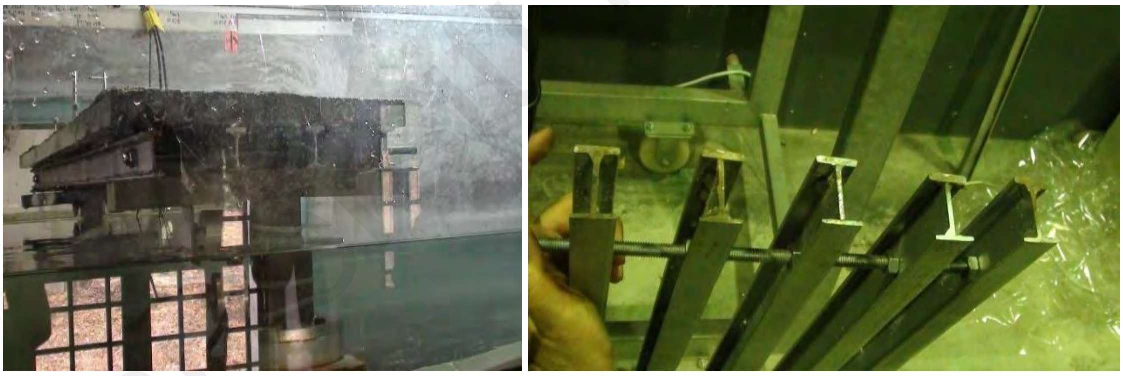

Figure 3.10: Girder bridge model installed in Flume

(c) Model C

The bridge Model C was a model of a typical spread box beam with concrete deck. The dimensions of the bridge model and beam are constructed to a scale Lr = 40. The dimensions are illustrated in Figure 3.11. Similar to Model B, three to six beams have been applied in this research. The beam distance is 112.00 mm, 64 mm, 40 mm and 25.5

mm utilized in three to six beams, respectively. In Figure 3.11 is shown the Model C6 in the flume.

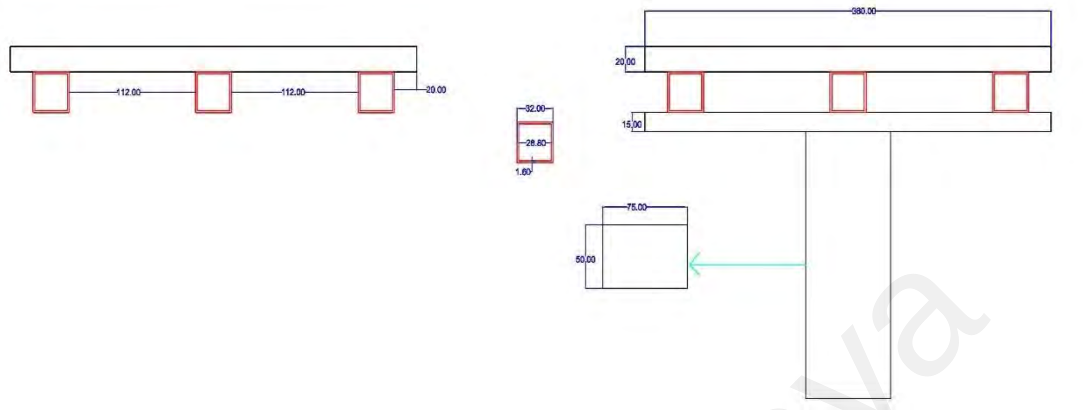

Model C3

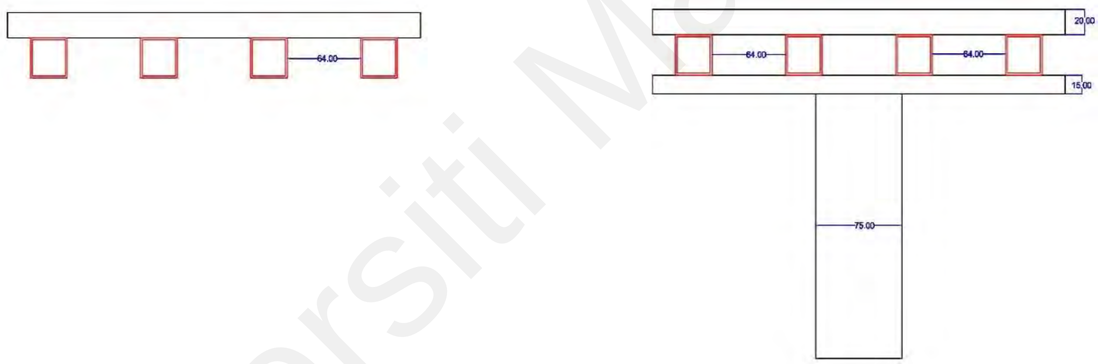

Model C4

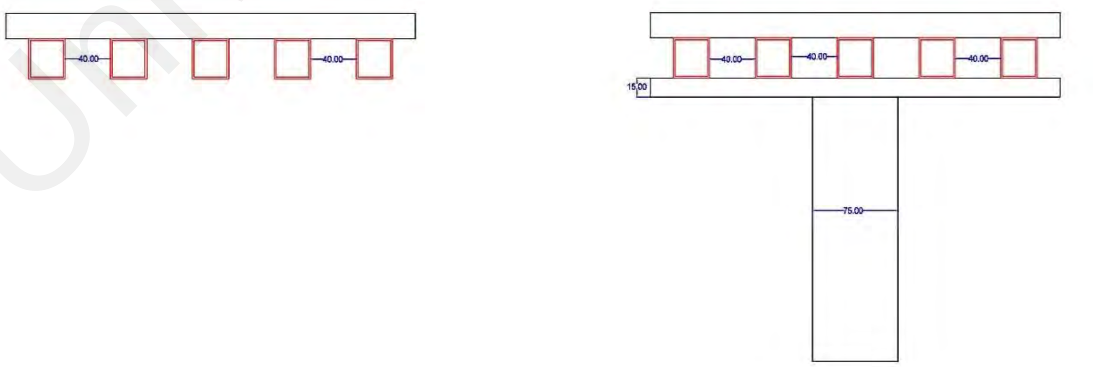

Model C5

Figure 3.11: Dimension of Model C3-Model C6

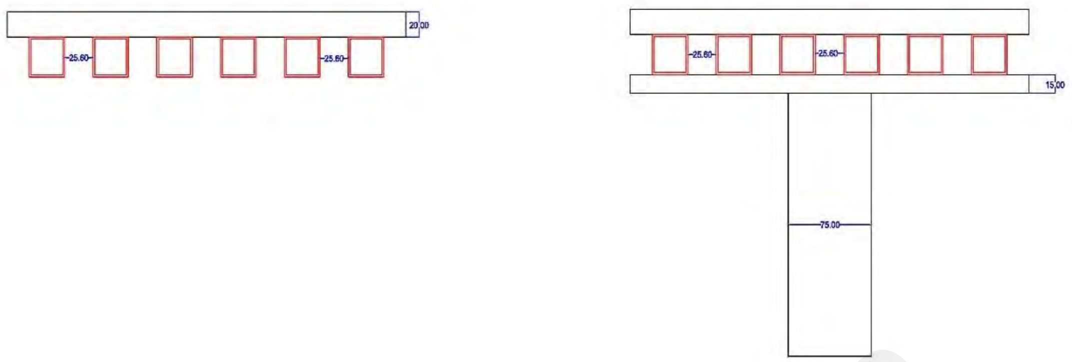

Model C6

Figure 3.11: Dimension of Model C3-Model C6 (continue)

Figure 3.12: Model C6 installed in the flume

(d) Model F

In Model F1-Model F4, baffle plate has been utilized to evaluate the effect of this device as a countermeasure of tsunami loads on model A. The dimension of the model is similar to model A and dimension of baffle plate is indicated in Figure 3.13.

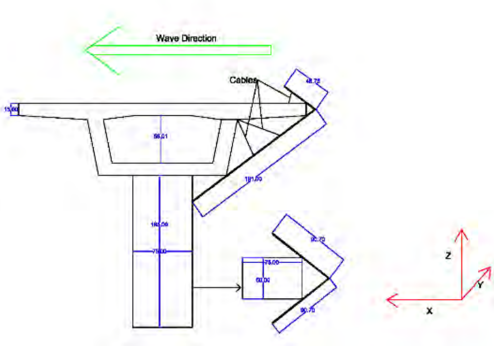

Model F1

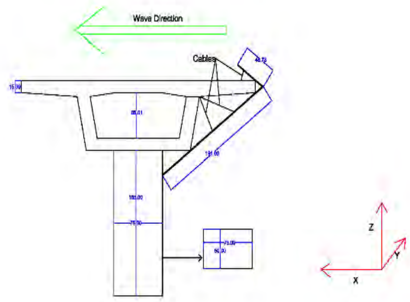

Model F2

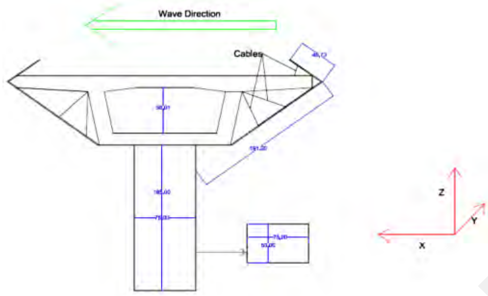

Model F3

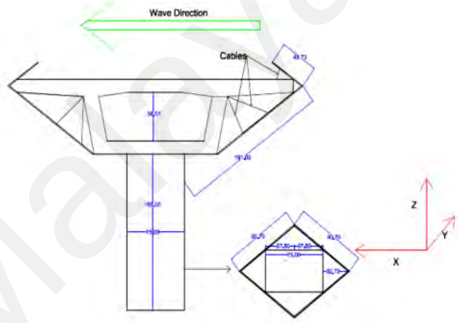

Model F4

Figure 3.13: Dimension of Model F1-F4

3.1.4 Platform

As illustrated in Figure 3.14, the platform was designed to characterize the beach profile at the location of the bridge model. Six piers were applied in order to create a rigid slop. All piers are adjustable in height except the last piers at the end of platform. These two piers hinged to the platform to support the slope. All piers were fixed to the concrete floor of the flume with four bolts. In order to limit the resonance of platform, four sets of cable were applied to connect the plates to the floor. Four different beach slopes were applied in this research to evaluate the effect of various beach slope on coastal bridge. The platform set up is indicated in Figure 3.15. Table 3.1 illustrated all employed angles in first and second slope in this research. The PB2 slope was performed to characterize the beach profile at the location of the Penang approach bridge. The first short steep slope rise with 32% presented the embankment on the proposed beach with a length of 2.2 m and second slope raised gently with 7 % representing the beach slope. The other beach profile was utilized to evaluate the effect of variable slope on tsunami wave. In Figure 3.14 is shown the employed adjustable pier and platform in the flume.

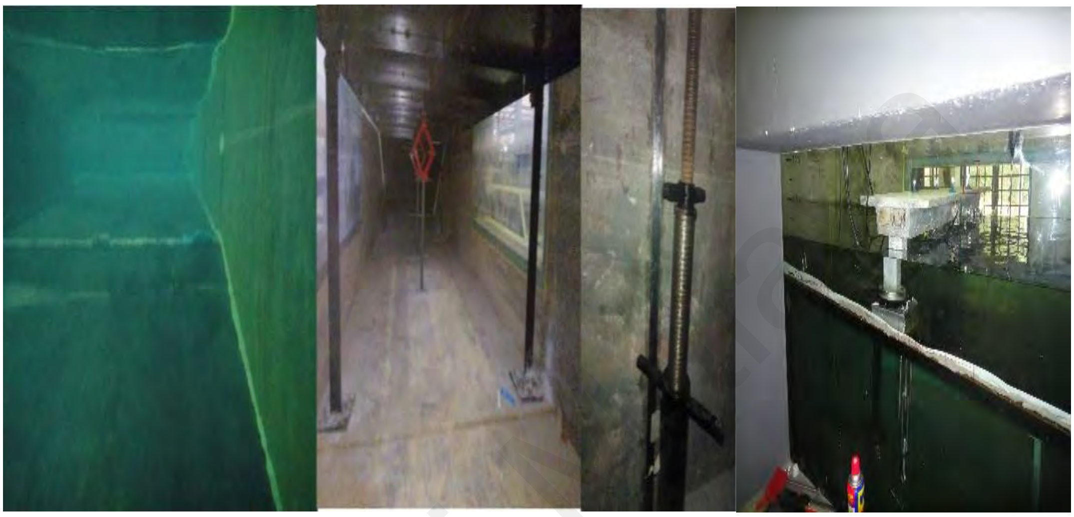

Figure 3.14: Platform instalation and adjustable piers in the flume

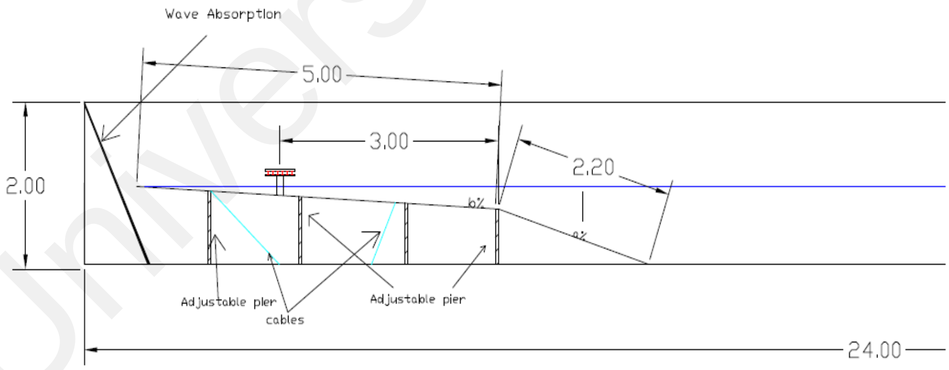

Figure 3.15: Platform set up

3.1.5 Instrument

The experiments, wave probes, load cells, Optitrack system schematic, data logger and data acquisition system were utilized. The detail of all these instruments are explained in the following section.

3.1.5.1 Wave Probes

Wave probes were applied in this research to evaluate the incident wave heights, transmitted wave height and water level at various locations in the flume. Six wave probes were utilized in the experiments. The wave probes include two parts i.e. bottom and top parts. The bottom part includes two vertical electrode rods in stainless steel with 1.8 mm diameter that are perpendicular to the direction of wave in the flume. While the wave probe is submerged in fluid, the stainless steel electrode determined the conductivity of the immediate fluid volume. The conductivity of electrode rods relatively influenced the variation of the water volume in the flume. Consequently, in order to obtain a complete coverage of the highest wave height created by the wave generator in the flume, it is significant to assure that the stainless steel rods are submerged sufficiently into the water. The accuracy of these wave probes are ± 0.1mm. Chakrabarti (1994) stated that the advantage of this type of wave probe is that it is independent of the wetness and water splashing on the measuring probe. The wave probe distance between H1-H3 are 1.7 m and between H4-H6 are 1.8 m. The location of wave probes are indicated in Figure 3.16.

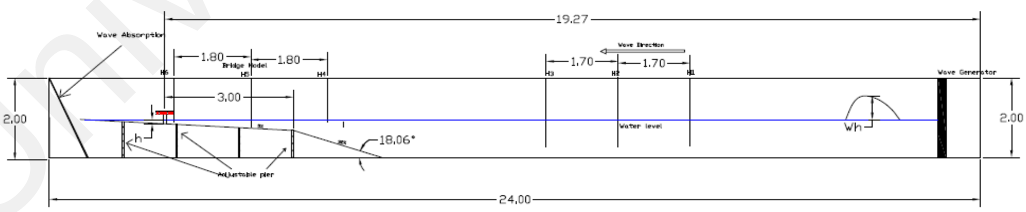

Figure 3.16: Side view of laboratory set up and wave probes location

For calibration purposes, all wave probes are connected to caliper. Wave probes are installed on top of the wall of wave flume and in the middle width of the flume through a transverse metal bar fixed to the rigid wood beam. Figure 3.17 illustrated the wave probe in the flume.

All of the wave probes connected into the signal processing system for the purpose of a data recording process. The static calibration of all the wave probes was properly carried out before running each set of experiments. The probes should be recalibrated quickly to manage the variety of water conductivity in a long series of experiments because of the change in water temperature.

Figure 3.17: Wave probes in the flume

Before performing the calibration, for 2 to 3 minutes time wave generator generated a wave to obtain a good combination of fluid and to verify water conductivity was uniform in all parts of the flume. The surface of metal rod in the wave probes was cleaned by using a soft towel before the calibration. The calibration process of wave probe in the flume was performed while the water was completely still. The probes were changed via a specified length to each other because the calipers were installed onto every wave probe such as indicators. Their voltage output presented zero in still water level, then all the wave probes were counterbalanced with zero value in their position. In order to obtain the required voltage, the “Gain” dial for all probes on the signal processing box was modified. A default gain of 0.4 volts/cm was employed for all the probes in order to obtain a standard calibration. All wave probes were subsequently moved back to their original location due to the fulfilment of the calibration process. Note that in reference to the highest wave height, which is 420 mm, the location of wave probes was appropriate and there was certainly no chance that the wave probe system clipped the wave height.

3.1.5.2 Load Cells

Two types of load cell were applied in this research, a six axis load cell (Figure 3.19) and 4 axis load cell (Figure 3.20). The six axis load cells were made from stainless steel and standard protection of IP68 that provide waterproof load cell and can be used up to 10m underwater. Six axis load cells were connected to the base plate to measure the horizontal, vertical and overturning moment at the piers of the bridge. The load cell is Sunrise M3716A with D=135MM and capacity FX, FY(N)= 400, FZ (N)=800, MX, MY (Nm)=40.00) MZ (Nm)=40.00 with sampling rate 1000 Hz. The typical nonlinearity and hysteresis is less than 0.5%, crosstalk less than 2% and the overload capacity is 300%. The axis load cell connects to the base plate of pier on top. The load cell at the bottom is connected to a hinge plate to the alignment of bridge model in the slope of platform and provided a level. Figure 3.18 illustrated adjustable base plate in the flume.

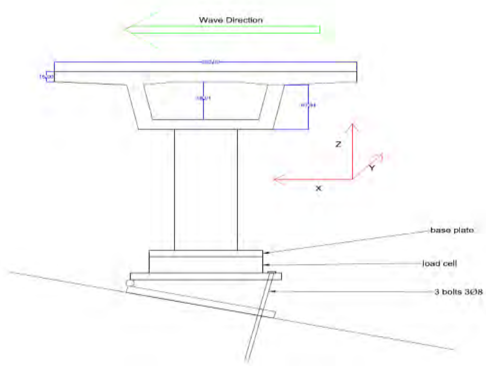

Figure 3.18: Adjustable base plate

The output data obtained from load cell include six channels. Channel 1 is Fx, channel 2 is Fy, channel 3 is FZ, channel 4 Mx, channel 5 is My, channel 6 is Mz. In order to calibrate, the six axis loads can be decoupled in three steps as follows:

Step 1: Obtain the raw data of Channels 1 through 6 into the Volt

[RAW] = (rawchn1, rawchn2, rawchn3, rawchn4, rawchn5, rawchn6)ty,

where rawchn1, rawchn2, rawchn3, rawchn4, rawchn5 and raw chn6 are in V.

Step 2: Convert the raw data into mv/V, assume the raw data output in Volt, Excitation voltage = EXC, Amplifier gain = GAIN

[DAT] = (chn1, chn2, chn3, chn4, chn5, chn6) *1000 / (EXC*GAIN),

where chn1, chn2, chn3, chn4, chn5 and chn6 are in mv/V.

Step 3: To calculate decoupled loads

[RESULT]T = [DECOUPLED]*[DAT]T

where [RESULT] = (FX,FY,FZ,MX,MY,MZ). Force Unit: N. Moment Unit: Nm

[DECOUPLED] is the below decoupled matrix.

Table 3.2: Decouple matrix

Decouple matrix					
- 5.26023	-0.82822	-7.26005	-282.603	- 4.48842	284.0116
- 3.99885	-329.1	-2.06366	161.63	- 7.02214	164.6179
- 896.259	-6.78126	-895.948	4.17719	-917.07	0.759944
0.03227	-0.01827	48.71672	-0.19332	- 49.6353	0.13131
- 57.1442	-0.42225	27.22186	0.13688	27.5172	-0.14478
0.33726	19.16262	0.17452	19.20376	- 0.30048	19.36831

Figure 3.19: Six-axis load cell installed in the flume

In this research, three channel was utilized. Table 3.3 indicated the output parameters.

Table 3.3: Output parameters

Output	Parameters description	Parameters characterization
Outputs	Fy	Uplift
	Fz	Drag Force
	Mx	Overturning Moment

Four axial load cells product from DDEN with 250N capacity were also utilized in this research. The protection rate of these load cells is IP67 that protected against water ingress. Thus, they are not ideal for very deep immersion in water. Two load cells were installed on the piers (P1, P2). Cell P1 covered 50% of pier height from bottom to the middle of the pier and cell P2 covered from middle to top of pier height. Figure 3.20 shows the location of P1 and P2. Two more load cells (P3, P4) were installed on the deck as seen in Figure 3.20. The load cells required the test models to be free to move at slight displacements in response to wave actions, without any restraint from adjacent objects.

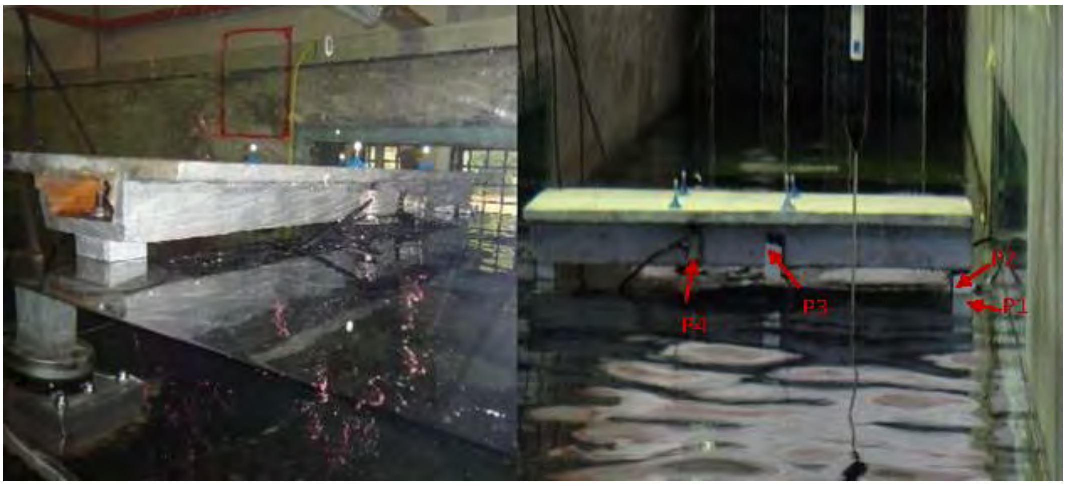

Figure 3.20: Axis load cells installation

In order to prevent changing the proposed bridge configuration in the experiment of load cell P1-P4 all data were measured in two phases. In phase 1, load cells P1-P4 were removed from model to measure the force in the 6 axis load cell and in phase 2 we installed them to the bridge model to measure the axial load acting by tsunami wave. All force data were measured with 1000 Hz sampling rate measurements computerized in the data acquisition system. As measured by Seiffert et al. (2014) in a similar experiment, the maximum and minimum force occur approximately in the range of 1 to 2 seconds and 1000 Hz sampling rate shows 1000-2000 samples per force event. Consequently, this sampling rate adequately illustrated the peak forces.

3.1.5.3 Optical Tracking System (Optitrack)

The hydrodynamic motion of the model during the test was measured by utilizing an Optical Tracking System (Optitrack) that attached at the top of the wave flume. Detecting all 6 degrees of the displacement of the model directly during the experiments is the main advantage of utilizing this device. The displacement of the bridge model may be determined by the camera at flume through the reflection of four balls fixed at the surface of the bridge. Figure 3. 21 illustrated the Optitrack system in the flume. Note that in this test three different cameras are used and all the data from all the cameras will be used and analyzed.

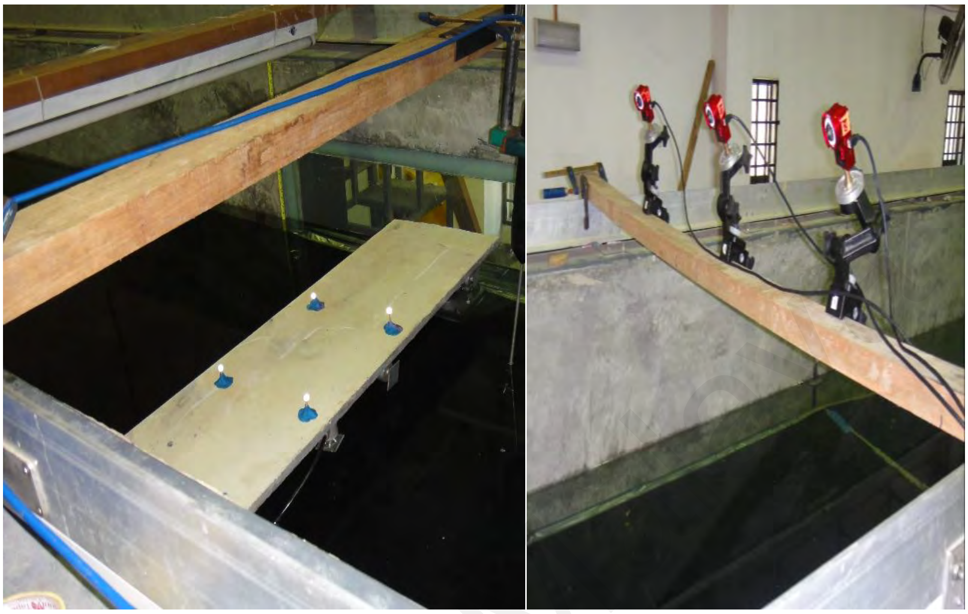

(a) (b)

Figure 3. 21: Optical Tracking System (a) reflective balls, (b) camera

3.1.5.4 Data Acquisition System

The data acquisition system applied in this research includes two sections, *i.e.* data logging hardware and data acquisition software. The details of both sections are provided in the following sections.

(a) Data Logger

The wave paddle, OPTITRACK, wave probes and load cells are connected to a data logger named Smart Dynamic Strain Recorder as illustrated in Figure 3.22. The data logger will then transmit all the required data, which is strained, DC voltage and thermocouples to a computer for further analysis. The frequency response of this logger is 10kHz and sampling speed to 200kHz at the fastest. In addition to numerical monitor and wave form display, dynamically variable amount can be displayed in analog form and in real time. At the time of measurement, measured data are automatically stored on a compact flash card up to 2GB. The hardware is compatible with most of the data acquisition software available in the market, including the WAVELAB data acquisition and processing software.

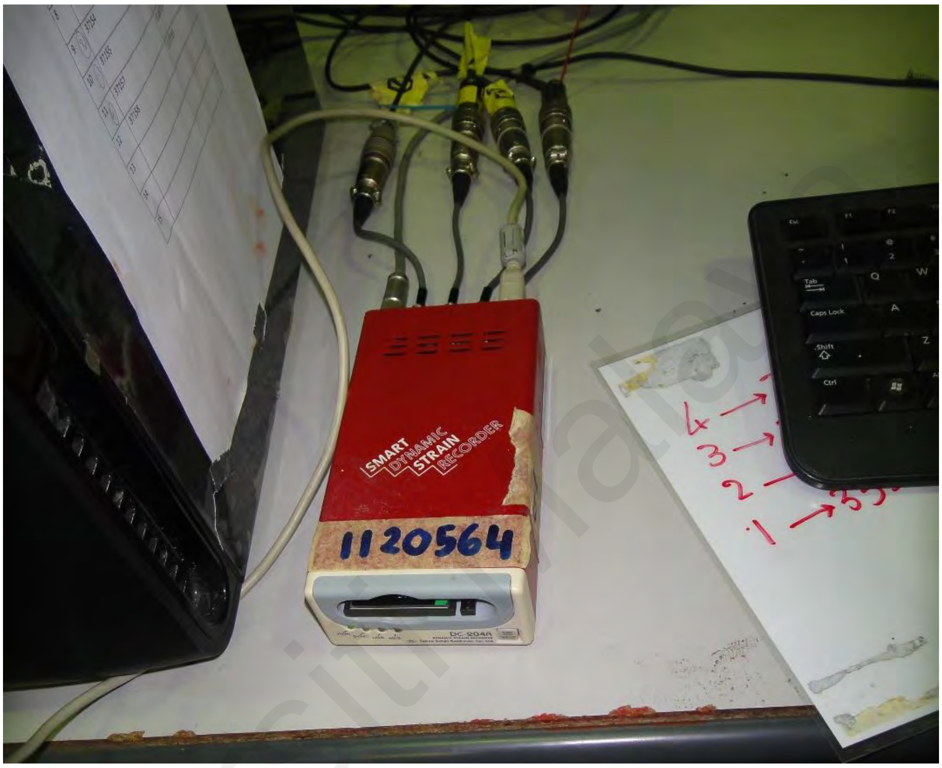

Figure 3.22: Data logger

The dynamic range of all the signals relative to the full-scale range of the A/D card (± 10 volts) was checked and adjusted in order to obtain the highest resolution possible. Payne (2008) recommended all incoming signals at maximum value should reach at least two-thirds of the absolute dynamic range so as to obtain the best resolution. Here in this study, a voltage range of ± 10 V was selected for the wave probes, giving a resolution as high as 0.1 mm. On the other hand, the working voltage range of the load cells was limited from -1 V to 9 V due to the constraint of the amplifiers, providing a resolution as high as 20 grams. The resolution level of the load cells was still considered satisfactory when compared to the smallest forces anticipated (approximately 300 grams) from the experiment. It gave a maximum deviation of 6% for small loads acting on the SCB model.

The signal quality was constantly checked and monitored during the experiments. Prior to the serious data acquisition, electrical noise generated by the equipment itself was identified by looking at each signal on the *WAVELAB* data acquisition program when the water was completely calm in the flume. The problem was eliminated by the use of the low-pass filtering function equipped in *WAVELAB* knowing that most electrical noise would be at frequencies that are very much higher than the maximum wave frequencies selected for the experiments. Filtering of the signals sampled by the data acquisition system also helped to prevent the signal components at frequencies greater than half of the data sampling frequency from breaking through into the sampled signal band as ‘aliasing’.

(b) Data Acquisition and Processing Software

Data acquisition and part of the analysis were carried out using the *WAVELAB* software developed by the Department of Civil Engineering, Aalborg University, Denmark. The software has a user-friendly graphical interface that is helpful for planning, performing and analyzing experiments. Besides data acquisition, it is capable of performing several other functions such as time series analysis, reflection analysis, wave height distribution, standard spectra generation, filtering, and others. The software has a unique capability to increase reliability of the analysis by prompting warning texts when the measurements or the results are less reliable. This feature prevents the experimenters from making a wrong interpretation of the test results.

In this study, *WAVALAB* was mostly used for data acquisition. Some of the main inputs in the data acquisition process are data file name and path, sample frequency, sample duration, the number of channels to be logged and calibration functions (optional). As mentioned previously, the software is equipped with a number of data analysis components. The time series analysis component was used to analyses wave elevations in both time and frequency domains and forces in time domain. Another tool applied in this study was the reflection analysis component, which adopted the Least Square Method (Mansard and Funke, 1980) for the decomposition of incident and reflected waves. This exercise requires identification of the wave probes and their spacing, sample frequency, calibration function for each wave probe and water depth. The details of the method are provided in Section 3.4.2. For further interpretation of the raw data, the data acquired by *WAVELAB* were stored in the form of data files and analyzed using the *MATLAB* routines. All data channels, which were logged in the form of raw voltage inputs, were loaded into a larger *MATLAB* program for further analysis. Calibration functions were applied in the program scripts to translate the raw data to the correct units. The data handling procedures used were intended to minimize the need for manual data entry. In addition, the programs were mainly used to produce wave energy density spectra, statistical interpretation and graphs plotting. In addition, a statistical software for data management and advanced statistical analysis, Excel by Microsoft, was utilized to establish the empirical equations for the prediction of the hydrodynamic performance of the tested SCB models, and to perform some statistical validations of the equations.

3.1.6 Test Program

A well-organized test program is of utmost importance in ensuring completion of the experiments within the time frame and fulfilment of the test objectives upon completion. For the present study, several test objectives were outlined and relevant experiments planned carefully and systematically so as to ensure they were achievable within three years of course study.

3.1.6.1 Experimental set up

As illustrated in **Figure 3.23** and discussed in section 3.1.15, the platform was designed to characterize the beach profile at the location of the bridge model. In the experiments, the bridge model was located at a distance of 19.30 m from the wave generator. Two different water depths in the flume were applied in this research i.e. H=1.0 m, 0.95m. Due to the platform these water depths lead to h= 0.16 m and 0.11 m water depth at the location of the bridge, respectively. Five different wave heights were utilized in this research classified in Table 3.4.

Table 3.4: Wave condition

Wave condition	Wave height	Water level at location of wave generator
Wave 1A	0.38 m	1 m
Wave 2A	0.34 m	1 m
Wave 3A	0.30 m	1 m
Wave 4A	0.26 m	1 m
Wave 5A	0.22 m	1 m
Wave 1B	0.38 m	0.95 m
Wave 2B	0.34 m	0.95 m
Wave 3B	0.30 m	0.95 m
Wave 4B	0.26 m	0.95 m
Wave 5B	0.22 m	0.95 m

where W_h= 0.38 m, 0.34 m, 0.30 m, 0.26 m, 0.22m. The bore heights for these solitary wave heights in the 1m water depth are 0.293 m, 0.278 m, 0.257 m, 0.226 m and 0.186 m, respectively. The bore heights in the 0.95 meter depth were 0.262, 0.245 m 0.220 m 0.194 m and 0.159 m, respectively. The solitary wave heights were applied to cover the wide range of tsunami wave height from large wave to small wave. In addition, the solitary wave heights applied in the flume covered the real tsunami wave height of 8.8 m, 10.4 m, 12m, 13.6 m, and 15.2 m. The water depths at the location of the bridge model represented realistic bridge prototype water depths of 6.4 m and 4.4 m. In this experiment, each test was repeated five times to ensure the repeatability and accuracy of the experiment. In the test condition, water depth, wave height, water and air temperature remained constant in each test and measured force on the bridge. The average vertical, horizontal, impact forces and overturning moment of these four tests were presented in experimental results.

In this research, force data were measured with a 1000 Hz sampling rate. As illustrated in Figure 3.24, the measured value might include the effect of resonance. This resonance with a frequency of 22 Hz is illustrated in the graph.

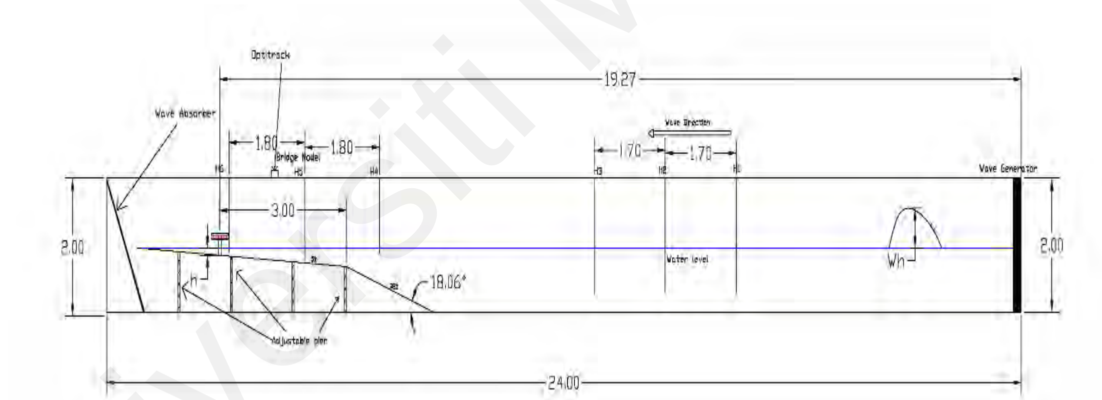

(a)

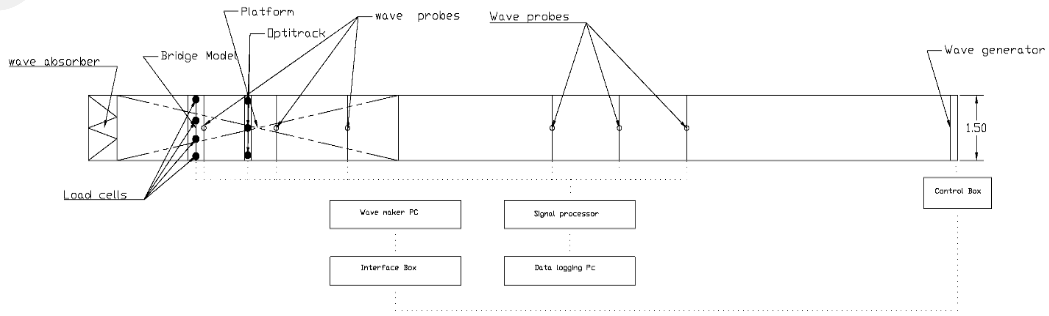

(b)

Figure 3.23: Experimental set up in the flume (a) side view (b) plan view

Due to the connection of the bridge model to the platform, this resonance was the natural period of the platform with about 25 Hz. In the experiments, data obtained directly from load cells and the moving-mean method was utilized to present a spline estimation for the signal result. This method was applied in order to eliminate the high-frequency resonance from the load cell signal. Therefore, 1/100 sec. moving-mean method was applied. After utilizing this method, the data was approximately equivalent to the data achieved by filtering the platform resonance frequency.

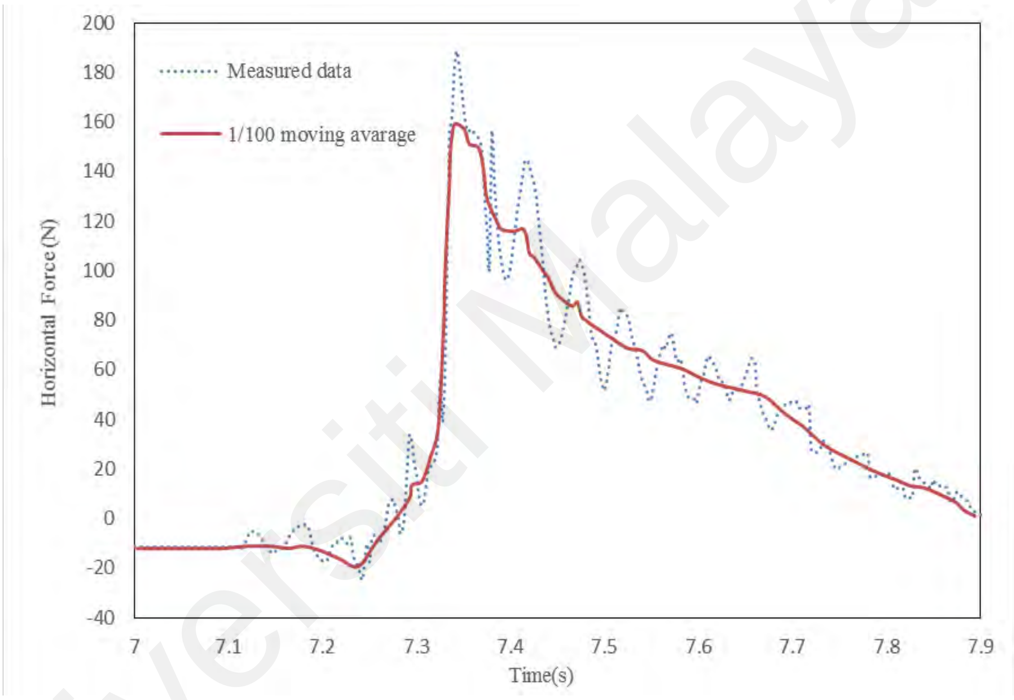

Figure 3.24: Time history of horizontal force

This approach was also used by Kenji Kosa et al. (2010) and Seiffert et al. (2014). This method was utilized for all the data i.e. horizontal, vertical and impact forces, as well as overturning moment in this research. Figure 3.24 shows the horizontal force with sampling rate of 1000 Hz and data after filtering 1/100 second moving-mean method.

3.1.6.2 Experiment series

The experiments in this study have been grouped into five series, according to beach slope and the bridge types as follows:

Series I: Bridge model A of various wave heights, water depths and beach slopes,

Series II: Bridge models B3-B6 with various wave heights and water depths in beach slope PB3,

Series II: Bridge models C3-C6 with various wave heights and water depths in beach slope PB3,

Series IV: Bridge models AB with baffle plate in various wave heights, water depths in beach slope PB2,

Series IV: Bridge models C3-C6 with various wave height and water depth in beach slope PB3,

Series IV: Bridge models C3-C6 with various wave height and water depth in beach slope PB3.

Table 3.5: Classification of variety of tests carried out for experiments in *Series I-Series IV*

Series Name	Bridge model	Wave height					Water depth	
		0.22	0.26	0.30	0.34	0.38	1m	0.95m
I	A	√	√	√	√	√	√	√
II	B3-B6	√	√	√	√	√	√	√
III	C3-C6	√	√	√	√	√	√	√
V	F1-F44	√	√	√	√	√	√	√

In this experiment, each test was repeated five times to ensure the repeatability and accuracy of the experiment. In the test condition, water depths, wave heights, water and air temperature remained constant in each test and measured force on the bridge. The average vertical, horizontal, impact forces and overturning moment of these five tests were presented in experimental results.

The experiment *Series I* aims to determine the tsunami force due to bore on Bridge model A on various wave heights, water depths and beach slopes. In this series, five wave heights in two different water depth and four various beach slopes were applied. A total of 200 tests were conducted for this series.

Series II and Series III aim to evaluate tsunami wave force due to bore, respectively, on bridge models B3-B6 and Bridge models C3-C6. In addition, effect of various Girders were investigated in these Series. In this series, five wave heights and two-water depths were utilized. The beach slope PB2 was applied in these tests. In total, 150 tests were performed in each series of experiments.

Series IV aims to study the effect of baffle plate to mitigate the tsunami load on coastal bridge. In Series IV, baffle plate was applied in bridge model A and create bridge model AB. Similar to Series II and Series, five wave heights and two water depths with beach slope PB2 were applied in the experiments. A total of 150 tests were carried out in the flume.

3.1.7 Summary of experiments

The experimental study of this research was carefully formulated to ensure the quality of the laboratory tests and measurements. Nevertheless, the tests were still subjected to some scale and laboratory effects that were difficult to quantify in practice. These effects can only be studied by comparing small and large scale models, which is beyond the scope of the present study. The hydrodynamic response of the test models was examined with approximately 1200 tests undertaken in stages over a period of 20 months at the University of Malaya and UTP University. The test data were vigilantly analyzed and presented in various forms.

3.2 Computational and Numerical Analysis

In this research LS-DYNA 971 R7 software as a finite-element analysis code (Gladman 2007) was utilized for the FSI (Fluid Structural Interaction) analysis in evaluating the uplift, horizontal and impact forces as well as the overturning moment in the proposed bridge model. There are several research works in industry that employ the FSI and ALE (Arbitrary Lagrangian Eulerian) method with the LS-DYNA Software or other Finite element code such as MSC/DYTRAN or ABAQUS (Ozdemir et al., 2010); Kim and Shin, 2008). However, evaluating the ability of FSI analysis and LS-DYNA software for tsunami bore-structure interaction in the wave basin has not been well validated for the scaled bridge with reinforced concrete material. The following section reviews the theoretical and numerical modelling and governing equation in FSI and ALE and continues with computational results and comparison with experimental results.

3.2.1 Theoretical Background

In the case of FSI, computational meshing could be categorized into two groups of elements i.e. structural elements and fluid (water, air) elements. The structural element is modelled with Lagrange formulation. In this part, the movements of mesh nodes are equivalent to the displacement of structural material. The fluid part, however, can be considered with Lagrangian specification by moving the interaction load through contact algorithms. The downside of this method is the need to minimize the problem forms with limited amplitude deformations. In particular, while the fluid mesh was close to the structural mesh with high deformations, the mesh becomes inappropriately distorted. This phenomenon leads to the generation of minimal time step for accurate calculations. Nevertheless, for high amount of deformation, the ALE techniques can develop new undistorted mesh elements of the fluid domain, resulting in accurate calculation. Generally, analysis using the ALE technique consider that the mesh movement is independent of the material movement (Ozdemir et al., 2010).

3.2.1.1 ALE method

The numerical code solves the Navier-Stokes (NS) equations to obtain the pressure field and consequently the forces on the structure. An arbitrary Lagrangian-Eulerian (ALE) formulation was used to track the fluid particles in the fluid-free surface. The code solves the NS equations and multiphasic contact and impact of the models. The ability to solve the NS equations allows the model to capture all of the effects related to fluid viscosity and rotation of the fluid particles. This feature makes the numerical code able to model wave breaking and fluid impact on the structure, which are crucial in modeling the tsunami loads on the structure. ALE analysis was applied in this research, benefitting from both Lagrangian-Eulerian algorithms. The fluid structure interaction (FSI) coupling algorithm combined with an Arbitrary Lagrangian-Eulerian (ALE) solver was used in the numerical models, as it is the most mature formulation to simulate the problem involving interaction between high velocity fluid and structure. ALE basically consists of three types of domains in space, which are referred to as spatial domain, material domain and reference domain. The spatial domain is considered to be in motion and the material domain has been evaluated as the domain utilized at time T= 0 by the material particles which engage the spatial domain at time t. However, the reference domain is determined as a fixed domain in the simulation. Consequently, both spatial and material domains are in motion with regards to the reference domain (Manawasekara, 2013b). Donea et al. (2004) and Souli and Benson (2013) stated that the ALE method is the most efficient solution to simulate the interaction issue involving turbulent fluid and rigid or flexible structure. The ALE method includes three varieties of domains i.e. spatial domain, material domain and reference domain.

(a) Governing equation for ALE

Souli et al. (2000) stated that in ALE the material derivative with regards to the reference coordinate may be defined as given by Equation 3.3 extracted by substituting the association between the material and reference configuration time derivatives as follows:

$$\frac{\partial f(X_i,t)}{\partial t} = \frac{\partial f(x_i,t)}{\partial t} - w_i \frac{\partial f(x_i,t)}{\partial x_i} \tag{3.3}$$

In Equation 3.3, X_i is the Lagrangian coordinate, x_i the Eulerian coordinate, i the referential coordinate. Note that u_i is material velocity and w_i is reference velocity. Furthermore, v and u is the material and mesh velocities, respectively. The relative velocity $w = v - u$. Souli et al. (2000) simplified the equations and present the governing equations for the ALE formulation as given by Equations 3.4-9 as follows:

The conservation of mass equation is given by

$$\frac{\partial \rho}{\partial t} = \rho \frac{\partial v}{\partial x_i} - w_i \frac{\partial \rho}{\partial x_i} \tag{3.4}$$

Equation 3.5 represents the momentum equation.

$$\frac{\partial y}{\partial x} = -\left(\sigma_{ij.j} + \rho b_i\right) - \rho w_i \frac{\partial v_i}{\partial x_j} \tag{3.5}$$

where σ_{ij} is the stress tensor and represented by Equation 3.6

$$\sigma_{ij} = -p\delta_{ij} + \mu\left(\upsilon_{i,j} + \upsilon_{j,i}\right) \tag{3.6}$$

The energy equation is described in Equation 3.7 as follows:

$$\frac{\partial E}{\partial t} = -\left(\sigma_{ij}\upsilon_{i,j} + \rho b_i \upsilon_j\right) - \rho w_j \frac{\partial E}{\partial x_j} \tag{3.7}$$

In Equations 3.4-7, ρ is the density of the fluid, p is the pressure, μ is the coefficient of kinematic viscosity,b_i and E are the body force and the energy, respectively.

3.1.1.2 FSI method

In FSI method, the fluid Lagrange mesh is sensitive to factors such as moving boundary conditions and in this research, a penalty coupling method is utilized to address the problem. Furthermore, the structure of coupling interfaces on both Lagrangian and ALE fluid based algorithm is carried out to assess the interaction force between fluid and structure (Manawasekara, 2013b). The penalty method is estimated by Equation 3.8 and characterized by replacing a spring at each penetrating node and the contact surface (Aquelet et al., 2006) where γ_i is spring stiffness , p_i penalty force and d_i is displacement.

$$p_i = \gamma_i d_i, \tag{3.8}$$

Utilizing penalty coupling provides an efficient solution for a fluid structure interaction. The penalty coupling monitors and solves the interactions issue involving a Lagrangian formulation modeling (the structural bridge model) and ALE formulation (fluid). The Lagrangian finite element formulation utilizes a computational mesh that employs the material deformation. This efficient method is for solving moderate deformation issues i.e. structural displacement and flow motion. Moreover, ALE codes provide the movement of material throughout the mesh element. The flow chart of fluid structure interaction algorithm is presented by Manawasekara (2013b).

3.2.2 Computational Modelling for Wave Tank and Tsunami Wave Generation

Previous simulation research work in applying the LS-DYNA to create the wave such as the tsunami wave include studies by Wemmenhove et al., (2010), Boon-intra (2010), Hayatdavoodi et al., (2014), Seiffert et al. (2014) and Manawasekara (2013b). These researches mostly focused on solitary wave on a single deck and were not applied to the complete bridge deck.

In the computational modeling, a piston-type wave generator was simulated similar to experiment (refer to Figure 3.25). The wave generation mechanism was introduced by Tokura and Ida (2005). However, they are not calibrated with the experimental result. The model includes concrete bridge model, wave generator, air and water. Figure 3.25 illustrated the boundary condition and the simulation dimension that is similar to the experiments. The length of flume in the simulation applied is 24 m and this is similar to length of flume in the experiment. The bridge model is 1:1 scale of bridge model in the experiments. The bridge dimension is similar to the experiment model presented in section 3.1.3. Two water depths similar to experiment were applied in the computational simulation i.e. 1 m and 0.95 m.

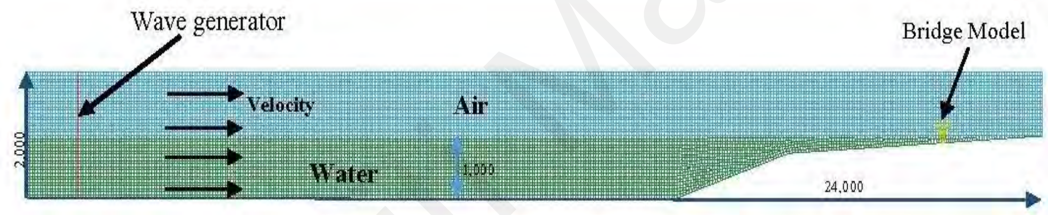

Figure 3.25: Side view of simulation model and boundary condition in the 1m water depth

According to the 2D simulation in this research, for accurate simulation, the fluids and models are made of layered solid elements over the depth as illustrated in Figure 3.26.

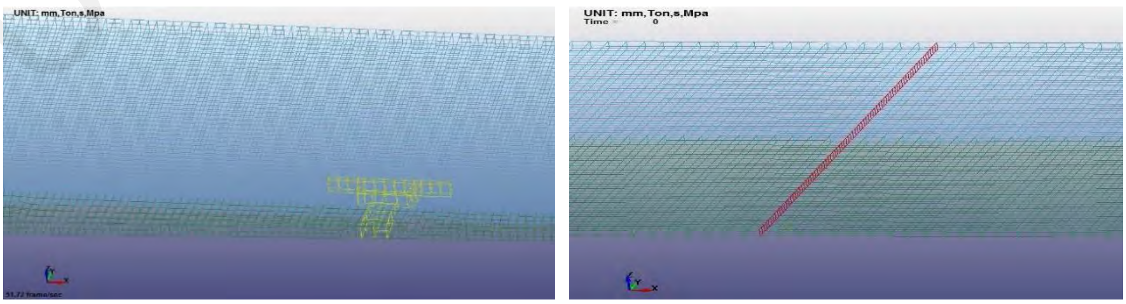

(a) (b)

Figure 3.26: Isometric view, (a) Close up isometric view of the bridge model, (b) Close up isometric view of wave-maker

The material parameters of model and fluid are illustrated in the screenshot of the input file in LS-DYNA in Figure 3.27. Further details on material parameters in LS-DYNA can be found in LS-DYNA Keyword User's Manual (2007). Various displacements were applied to the wave generator through BOUNDARY-PRESCRIBED-MOTION-RIGID, LS-DYNA keyword to generate proposed solitary wave (0.38 m, 0.34 m, 0.30 m, 0.28m 0.24 m) in the experiments. As described previously, the penalty coupling was applied to define the FSI.

```
*PART
$#                                                                     title
wave_maker
*MAT_RIGID_TITLE
rigid
$#     mid        ro         e        pr         n    couple         m     alias
         4 7.8000E-7 2.0000E+5  0.300000     0.000     0.000     0.000
*PART                                                                     title
air
*MAT_VACUUM_TITLE
air
$#     mid       den
         3 1.2300E-12
*HOURGLASS_TITLE
HourGlas_5
$#    hgid       ihq        qm       ibq        q1        q2    qb/vdc        qw
         5         1 1.0000E-6         1  1.500000 6.0000E-2  0.100000  0.100000
*PART
$#                                                                     title
water
$#     pid     secid       mid     eosid      hgid      grav    adpopt      tmid
         3         2         2         8         5         0         0         0
*MAT_NULL_TITLE
water
$#     mid        ro        pc        mu     terod     cerod        ym        pr
         2 1.0000E-9-1.000E+20 1.0000E-9     0.000     0.000     0.000     0.000
```

Figure 3.27: The material parameters of the model and fluid in input file of LS-DYNA

Abbreviation, hgid: hourglass ID, ihq: hourglass control type, qm: hourglass coefficient, ibq: bulk viscosity type, q1:quadratic bulk viscosity coefficient, qb: hourglass coefficient for shell bending, vdc: viscous damping coefficient, qw: hourglass coefficient for shell warping, ro: mass density, e: young modulus, pr: Poisson's ratio, mid: material identification, den: material density, pc: pressure cutoff, mu: dynamic viscosity coefficient.

In the experimental flume as illustrated in Figure 3.1 and Figure 3.4, a wave absorber was applied opposite the wave generator to prevent the wave reflection to the bridge model. In the numerical simulation, this is provided by a relaxation zone. This was also applied by previous researchers such as Mayer et al. (1998), Christensen and Deigaard (2001) and Piro (2013). Mayer et al. (1998) stated that partial velocity and surface elevation are relaxed given by the following equation:

$$\theta(x,t)=\beta(x)\theta(x,t)+(1-\beta(x))\theta_p(x,t) \tag{3.9}$$

In Equation 3.9, θ may be replaced by partial velocity and surface elevation represented by ν and ζ, respectively. β is the relaxation parameter and θ_p is the prescribed value for ν and ζ. The relaxation factor is given as follows

$$\beta(\bar{x})=1-\frac{\exp(\bar{x}^{3.5})-1}{\exp(1)-1} \; where\,\bar{x}\in[0,1] \tag{3.10}$$

In Equation 3.10, in the relaxation zone, $\bar{x}$ factor is the normalized horizontal coordinate. However, the application of a wave absorber in the simulation process is not only a very time consuming and complicated process, but the behaviour of the wave absorber also depends on the wave character and may not absorb it perfectly. Consequently, in the computational analysis of this research, the open boundary was applied after the bore had hit the bridge and left the flume and simulation time will be stopped at this moment.

Figure 3.28 compares simulation without and with relaxation zone. As illustrated in this figure in the case of (a), wave after contact with the wall of the flume was reflected to the bridge, but in case (b) the wave after hitting the bridge left the flume. More details on relaxation zone through open boundary in LS-DYNA can be found in Petel (2011) and Yeom (2009).

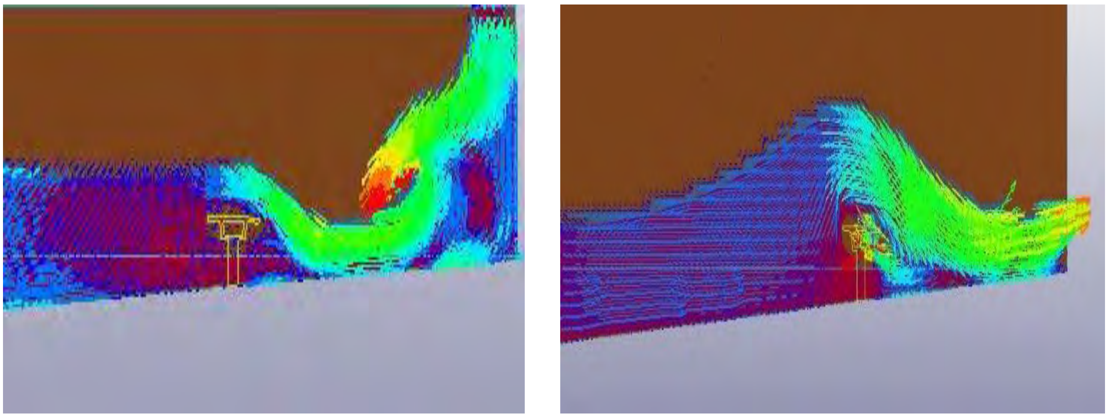

(a) (b)

Figure 3.28: Relaxation zone effect (a) simulation without relaxation zone, (b) simulation with applied relaxation zone with open boundary

3.2.3 Grid Independency and Verification

The 2D computational domain was discretized with structured, free surface and non-uniform grid distributions (indicated in Appendix A). As described previously in Figure 3.26, the mesh depth was fixed at 0.05m in all cases. To obtain the grid independency, four different mesh sizes were applied in this research. Note that d_x is mesh size in the horizontal direction and d_y is the mesh size in the vertical direction. These two values are equal in all cases. Flume dimension and numerical model are constant in all simulations. The grid independency for each wave height and water level was studied separately. However, due to limited space in Table 1, only the results of grid independency for 0.38 m wave height and 1m water level are illustrated. Based on the results in Table 1, d_x=d_y= 0.025 m was selected in this research. This mesh size was used in all cases in simulation with the LS-DYNA. In this research, a Symmetric Multi-Processing (SMP) (SGi Altix 4700) computer was used with 32 CPU core and 64 GB RAM. The operating system is Suse Enterprise 10 and CPU type is 64 x Dual Core Intel Itanium2 64 bits Processors.

Table 3.6: Grid independency test for 1m water depth in 0.38 wave height

Number of grids	240*20	480*40	960*80	2000*167
d_x horizontal mesh size	0.10	0.05	0.025	0.0125
d_y vertical mesh size	0.10	0.05	0.025	0.0125
d_z depth mesh size	0.10	0.05	0.025	0.0125
Total number of mesh	3422	14133	55823	222730
Horizontal force (N)	2104.74	2069.32	2018.75	2017.31
Uplift force (N/m^2)	670.21	601.39	594.95	593.56
Overturning moment (Nm)	73.67	70.11	66.53	66.04

3.3 Evaluating Accuracy of Experimental and Numerical Results

Accuracy of experimental and numerical results were presented as Root Means Square Error (RMSE) (Equation 3.11), coefficient of determination (R^2) (Equation 3. 12) and Pearson coefficient (r) (Equation 3.13). These statistics are defined as follows:

a) Root Means Square Error (RMSE):

$$RMSE = \sqrt{\frac{\sum_{i=1}^{n}(P_i - O_i)^2}{n}} \tag{3.11}$$

b) Pearson correlation coefficient (r):

$$r = \frac{n\left(\sum_{i=1}^{n} O_i \cdot P_i\right) - \left(\sum_{i=1}^{n} O_i\right)\cdot\left(\sum_{i=1}^{n} P_i\right)}{\sqrt{\left(n\sum_{i=1}^{n} O_i^2 - \left(\sum_{i=1}^{n} O_i\right)^2\right)\cdot\left(n\sum_{i=1}^{n} P_i^2 - \left(\sum_{i=1}^{n} P_i\right)^2\right)}} \tag{3.12}$$

c) Coefficient of determination (R^2):

$$R^2 = \frac{\left[\sum_{i=1}^{n}\left(O_i - \overline{O_i}\right)\cdot\left(P_i - \overline{P_i}\right)\right]^2}{\sum_{i=1}^{n}\left(O_i - \overline{O_i}\right)\cdot\sum_{i=1}^{n}\left(P_i - \overline{P_i}\right)} \tag{3.13}$$

where O_i and P_i are known as the experimental and numerical values of test respectively, and *n* is the total number of test data. $\overline{P_i}$ and $\overline{O_i}$ represent average values of P_i and O_i.

CHAPTER 4: RESULTS AND DISCUSSION

4.1 Tsunami Wave and Bore Generation

As explained in chapter 3, solitary wave was created by wave generator and was formed at the location near to offshore region from H1-H3, while the various solitary waves in the experiment are illustrated in Figure 3.23. Goring (1978) stated that a solitary wave includes an individual hump of water completely above still water level with a very long wavelength. Hall Jr. and Watts (1953) utilized a piston-type wave generator for generating the solitary wave for the first time. In the current experiment, the solitary wave was generated with piston type generator produced by Edinburgh design. Wiegel (1980) stated that the surface elevation of a solitary wave may be described by Equation 4.1.

$$\eta_w = Hsech^2\left[\sqrt{\frac{3H}{4d^3}}(x - ct)\right] \tag{4.1}$$

where η_w is the surface wave elevation, H is the wave height, c is wave celerity given by $c = \sqrt{gd}(1 + H/2d)$, d is water depth, t is time, g is the gravitational acceleration. Figure 4.1 compares the surface elevation in the solitary wave between the experiment and Equation 4.1 along with corresponding time history. In this figure, the water depth of d=1 m was applied in the flume and wave height was H=0.38, 0.34, 0.26, 0.24, 0.22 meters. It might be described that in the figures, lower forecast time periods are related to improved prediction accuracies. This may be predicted considering higher correlations between the values divided by lower times.

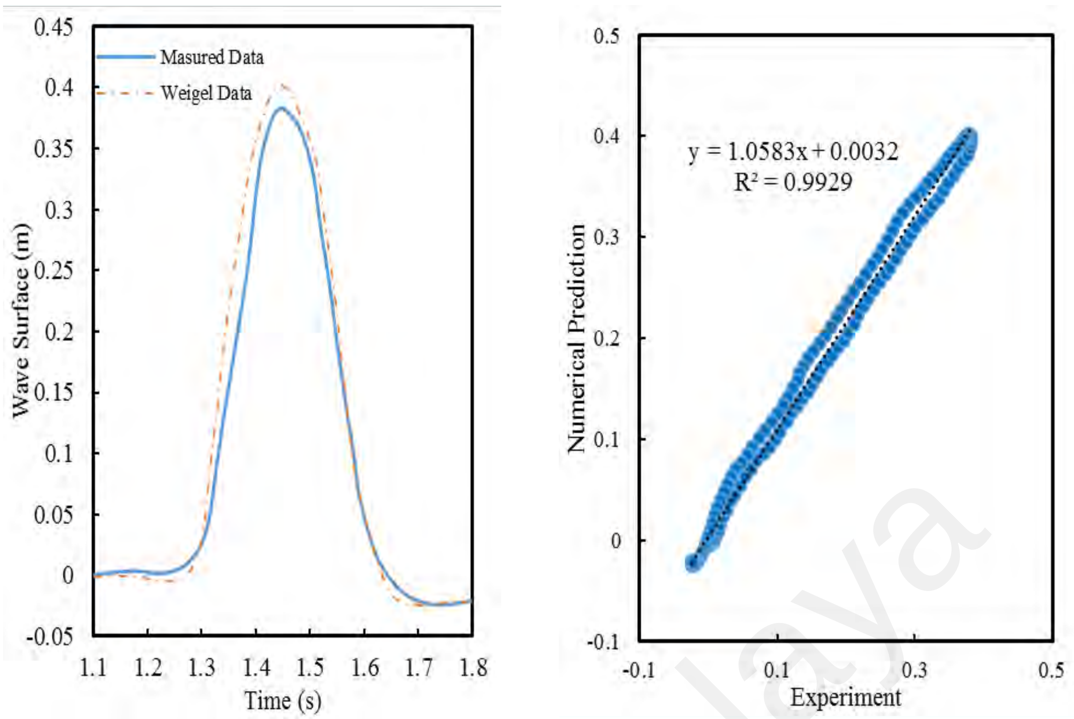

(a)

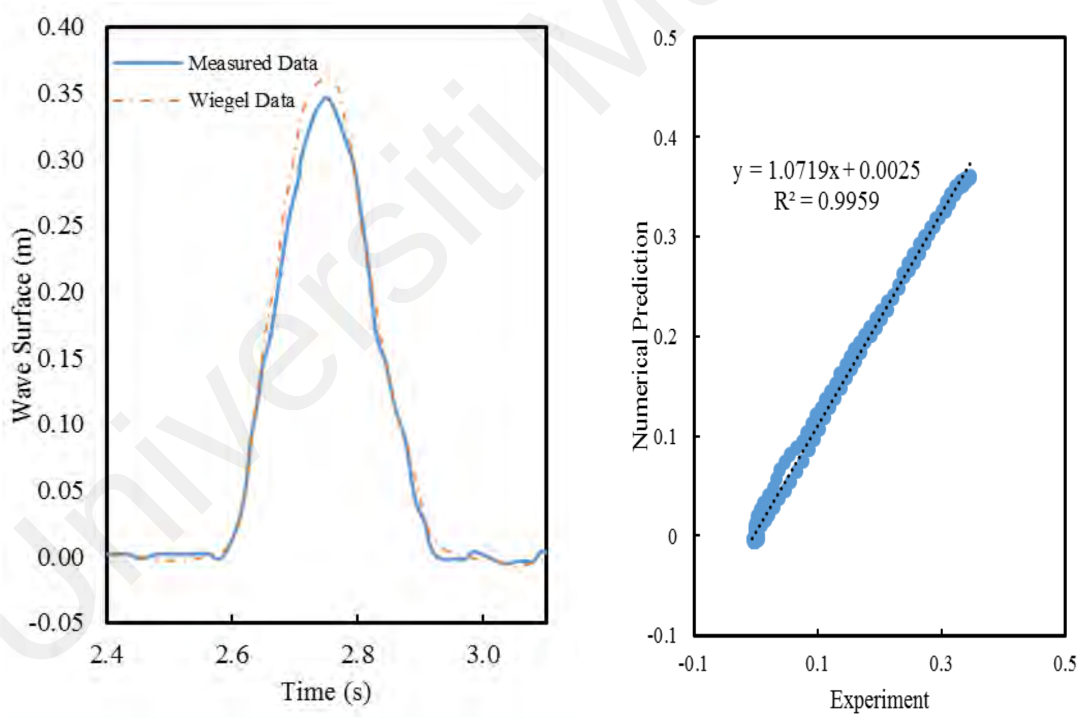

(b)

Figure 4.1: Comparison between the surface elevation in the 0.38 m solitary wave between experiment and Wiegel Method, left solitary wave elevation in the experiment and Wiegel, right, Scatter plots of actual and predicted values of solitary wave, a) 0.38 m wave height, b) 0.34 m wave height, c) 0.30 m wave height, d) 0.26 m wave height e) 0.24 m wave height

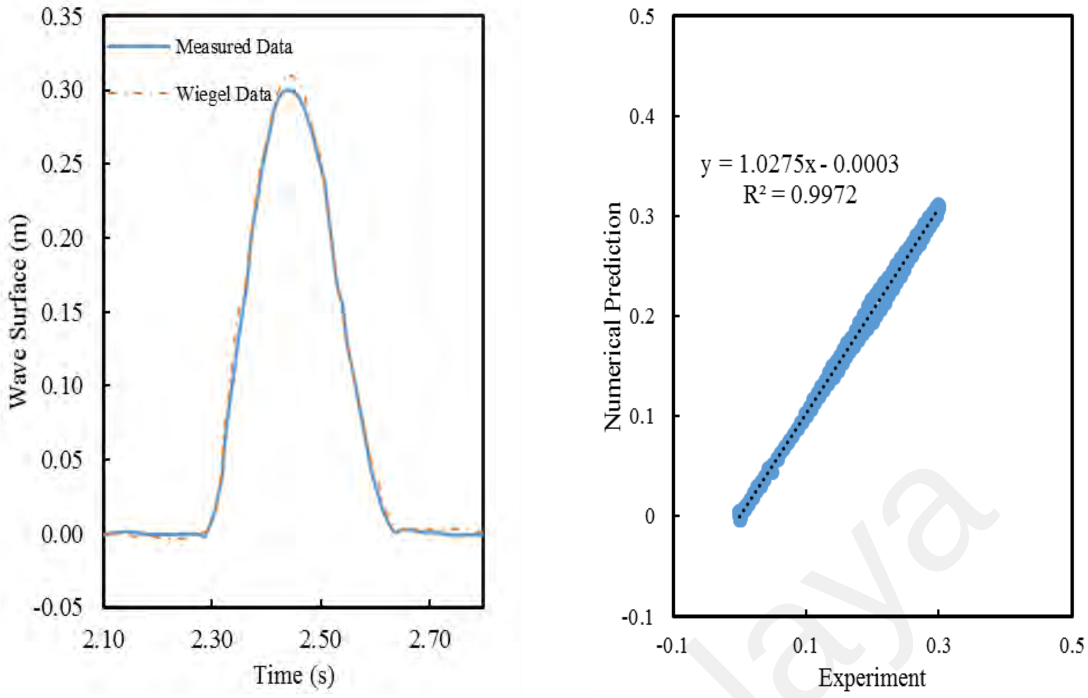

(c)

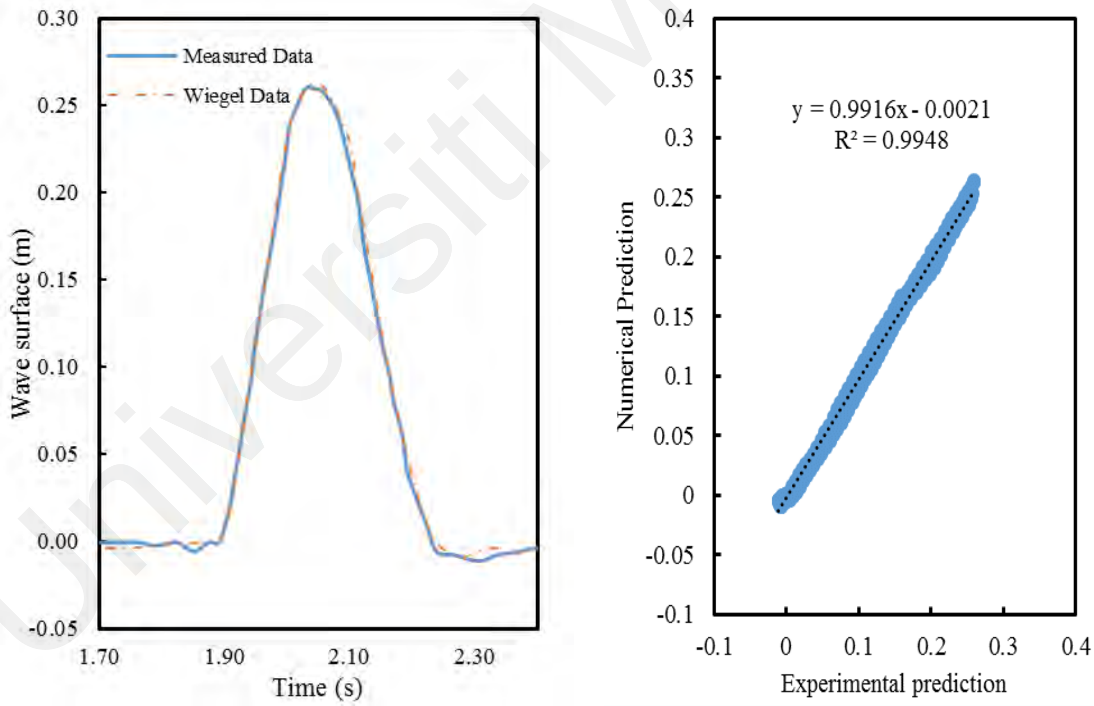

(d)

Figure 4.1: Comparison between the surface elevation in the 0.38 m solitary wave between experiment and Wiegel Method, left solitary wave elevation in the experiment and Wiegel, right, Scatter plots of actual and predicted values of solitary wave, a) 0.38 m wave height, b) 0.34 m wave height, c) 0.30 m wave height, d) 0.26 m wave height e) 0.24 m wave height (continue)

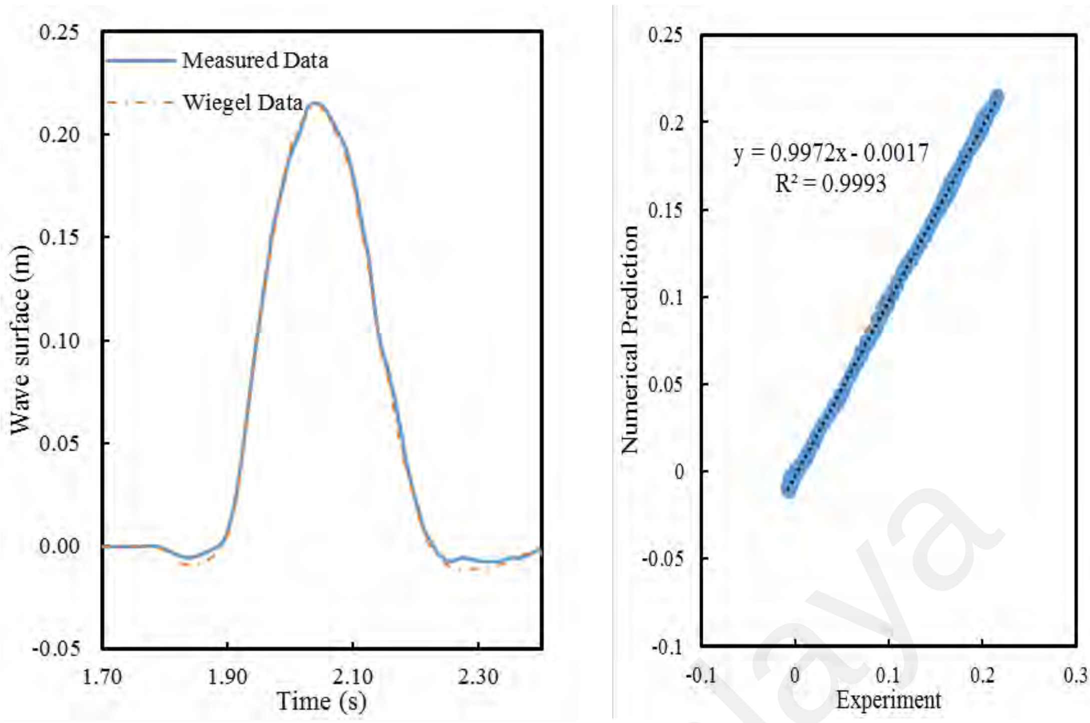

(e)

Figure 4.1: Comparison between the surface elevation in the 0.38 m solitary wave between experiment and Wiegel Method, left solitary wave elevation in the experiment and Wiegel, right, Scatter plots of actual and predicted values of solitary wave, a) 0.38 m wave height, b) 0.34 m wave height, c) 0.30 m wave height, d) 0.26 m wave height e) 0.24 m wave height (continue)

Figure 4.1 shows that there exist good accuracy levels between experimental and Wiegel Method. The result shows that the crest of wave in higher wave height is slightly overestimated but Wiegel Method is predicted with a good agreement. Coefficient of determination of results are stated as 0.9993 to 0.9929 with increase in wave. This proved that Wiegel Method in lower weight height provides better wave height prediction. The comparison of wavelength in Figure 4.1 (a – e) shows that Wiegel Method estimated the wavelength of solitary wave accurately. The better predictions at lower wave height could be due to relatively less wave turbulence during the experiments. For the H:0.38, the prediction accuracy further dropped down.

The sharp edges of wave surface are made smooth in the calculations with application of a smoothing factor 0.9999 formula. The location of wave gauge was H2 as shown in

Figure 3.16. The result illustrated in Figure 4.1 shows there is good agreement between experimental and numerical result, especially in side surface of solitary waves. There is slight difference in solitary wave prediction by Wiegel (1980) and experiments, especially in top of the wave. However, the agreement increases the lower the wave height. This small disagreement can be attributed to error in the laboratory experiments in addition to energy dissipation during the wave propagation.

The solitary wave that reaches to the steep of the platform convert to the almost vertical wave form (Case I in Figure 4.2) and then tends to change to case II to break in shallow water as a plunging-type breaker after losing its stability. Case II-Case IV indicate the procedure.

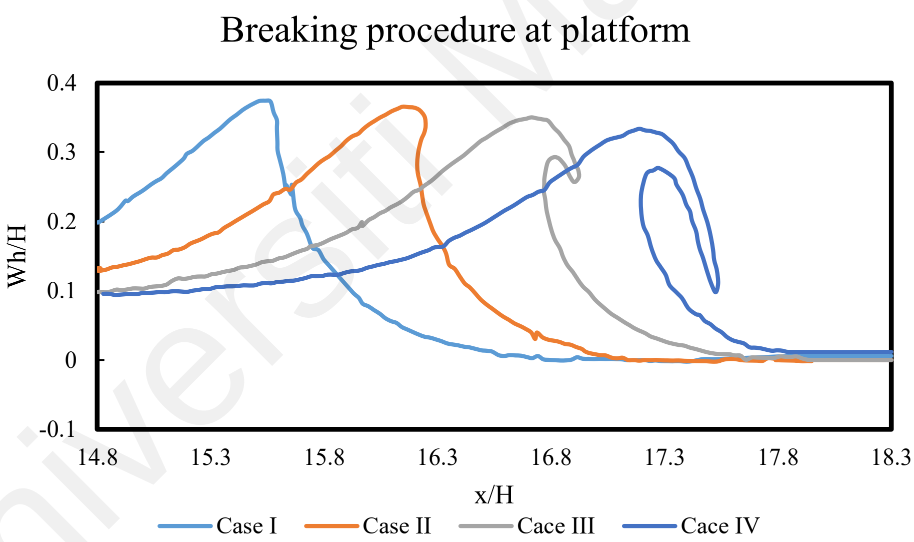

Figure 4.2: Breaking procedure in case 1A

The wave then transformed into bore by shoaling a solitary wave at a distance of 17 m from wave generator. The turbulent bore then hit the bridge model. The bore profile before hitting the model for Case1A- Case 5A is illustrated below. The x coordinate is measured from the wave maker to the model and η_b is presented bore elevation.

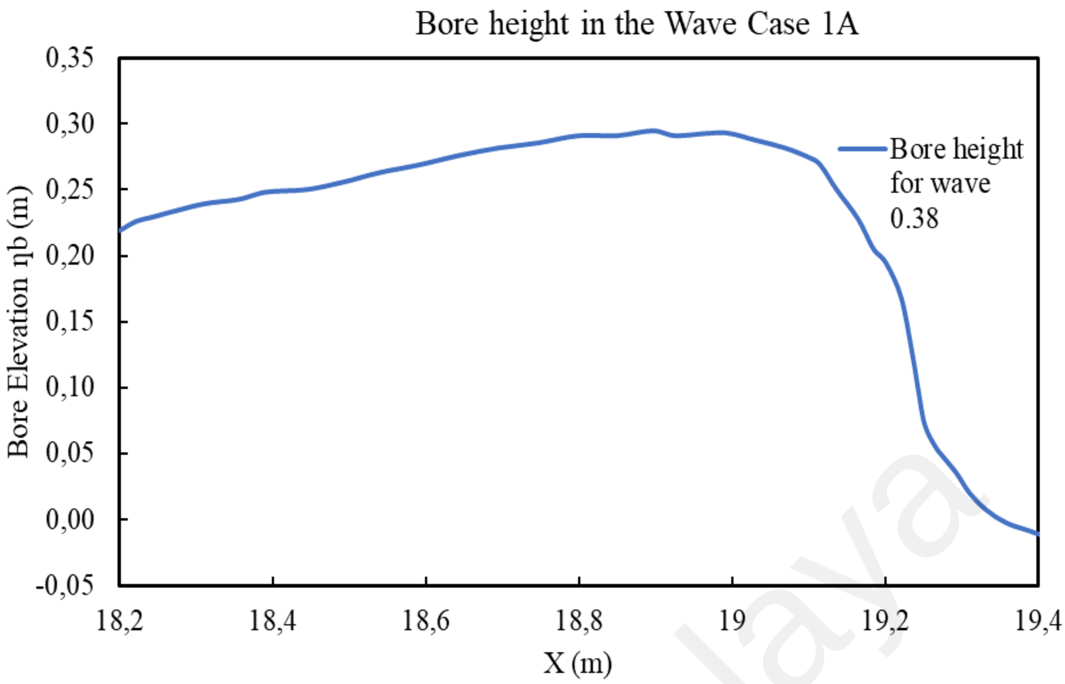

(a)

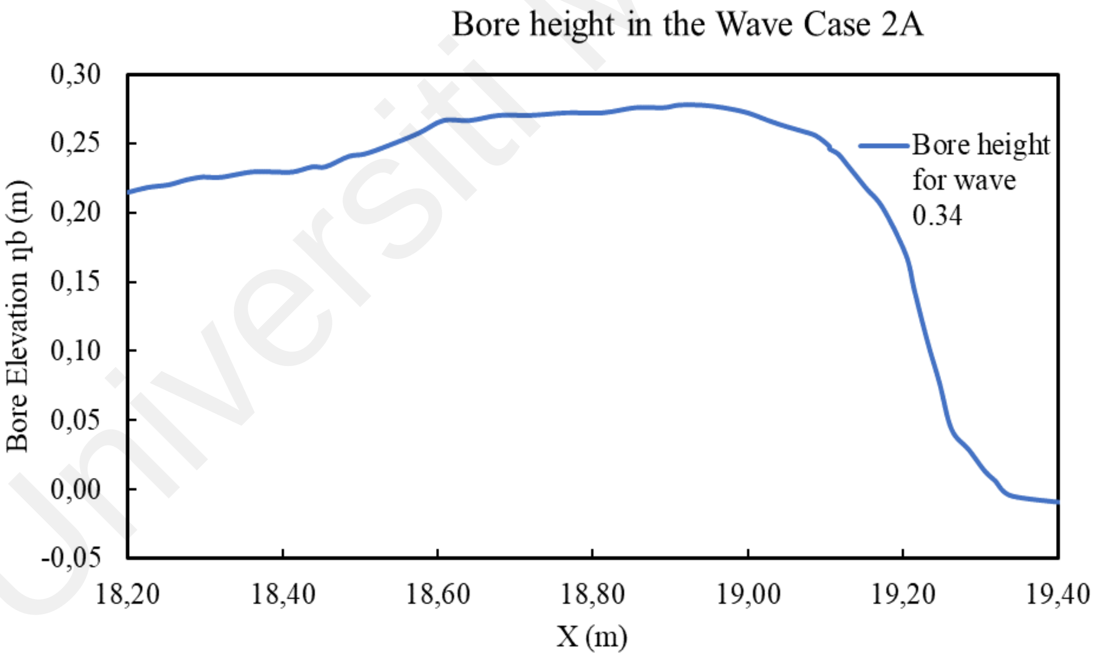

(b)

Figure 4.3: Bore elevation (a) Wave case 1A, (b) Wave case 2A, (c) Wave case 3A, (d) Wave case 4A, (b) Wave case 5A

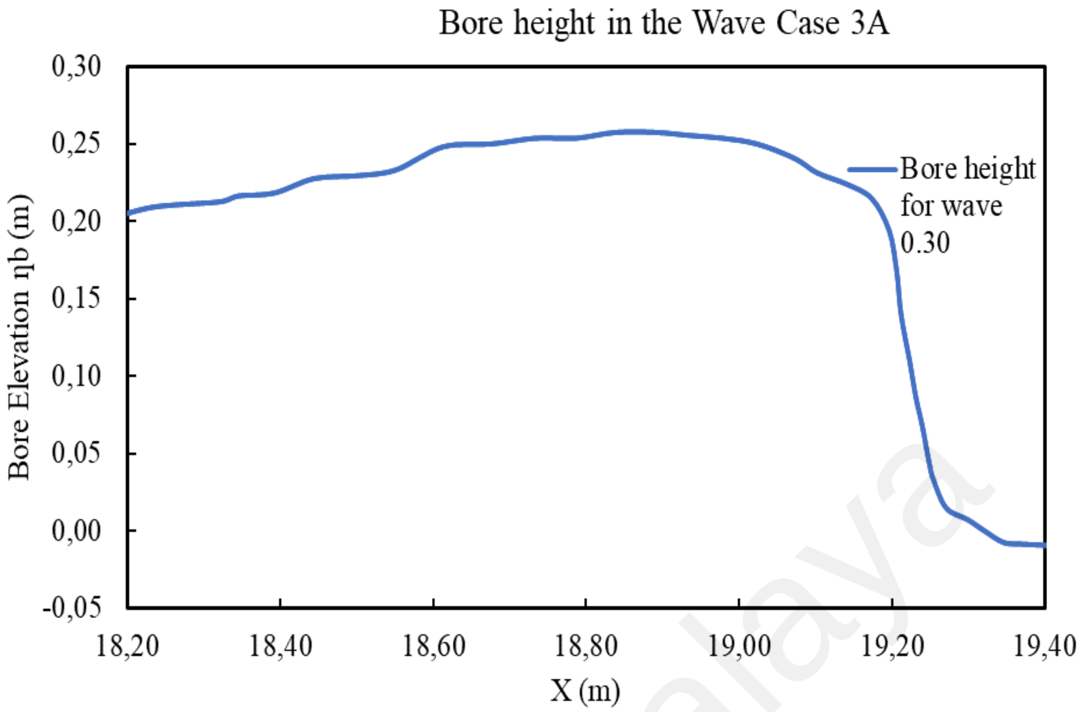

(c)

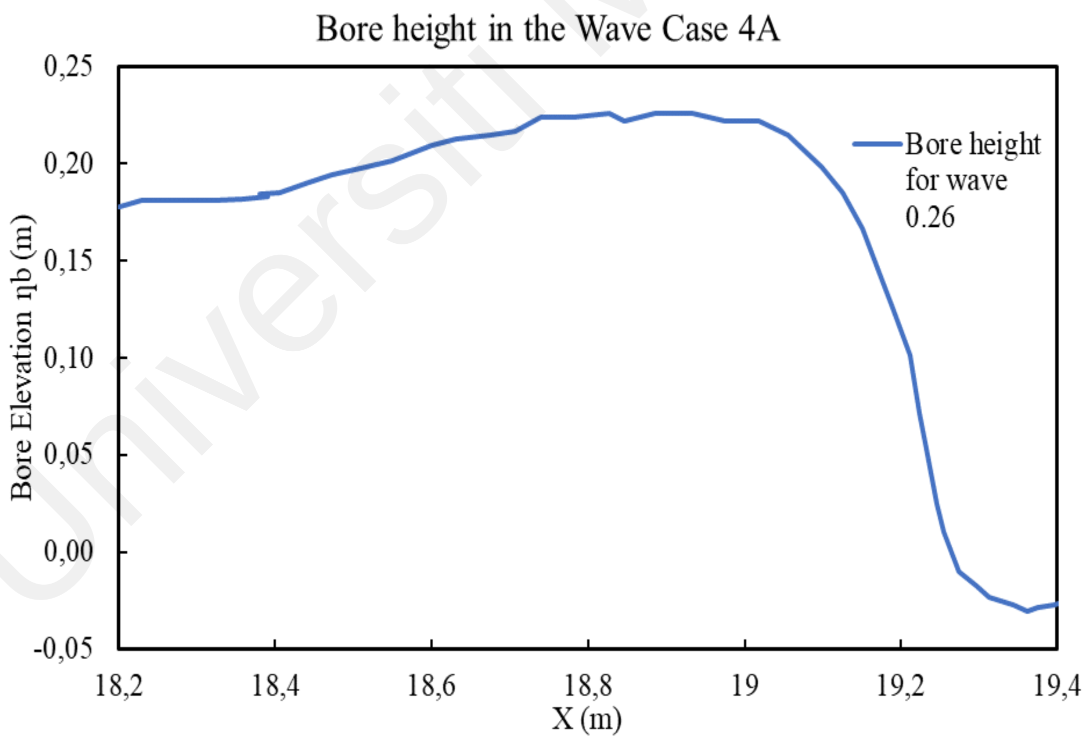

(d)

Figure 4.3: Bore elevation (a) Wave case 1A, (b) Wave case 2A, (c) Wave case 3A, (d) Wave case 4A, (b) Wave case 5A (continue)

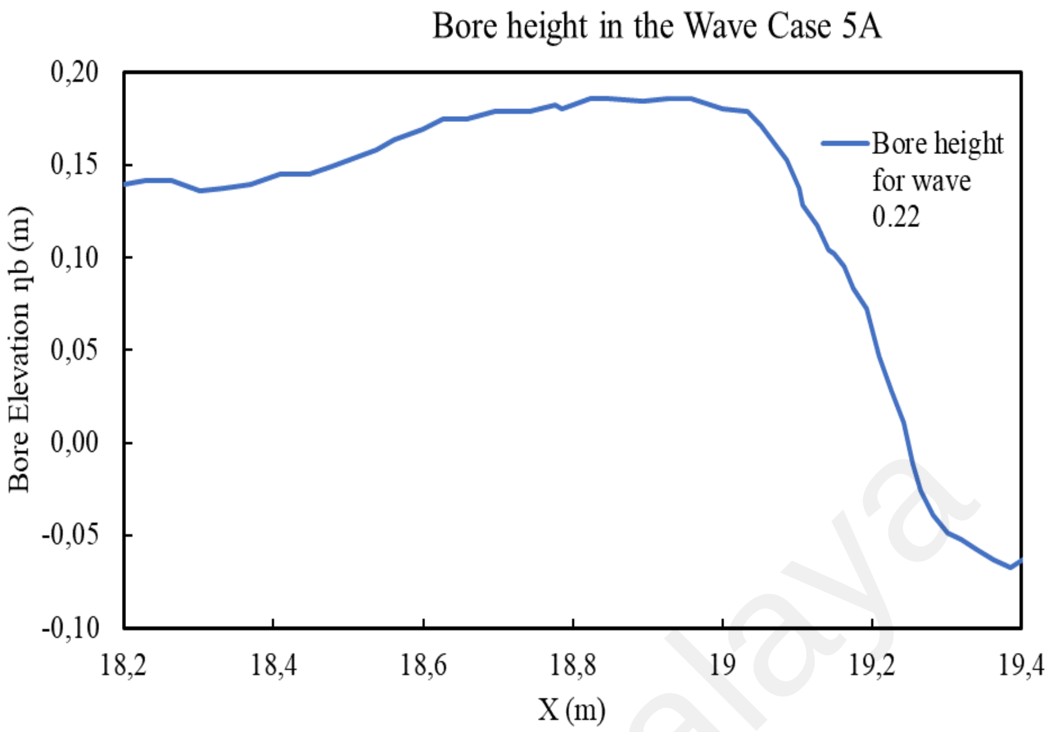

(e)

Figure 4.3: Bore elevation (a) Wave case 1A, (b) Wave case 2A, (c) Wave case 3A, (d) Wave case 4A, (b) Wave case 5A (continue)

The bore profile measured by the wave gauges in the flume is illustrated in Figure 4.3 The result indicates that a general trend was found, which is that the bore elevation increased by increasing the wave height. However, in contrast with solitary wave height that increased 0.04 m for each wave, the bore elevation is increased unequally. The bore elevation is increased 21.5 percent between Case 5A and Case 4A, 13.8 percent between Case 4A and Case 3A, 8.2 percent between Case 3A and Case 2A and 5.4 percent between Case 2A and Case 1A.

4.2 Correlation Between the Solitary Wave Height and Bore Height

This section is assessed the correlation between the solitary wave height and bore height

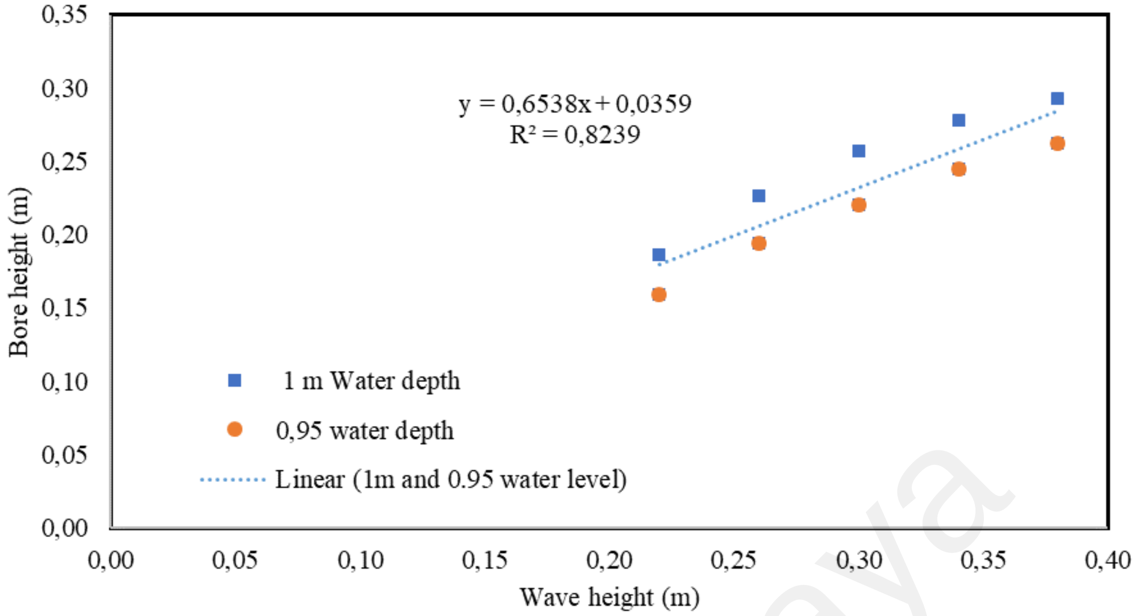

Figure 4.4: Correlation between the solitary wave height and bore height in 0.95 m and 1 m

The correlation between the solitary wave height and bore height in 0.95 m and 1 m water level at location of bridge models are shown in Figure 4.4 and Table 4.1. The results illustrate that in the same solitary wave height with increasing the water level, the bore heights increased. Of all cases, the maximum bore height occurs in Case 1A. This is due to higher water depths at the location of bridge models. As we discussed in chapter 3, due to the platform, 1m and 0.95 m water level in the flume lead to h= 0.16 m and 0.11 m water depth at the location of the bridge, respectively. The result illustrates that water level has a significant influence on the bore height.

Table 4.1: Solitary wave height and bore height in 0.95 m and 1 m

Wave condition	Wave height (m)	Water level at location of wave generator m	Bore height (m)
Wave 1A	0.380	1	0.293
Wave 2A	0.340	1	0.278
Wave 3A	0.300	1	0.257
Wave 4A	0.260	1	0.226
Wave 5A	0.220	1	0.186
Wave 1B	0.380	0.95	0.262
Wave 2B	0.340	0.95	0.245
Wave 3B	0.300	0.95	0.220
Wave 4B	0.260	0.95	0.194
Wave 5B	0.220	0.95	0.159

Fukui et al. (1963) conducted analytical research and hydraulic experiments to determine the relationship between tsunami bore velocity and water surface elevation as proposed in Equation 4.2;

$$U = \frac{C\eta_b}{D} = \eta_b \sqrt{\frac{gD(D+h)}{2D(D+\mu\eta_b)}} \tag{4.2}$$

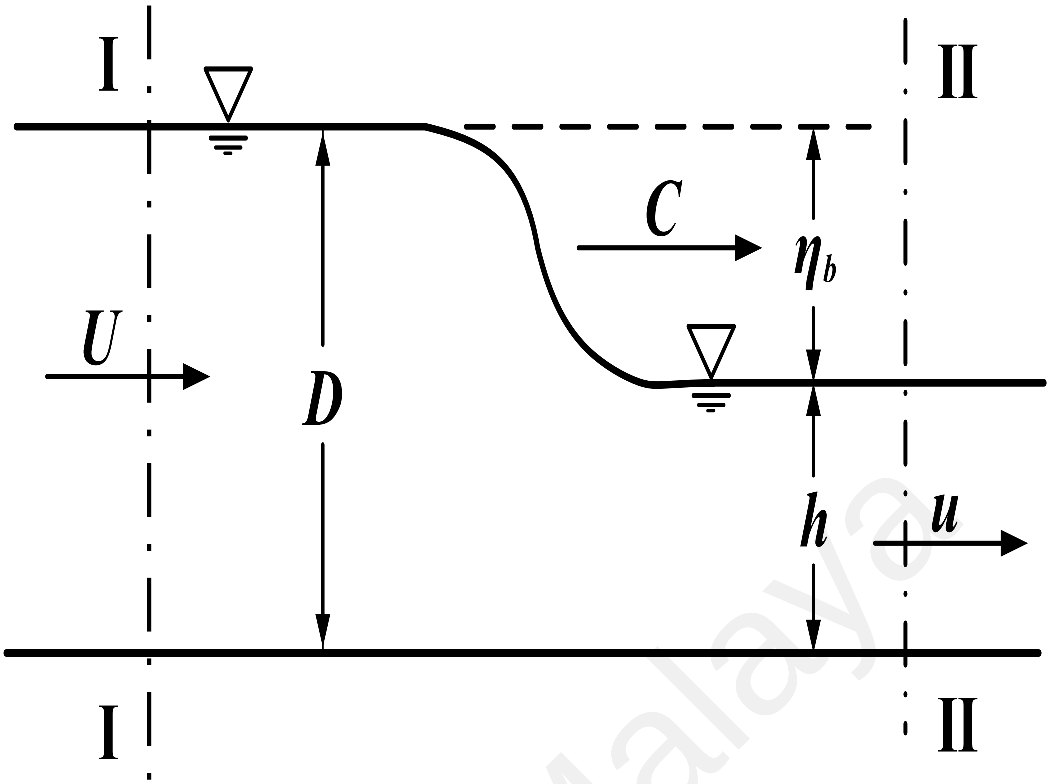

Figure 4.5: Bore profile illustration by Fukui (1963)

where U is the bore velocity, g the gravitational acceleration, $D = h + \eta_b$ is the total depth from the bottom, η_b the time-dependent bore height. μ is the velocity coefficient derived from the ratio of water level and wave height. This equation was applied by Wijatmiko and Murakami (2012) and Nott (2003). Figure 4.5 illustrates all these factors. Five solitary wave heights W_h applied in the experiments were 0.38 m, 0.34 m, 0.30 m, 0.26 m, 0.22m. The bore heights for these solitary wave heights in the 1m water depth are 0.293 m, 0.278 m, 0.257 m, 0.226m and 0.186 m, respectively.

Figure 4.6 indicated the comparison between experimental results and Fukui et al. (1963) equation for a 1 water level in the location of H6. The solid line illustrates the bore height prediction and the circles illustrate the experimental data for the 1 water depths in the flume and 0.16 in the location of the bridge.

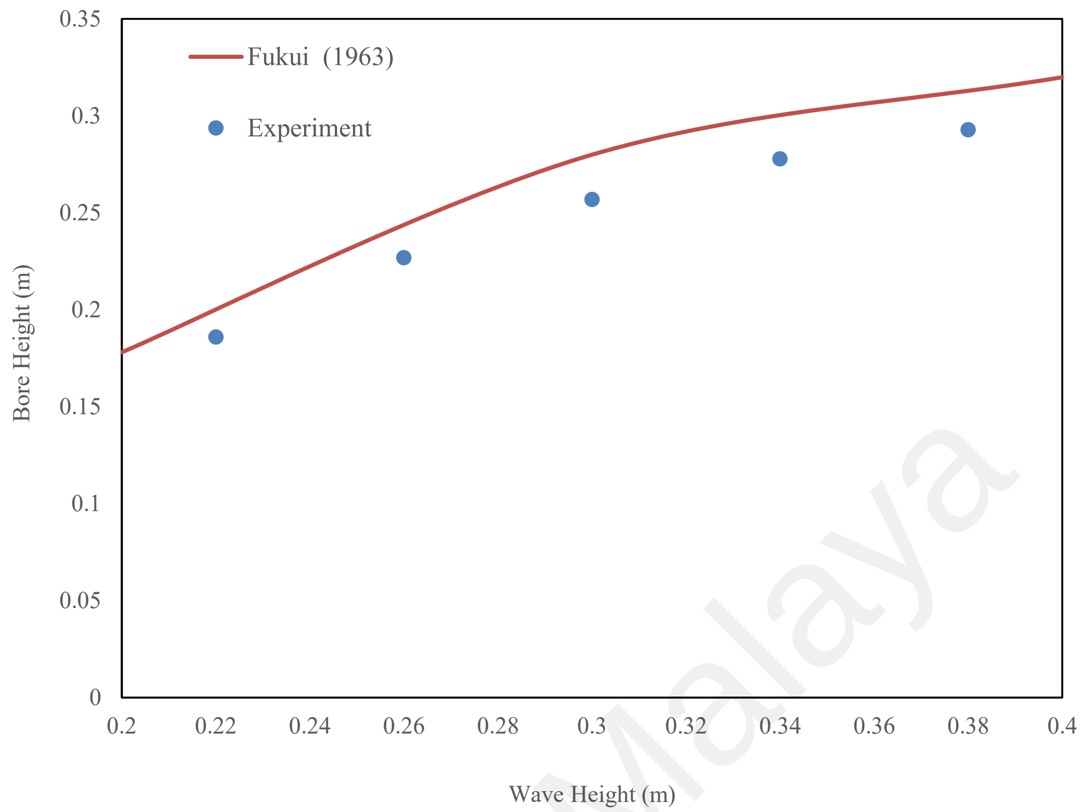

Figure 4.6: Comparison between bore height and Fukui et al. (1963)

Figure 4.6 shows that Fukui et al. (1963) predict the bore height reasonably well when bore velocity was available. There was a slight difference between the numerical and experimental results, which was due to the difference in the applied angle to the platform. In this case, the lower bore height is in slightly better agreement with the numerical approach.

4.3 Bore and Velocity Characteristic

In this section the bore and velocity characteristic in the location of the bridge is evaluated in which the bridge model is not installed on platform. This location was 19.09 m from wave generator,. Figure 4.7 (a-e) and Figure 4.8 (a-e) illustrated the time history of the bore height and velocity in the location of the bridge in five various wave heights, which were 0.38 m, 0.34 m, 0.30 m, 0.26 m, 0.22m applied in water depths 1 m and 0.95 m, respectively. A smooth variation can be observed from these figures.

In these figures and the following discussion, the moment when the wave first attacks the bridge model is taken as time as illustrated in the result. Note that time t=0 of the time series may not certainly state the time at which the experiments are begun. It is worth mentioning that the leading side of the wave achieves essentially the highest velocity and then quickly attains the location of the bridge model while the bore elevation is quite small. As the wave rises in height, the velocity reduces notably, so the greatest wave elevation is obtained at the moment at which the velocity is maximum. Consequently, the highest flow velocity does not correspond with the highest wave level.

Although there are minor variations among those time histories, the overall experimental results prove that the velocity and water depth in each water depth at the location of the bridge model vary in the same trend with good consistency over time. This denotes that the experiment was carried out in a well-controlled manner and the results are reproducible.

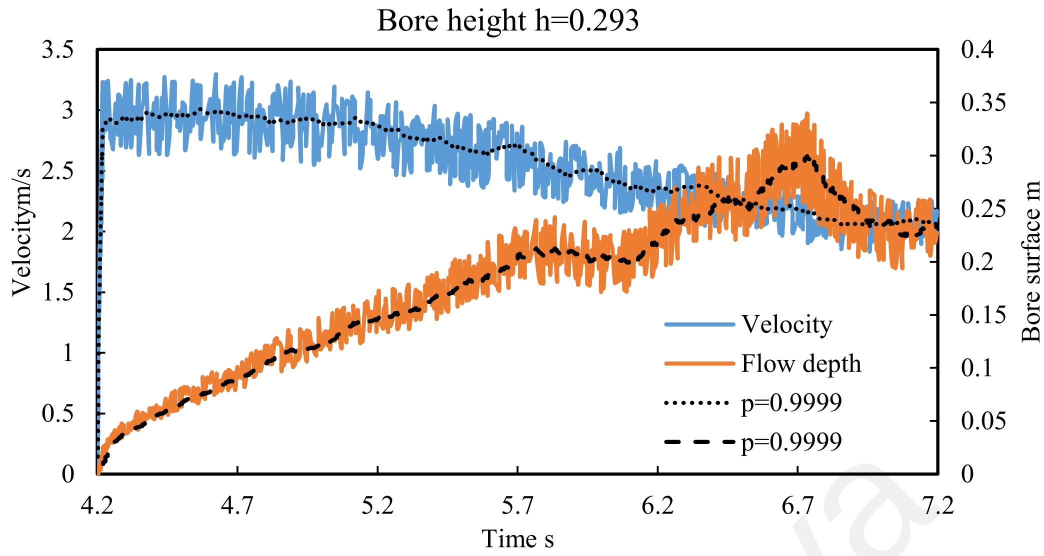

(a)

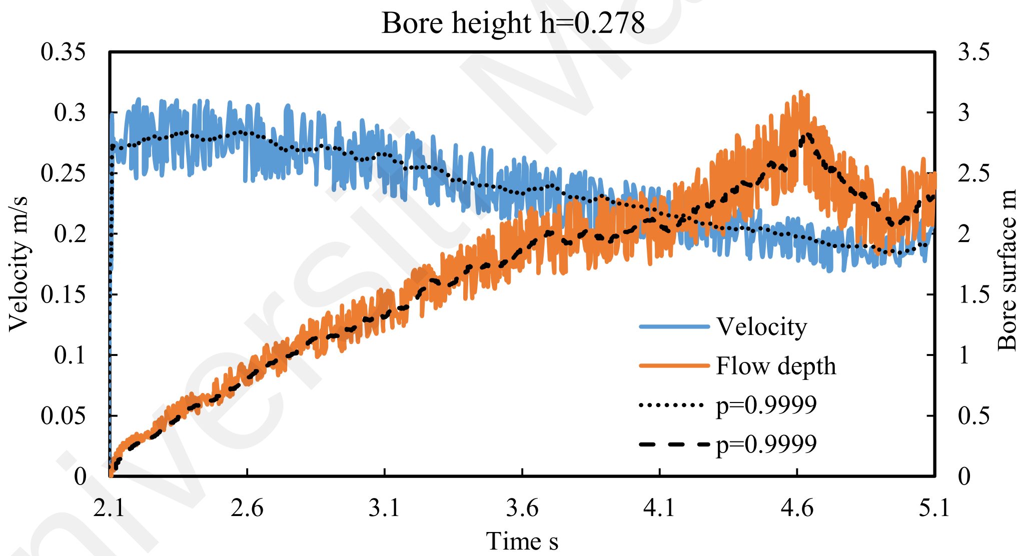

(b)

Figure 4.7: Time history of flow velocity and flow depth in location of the bridge models in 1m water level, a) 0.38 m wave height, b) 0.34 m wave height, c) 0.30 m wave height, d) 0.26 m wave height e) 0.24 m wave height

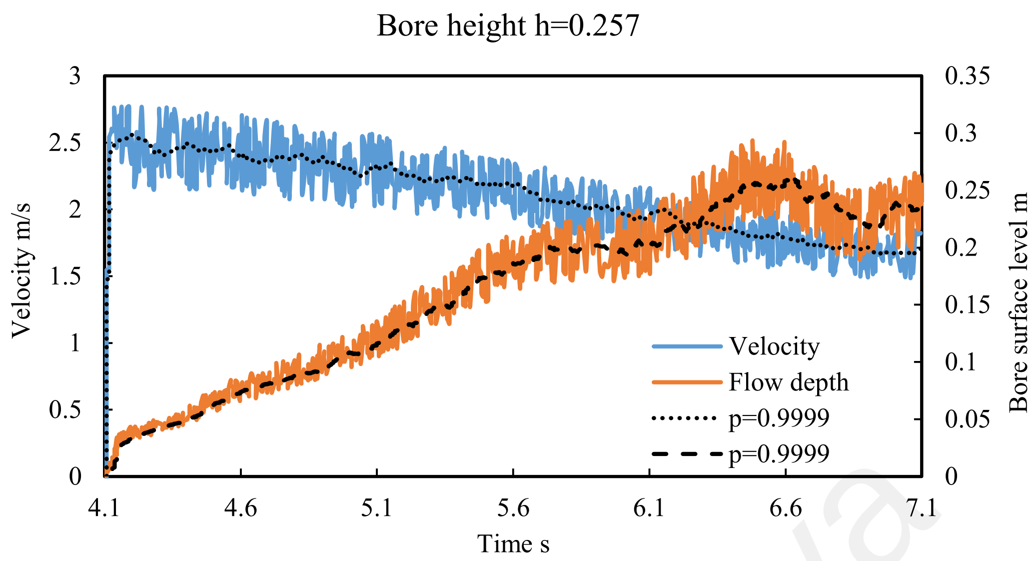

(c)

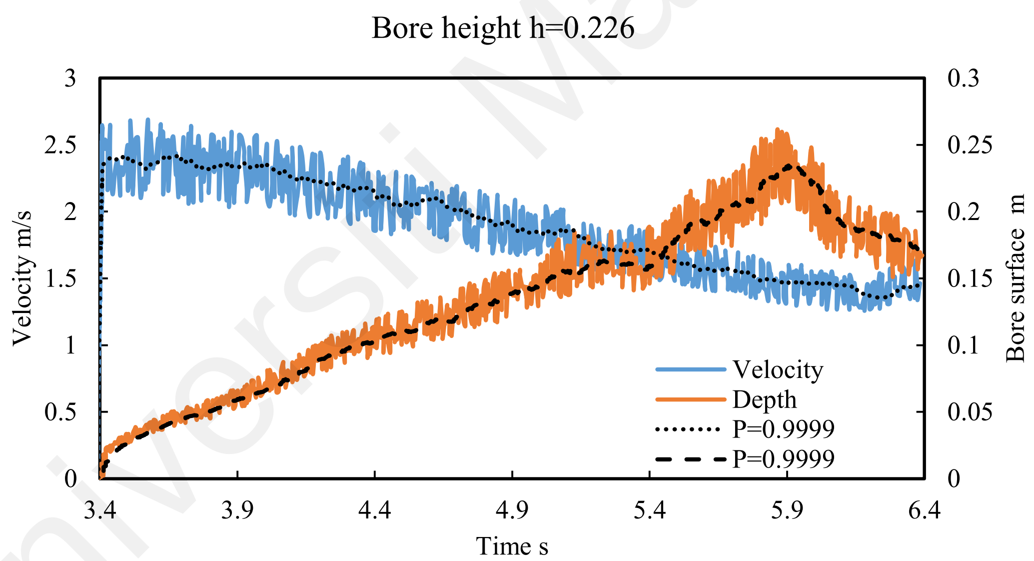

(d)

Figure 4.7: Time history of flow velocity and flow depth in location of the bridge models in 1m water level, a) 0.38 m wave height, b) 0.34 m wave height, c) 0.30 m wave height, d) 0.26 m wave height e) 0.24 m wave height (continued)

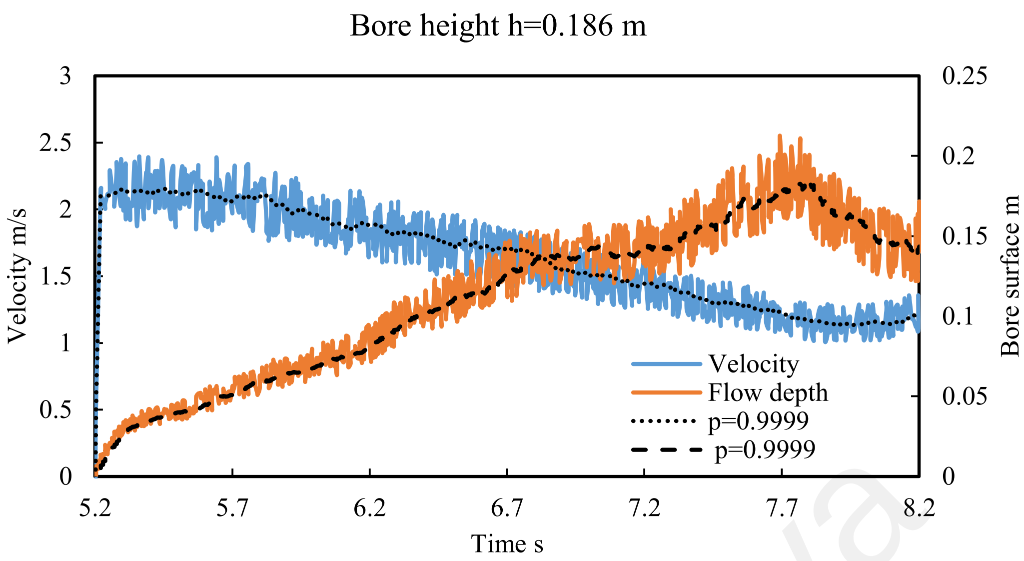

(e)

Figure 4.7: Time history of flow velocity and flow depth in location of the bridge models in 1m water level, a) 0.38 m wave height, b) 0.34 m wave height, c) 0.30 m wave height, d) 0.26 m wave height e) 0.24 m wave height (continued).

Although the solitary wave height increases linearly, this improvement is not linear in bore height. The bore height between subsequent bore increases with decrease in wave height. This is explained by the fact of complex interaction of breaking wave in shallow water in that the large waves have more energy, are steeper, and thus tend to break slightly closer to bridge model than the small ones, and therefore the energy of smaller wave dissipates more that long wave (An and Cai, 2010). This is leads to decrease the bore height with decrease in solitary wave (Xiao et al., 2010).

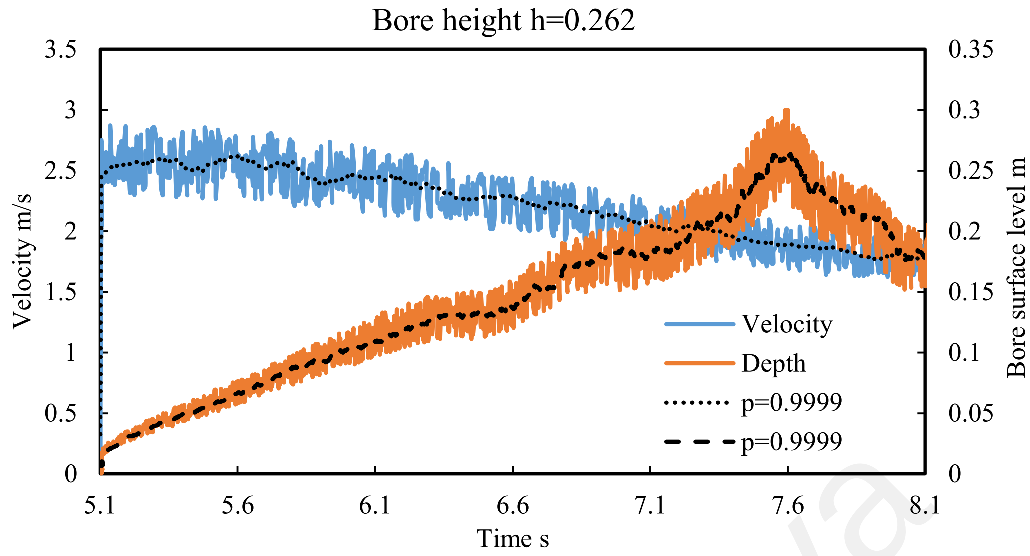

(a)

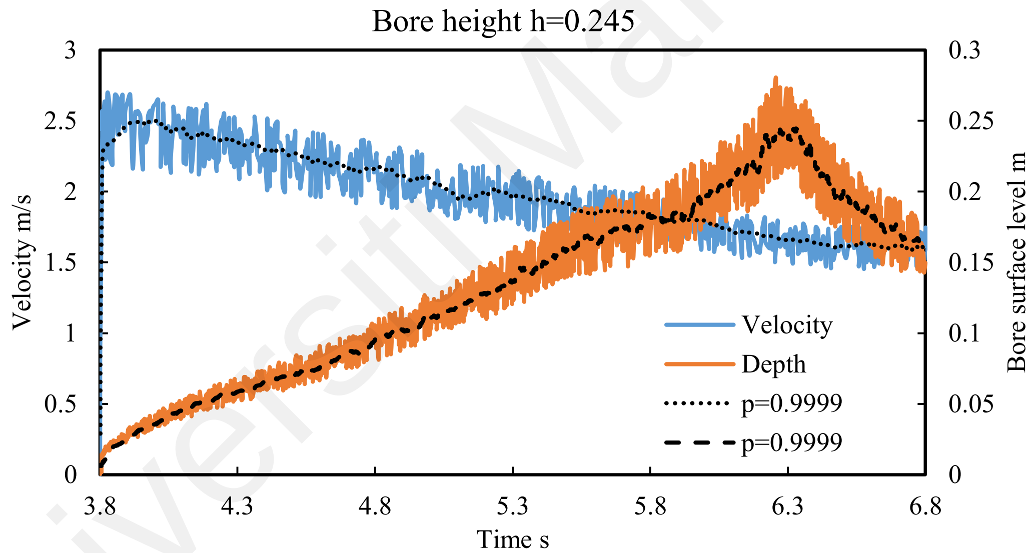

(b)

Figure 4.8:Time history of flow velocity and flow depth in location of the bridge models in 0.95 m water level a) 0.38 m wave height, b) 0.34 m wave height, c) 0.30 m wave height, d) 0.26 m wave height e) 0.24 m wave height

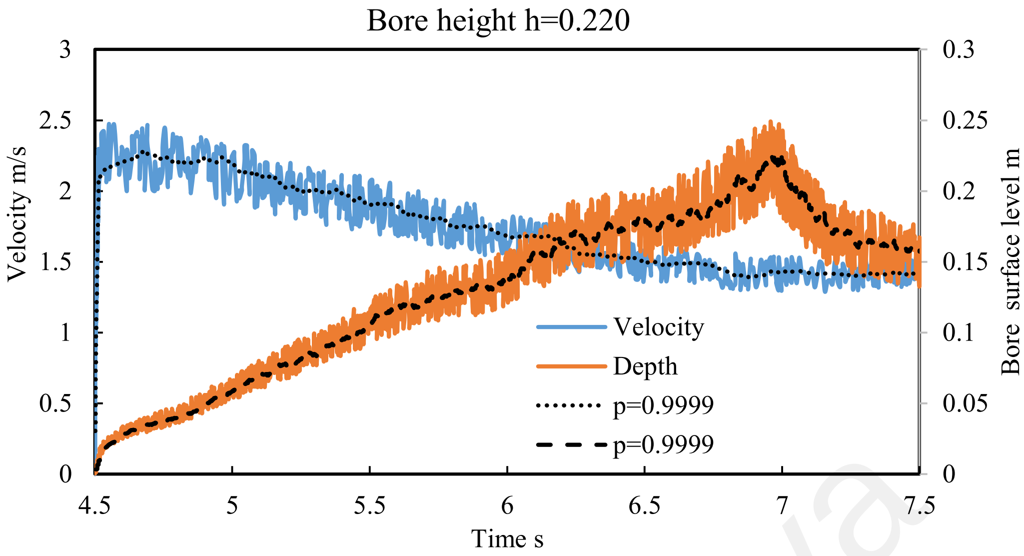

(c)

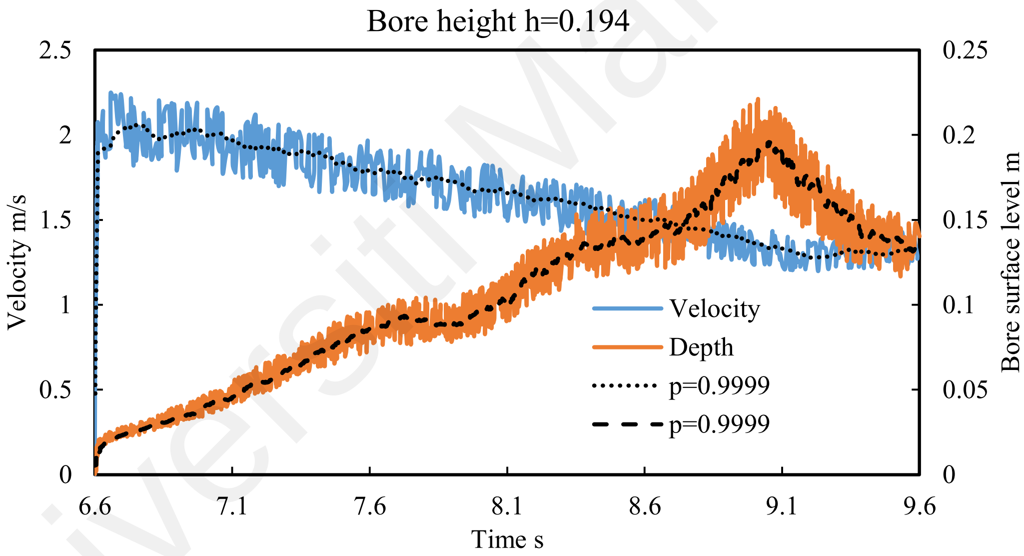

(d)

Figure 4.8:Time history of flow velocity and flow depth in location of the bridge models in 0.95 m water level a) 0.38 m wave height, b) 0.34 m wave height, c) 0.30 m wave height, d) 0.26 m wave height e) 0.24 m wave height (continued)

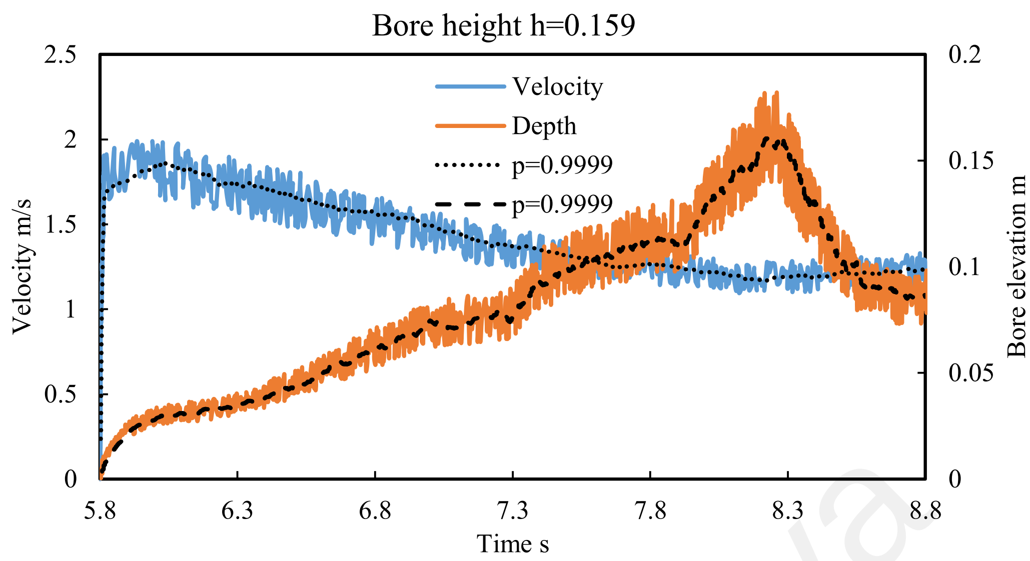

(e)

Figure 4.8:Time history of flow velocity and flow depth in location of the bridge models in 0.95 m water level a) 0.38 m wave height, b) 0.34 m wave height, c) 0.30 m wave height, d) 0.26 m wave height e) 0.24 m wave height (continued)

Comparison of the result of velocity in Figure 4.7 and Figure 4.8 indicated that although the initial velocity in case of 1m and 0.95 meters water depth had slight differences, this difference would be more significant in the location of the bridge. The variance between the velocity in the 1 m water depth and 0.95 m in the position the bridge reduce with reduction of wave height. We observe in these figures a substantial difference in the behaviour and height of bore on different shallow water of the same solitary wave heights. This is proof of the effect of shallow water on bore height when a wave breaks in shore condition. Furthermore, the figures also show the effect of shallow water on bore height, where increase in the shallow water in the location of the breaking bore results in increase in turbulent bore height. This is in contrast with the breaking bore in dry bed (Manawasekara, 2013a).

Figure 4.9 shows correlation between waves and bore in water depth 1 m and water depth 0.95 m in the beach slope PB3. As shown in this figure, with increase in the bore height, the bore velocity increased with y = 9.5118x - 0.6456 and R^2 = 0.9941 in 1 m and in 0.95 water depth, $R^2 = 0.9189$ and the equation between wave height and bore height was $y = 6.4297x + 0.1048$.

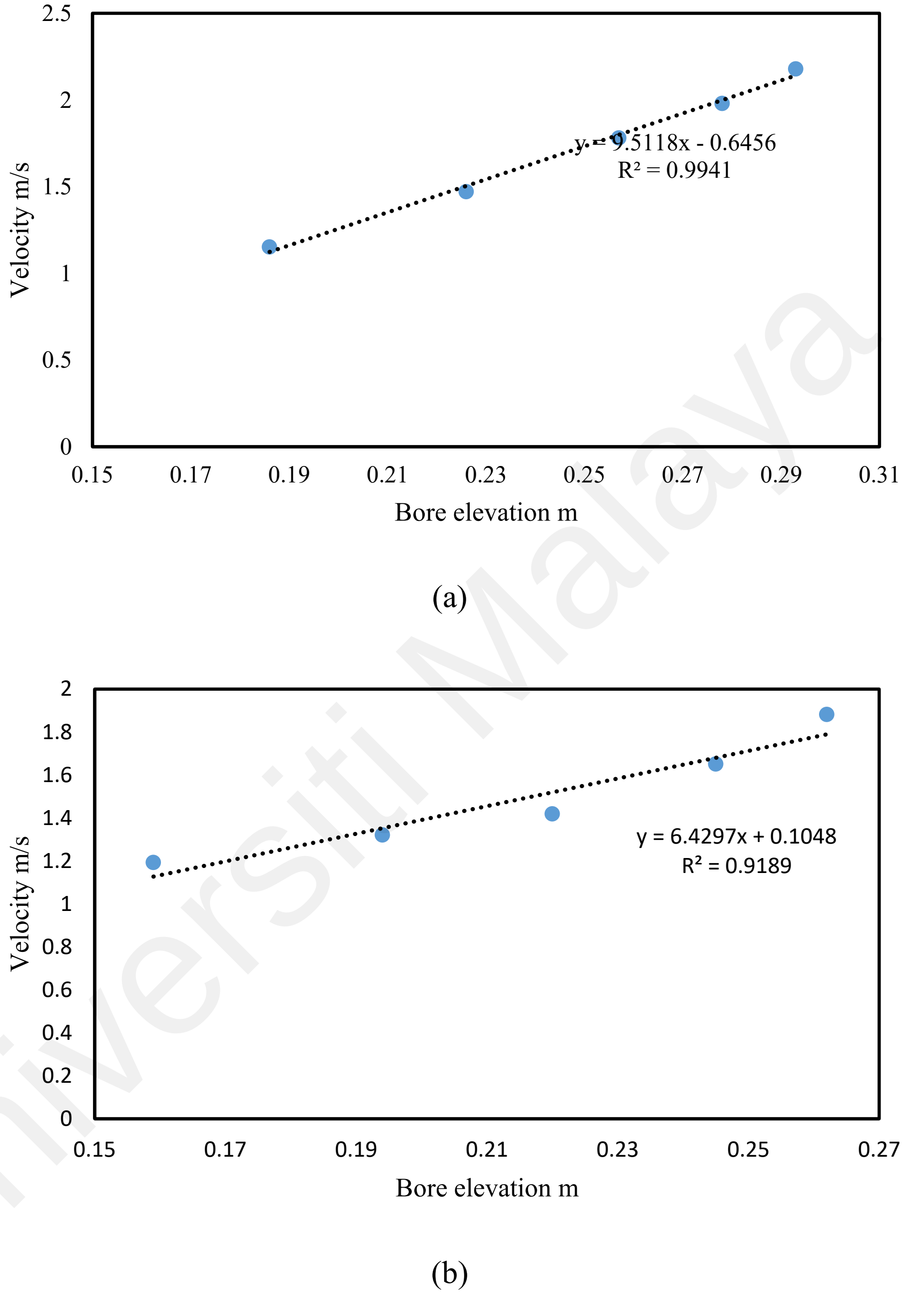

Figure 4.9: Correlation between velocity and bore (a) water depth 1 m and platform PB3, (b) water depth 0.95 m and platform PB3

In order to estimate the Froude number for each time step, Equation 4.3 is applied.

$$Fr = \frac{V}{\sqrt{gL}} \tag{4.3}$$

where V is velocity and L is depth and g is the gravitational acceleration. In this equation, L is the accumulation of bore height η_b and shallow water h in the location of the bridge, which was 0.16 and 0.11 m in 1 m and 0.95 m, respectively.

Figure 4.10 presented value of estimation of Froude number. From this figure, during the initial impact, high Froude number values can be detected due to lower flow depth and greater velocities, which reduce after some time while flow velocity decreases and flow depth raises. Value of the Froude number continues to reduce further as flow depth and velocity decrease with time. From the figure it is shown that, although the initial velocity in 1 m depth were higher than 0.95, the shallow water in the location of the bridge in 0.95 m was 0.05 meter lower that 1 m depth. This lead to decrease the value of Froude in 0.95 m water depth. Consequently, there were no significant differences between the two cases.

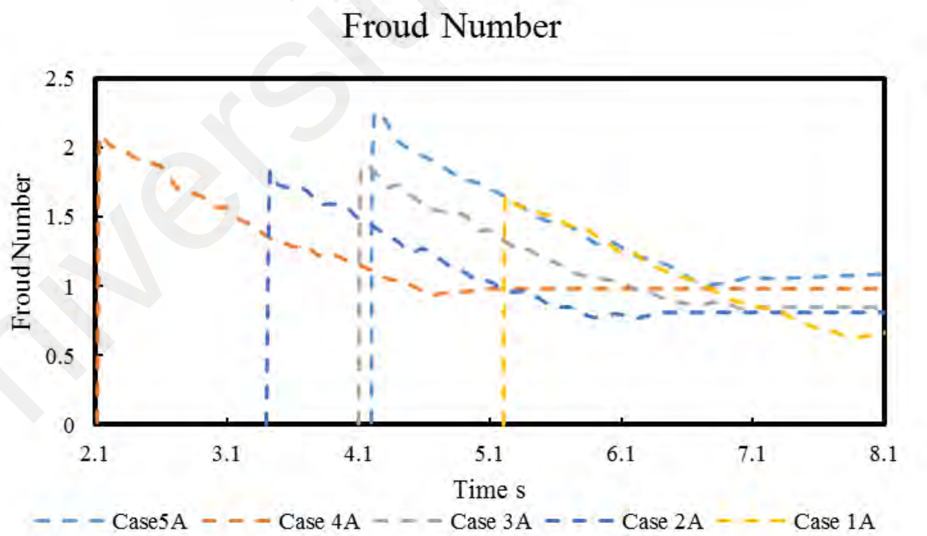

(a)

Figure 4.10: Estimation of Froude number (a) water depth 1 m and platform PB3, (b) water depth 0.95 m and platform PB3

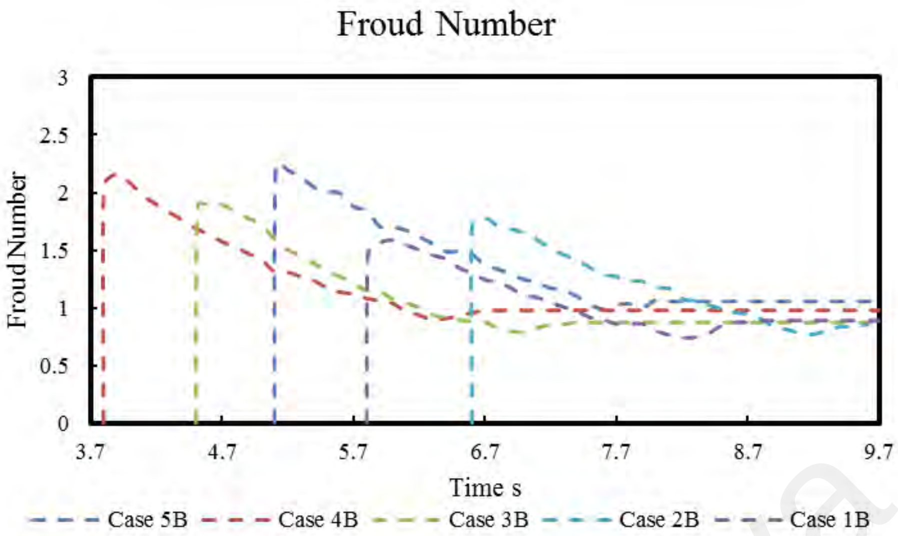

(b)

Figure 4.10: Estimation of Froude number (a) water depth 1 m and platform PB3, (b) water depth 0.95 m and platform PB3 (continue)

4.4 Tsunami load evaluation on bridge Models

The overall tsunami load on a proposed bridge model is evaluated as individual components i.e. horizontal, vertical and impact forces and overturning moment. The horizontal element behaves perpendicularly at the centre of gravity of the bridge pier whereas the vertical element acts in upward and downward orientations at the centre of gravity of the complete bridge against the tsunami bore flow. However, the overturning moment is evaluated about the centre of gravity of the bridge model in the pier location. In this research, similar to the research by Seiffert et al. (2014), the total amounts of the horizontal (Fx), uplift (Fz) forces and overturning moment (My) on the bridge model are normalized by two-dimensional forms as given by the following equations 4.4- 4.6:

$$F_X = \frac{\| f_X \|}{l_s (t_D + t_B + t_p)} \tag{4.4}$$

$$F_z = \frac{\| f_z \|}{l_s} \tag{4.5}$$

$$M_y = \frac{\| M_y \|}{l_s} \tag{4.6}$$

where $l_s$is span length, $t_D$is deck thickness, $t_B$is the height of the girder and t_P is height of pier. f_x and f_z are maximum and minimum value of horizontal and uplift forces, respectively. These parameters are illustrated in Table 3.3.

In this research, due to the lower values of negative forces, the effects of negative horizontal and vertical forces were neglected. In the experiment, in all cases, each test was replicated five times and after eliminating the highest and lowest values, the average was presented in the results section. This procedure ensures the repeatability and reliability of the experiment giving errors of below 4.5 %, which is acceptable.

4.4.1 Bridge Model A

Experimental results for two different water depths i.e. 1m and 0.95 for horizontal, uplift force and overturning moment for Bridge Model A are shown in Figure 4.11, Figure 4.12, Figure 4.13 respectively. As illustrated by these results (Figures 4.1-4.3), the largest horizontal force, uplift force and overturning moment appeared in larger wave heights and water depths.

Figure 4.11: Horizontal bore force in the 1 m and 0.95 m water depth

Figure 4.11 illustrates the normalized maximum horizontal force on the bridge model for five different tsunami wave heights and two water depths. In this figure, the horizontal force was normalized by Equation 4.1. The result shows that maximum horizontal force occurred in the highest wave height (0.38 m) and deepest shallow water (h=0.16 m) with 2018.75 N/m^2. In both shallow waters, the highest horizontal force occurred at the larger wave height and bore height. In the case of 1 m water depth, the horizontal force fluctuated between 0.38 m and 0.22 m, which was around 120 percent of the lower wave height. In the case of 0.95 m water depth, the horizontal fluctuation between highest and lowest wave height was around 240 percent of lower horizontal force. This means that in the case of less shallow water, the increase of wave height increased the horizontal force more than in the case of more shallow water. However, the value of horizontal force in the case of more shallow water was much larger than the case of 0.11 m shallow water (0.95 water depth). The increase in horizontal force in the case of 1m water depth in 0.26

m water depth and 0.3 m water depth was very gradual. However, between wave heights of 0.3 to 0.34 m, the increase was sharp. The results also demonstrated that the increase of the horizontal load in both cases was nonlinear.

Figure 4.12 shows the experimental results of uplift forces on the bridge model. As mentioned in Equation 4.2, uplift force was normalized by dividing the uplift force by the span length. The highest uplift force of 594.95 N/m occurred at the largest wave height and deeper shallow water, which is similar to the horizontal force. The results also illustrated that uplift force increased with increasing wave height and shallow water. However, these increases, such as the horizontal force, were not linear. In the case of 1 m water depth, uplift force sharply increased by raising the wave height from 0.22 to 0.26 m. However, from 0.26 to 0.38 m wave height uplift force increased more gradually. As illustrated by the experimental results, for both water depth cases, variation between uplift forces between 1 m water depth and 0.95 m water depth increased by increasing the wave height.

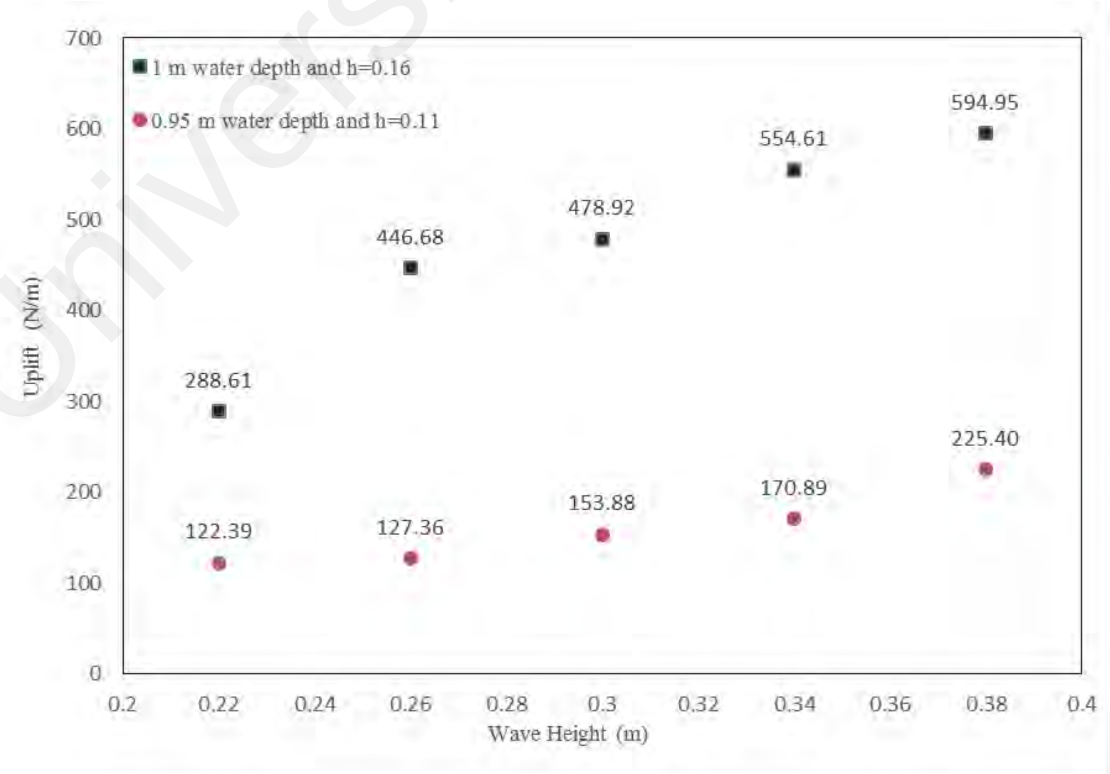

Figure 4.12: Uplift force in the 1 m and 0.95 m water depth

Figure 4.13 shows the overturning moment increasing with increasing wave heights and water depths. In this case, forces such as horizontal load and uplift load and higher overturning moment occurred at larger wave height. Comparing the case of 1 m and 0.95 m water depths, it is seen that in the case of lower shallow water, the overturning moment increases more gradually than higher shallow water. This behaviour may relate to the fact that in the deeper shallow water, increasing the wave height leads to more enhanced impact force due to splashing water on the bridge model. As presented in the results (Figure 4.11-13), the largest horizontal force, uplift force and overturning moment appeared in higher wave height and deeper shallow water.

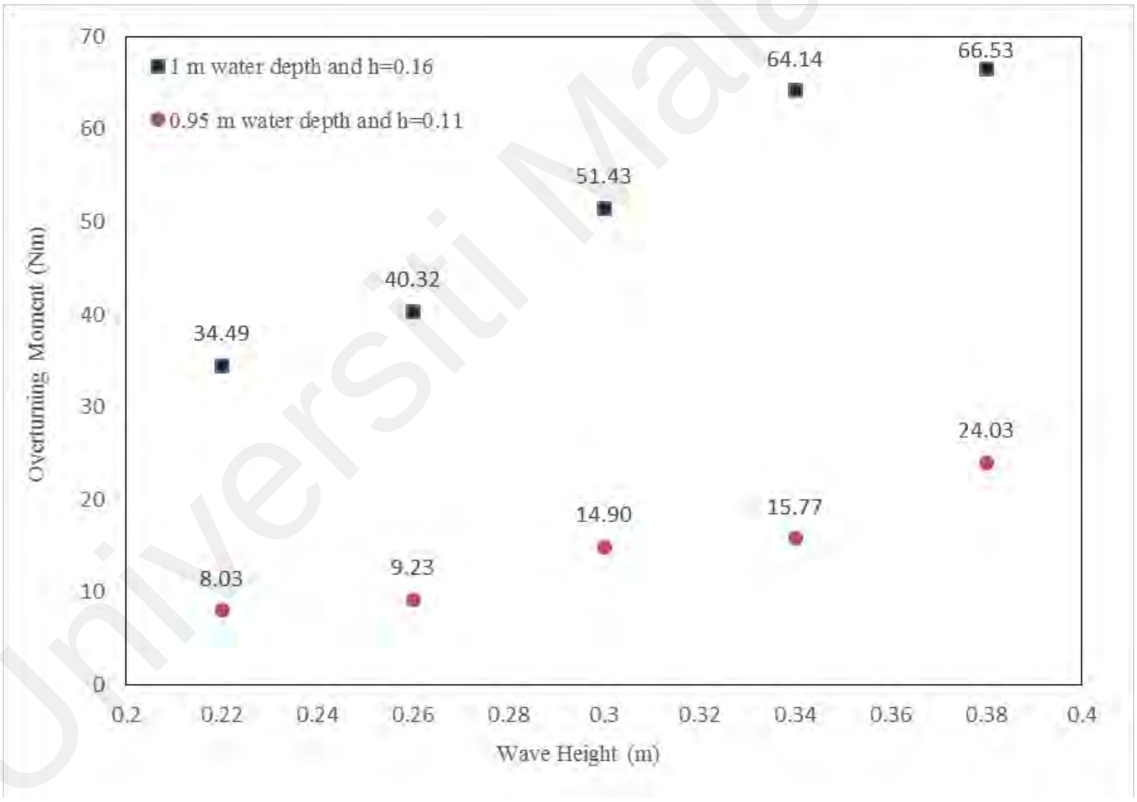

Figure 4.13: Overturning moment in the 1 m and 0.95 m water depth

The values of horizontal forces in Figure 4.11 are much higher than uplift forces in Figure 4.12. This is due to the normalization process of these loads. This relates to Equations 4.1 and 4.2, where Equation 4.1 normalizes the horizontal force by dividing the total height of the bridge multiplied by the bridge width. In contrast, Equation 4.2 normalizes the uplift force by dividing the horizontal force by only the span length.

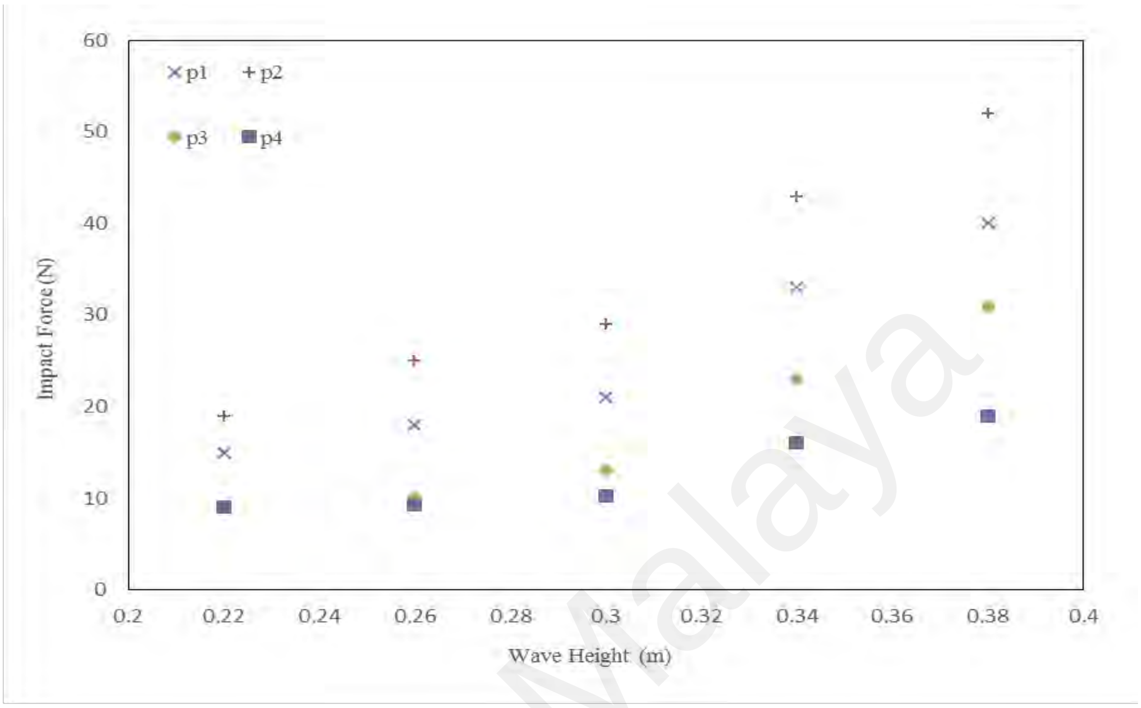

(a)

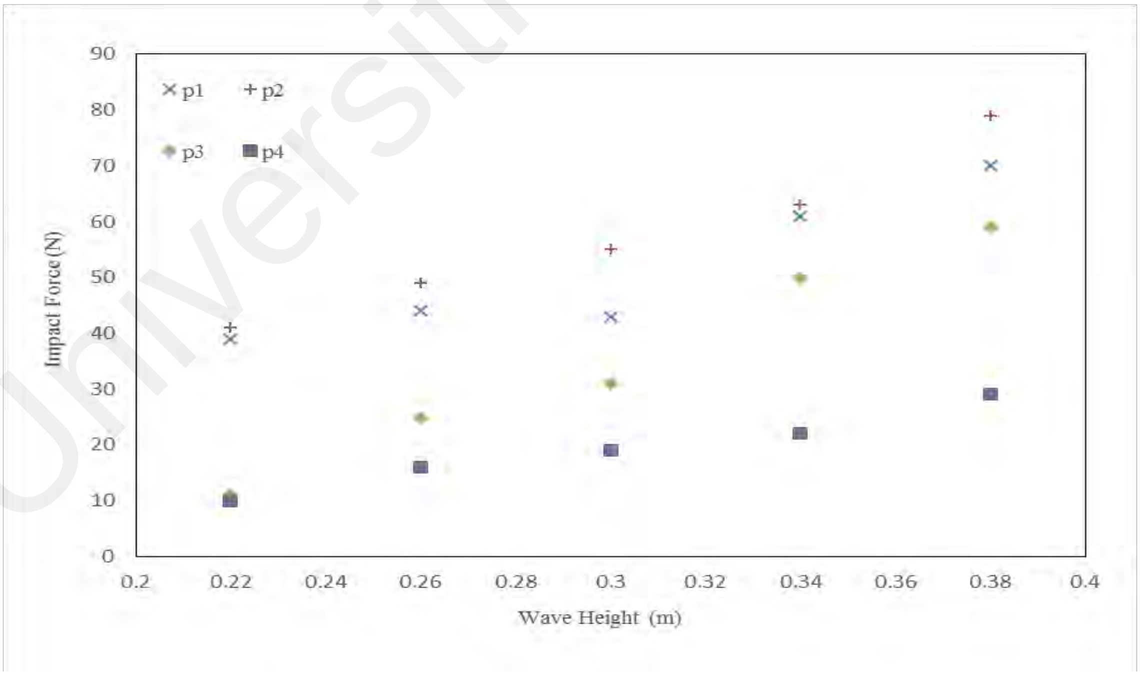

(b)

Figure 4.14: Impact load evaluation in bridge (a) Impact load at 0.95 m water depth, (b) impact load at 1 m water depth

Impact loads at four various points subject to tsunami bore are illustrated in Figure 4.14. These results were obtained from four axial load cells installed on the bridge. The results show that in this section, such as lateral load on piers, shallow water depth plays a vital role in fluctuation. The highest value occurred at P2, which is in the second part of the pier. This means that the maximum impact force occurred at the upper part of the pier on the bridge over the sea. However, the maximum impact force on the bridge in a dry bed occurs at the bottom of the bridge as presented by Lau (2009).

4.4.2 Bridge Model B

In this section, the number of girders is changed, whereas the dimensions of the deck and girders remain fixed. This is corresponding to changing the girder spacing, whereas the dimension of the deck is kept constant. The variation of the wave loads with two water depths, i.e., 1 m and 0.95 for a combination of five wave heights, are investigated.

Figure 4.15 is shown the variation of the horizontal forces with a number of girders in bridge model B in 0.95 and 1m depth.

The result in Figure 4.15 (a) shows the variation of the horizontal force in bridge model B3, B4, B5, and B6 in 0.95 m water depth. The result indicated that the more significant horizontal force occurred on higher wave height. In 0.95 m, water depth horizontal force in wave height 0.22 and 0.26 are almost in the same range, and the value of the horizontal force is raised on wave height 0.30 and then gradually increased on higher wave height. In a comparison of the number of girders in 0.95 m water depth, the horizontal force stays at the same level in 0.22 m and 0.26 m water depth.

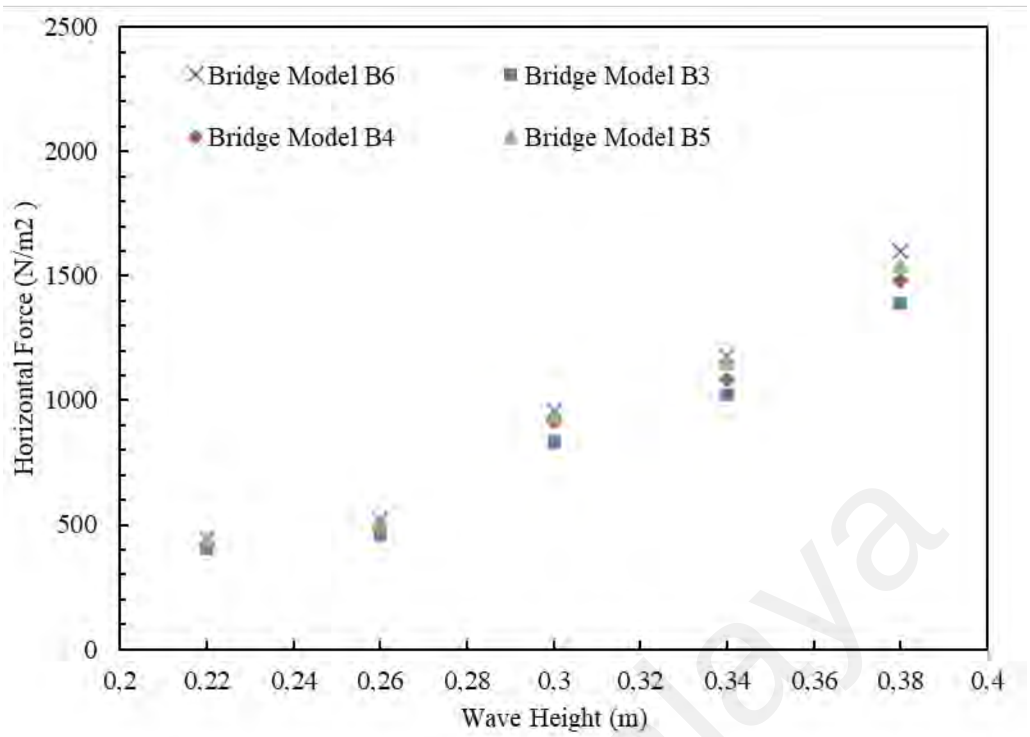

(a)

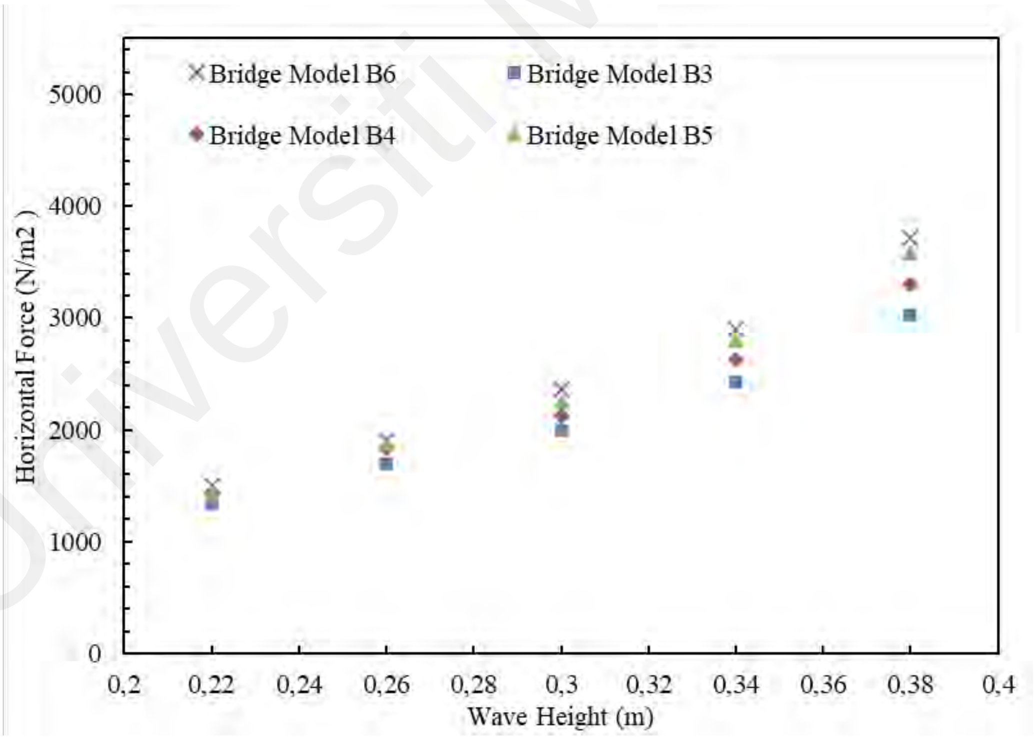

(b)

Figure 4.15: Horizontal bore force, for bridge Model B3-B6, (a) 0.95 m water depth (b) 1 m water depth

In wave height 0.30 m until 0.38, the horizontal force gradually increased by raising the number of girders from 3 to 6 girders. In 0.30 m and 0.34, the horizontal force by increasing the number of girders from 3 to 6 is grown 18 % and 19 %, respectively. However, the variation is not very significant.

The dependency of the horizontal force on the wave height is tended to be almost linear in water depth 1 m as illustrated in Figure 4.15 (b). Regarding the effect of the number of girders in water depth 1, as the wave height increases, the difference between the horizontal forces in Bridge Model B3-B6 became larger.

Such behavior, however, appears to be slightly different in the lower water depth i.e., 0.95. In both water depth, the highest variation of horizontal force has occurred on a higher wave height. Horizontal force on 0.95 water depth and 0.38 increased by 15% with increase in the number of girders from 3 to 6. Whereas, this variation in 1 m water depth was 23 %.

Uplift force at the Bridge Model B in the different wave heights and water depth 0.95 and 1m due to a tsunami wave is shown in.Figure 4. 16 and Figure 4. 17 respectively.

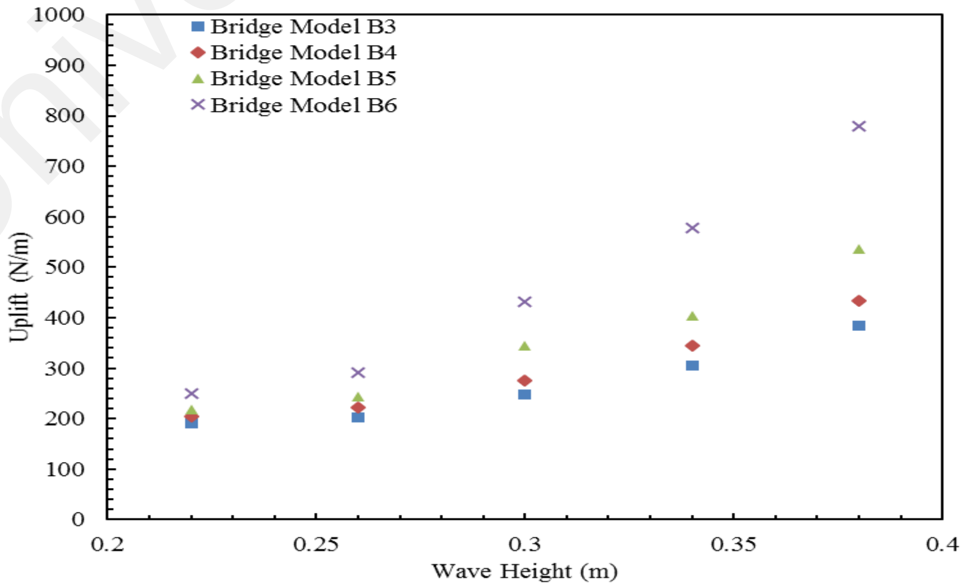

Figure 4. 16: Uplift force in the 0.95 m water depth for bridge Model B3-B6

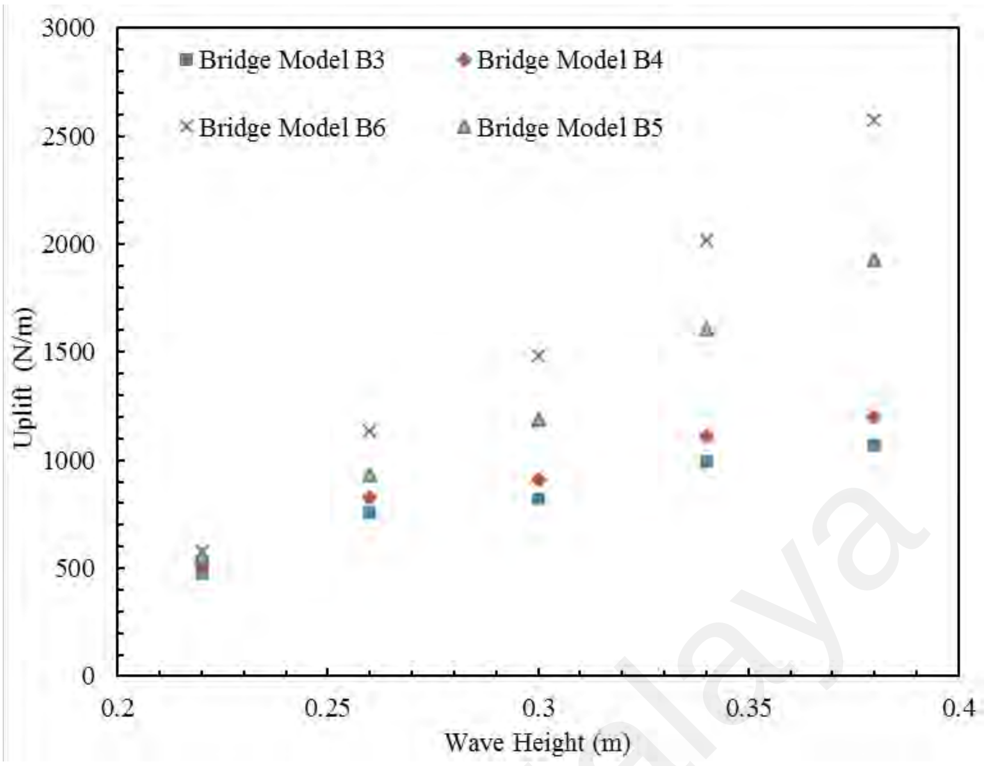

Figure 4. 17: Uplift force in the 1 m water depth for bridge Model B3-B6

As result indicated in Figure 4. 16 and Figure 4. 17, uplift significantly increased with increase in the number of girders. However, as the results indicate, the correlation of number of girders with variation of uplift force is not linear. In 0.95 m water depth, uplift rose 103 % with increase the bridge girder from 3 to 6. In 1 m water depth, this variation between Bridge Model 3 to Bridge Model 6 is increased by 140 % on wave height 0.38 m.

In 0.95 and 1 m water depths, the value of uplift force on the bridge model with 3 girders (bridge model B3) and 4 girders (bridge model B4) has not significantly increased. However, the variation of uplift increased considerably between bridge models with 5 and 6 girders (Bridge Model B5 and B6). This is due to air trapped between girders as discussed by Henry (2011) and Hayatdavoodi et al. (2014).

Overturning moment on Bridge Models B3-B6, due to tsunami waves on 0.95 m and 1 m water depths, are shown in Figure 4.18.

The variation of the overturning moment is increased rapidly as the wave height became larger. As shown, the variation of the overturning moment on the largest wave height (0.38 m) in water depth 0.95 m and 1 m is increased by 160 % and 212 %, respectively. The overturning moment is shown the highest value with Bridge Model B6 for the highest wave amplitude (0.38 m) in both cases of water depth.

In comparison, the influence space between bridge girders on horizontal and uplift forces, the result indicated that the number of girders had a greater influence on the uplift force. The uplift force in 0.34 m and 0.38 m experienced considerable variation with increasing wave heights. For linear wave conditions, the variation of horizontal force with the varying depth is almost linear.

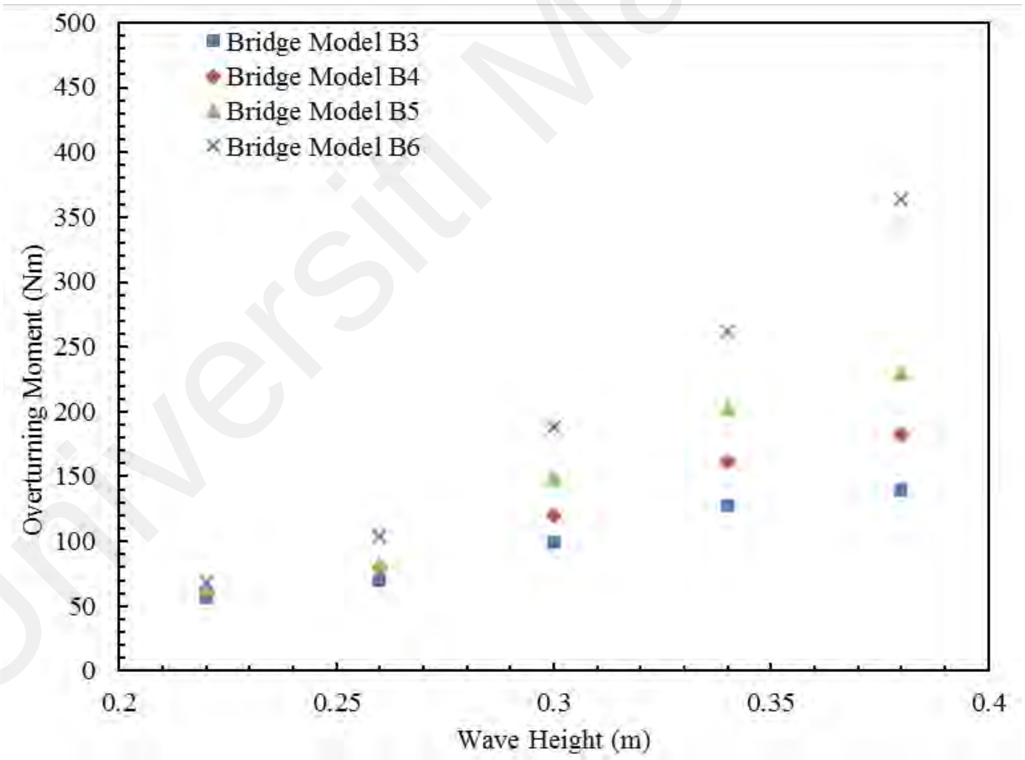

(a)

Figure 4. 18: Overturning moment for bridge Model B3-B6 (a) 0.95 m water depth, (b) 1 m water depth

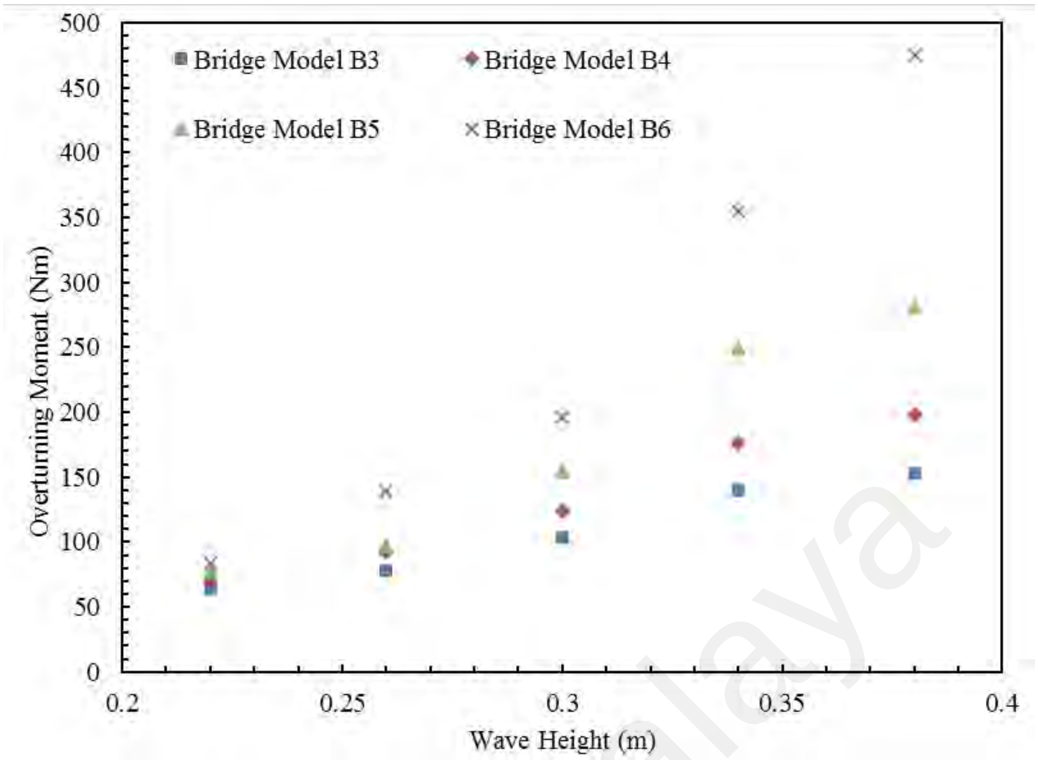

(b)

Figure 4. 18: Overturning moment for bridge Model B3-B6 (a) 0.95 m water depth, (b) 1 m water depth (continued)

4.4.3 Bridge Model C and Impact of Girder Configuration

The purpose of this section is to investigate the tsunami wave load at the Bridge model C with four different girders of various wave height i.e., in 0.38 m, 0.34 m, 0.30 m, 0.26 m, and 0.22 wave heights on 0.95 m and 1 m water depths. Furthermore, a comparison of horizontal force, uplift, and overturning moment in different wave heights and water depths between Bridge Model C and Bridge Model D with 3,4,5 and 6 girders are another objective of this section. The result is indicated in Figures 4.19 to 4.21.

The result of the horizontal force is shown in Figure 4.19; in most cases, the horizontal force is increased with a rise of wave heights. Only in 0.95 m water depth and low wave heights (0.22 m and 0.26 m) does the horizontal force not significantly improve. This means that in the case of less shallow water, the number of girders did not influence the value of horizontal force. In these cases, due to low wave amplitude, wave height had a greater effect more on piers of bridges.

The result in Figure 4.19 a-d revealed that the highest horizontal force occurred in the highest wave height and shallow water. In bridge Model C6, in 1 m water depth, the value of horizontal force is grown 150 % with an increase in the wave height from 0.22 to 0.38 m.

Result also indicated that an increase in the number of girders increased horizontal force. For instance, in 1 m water depth and 0.38 m wave height, the horizontal force grew 30 % with increasing the number of girders from 3 to 6. This is due to the horizontal component of the wave forces having more surface area to impact when the number of the girders was increased.

Comparison of horizontal force in Bridge Model B with I girder and Bridge model C with box girders presented in Figure 4.19 a-d shows that Bridge Model C with box girder experienced slightly lower horizontal force. The higher horizontal force value on Bridge Model B is due to the effect of the configuration of the I beam on the interaction of the bridge model with tsunami bore.

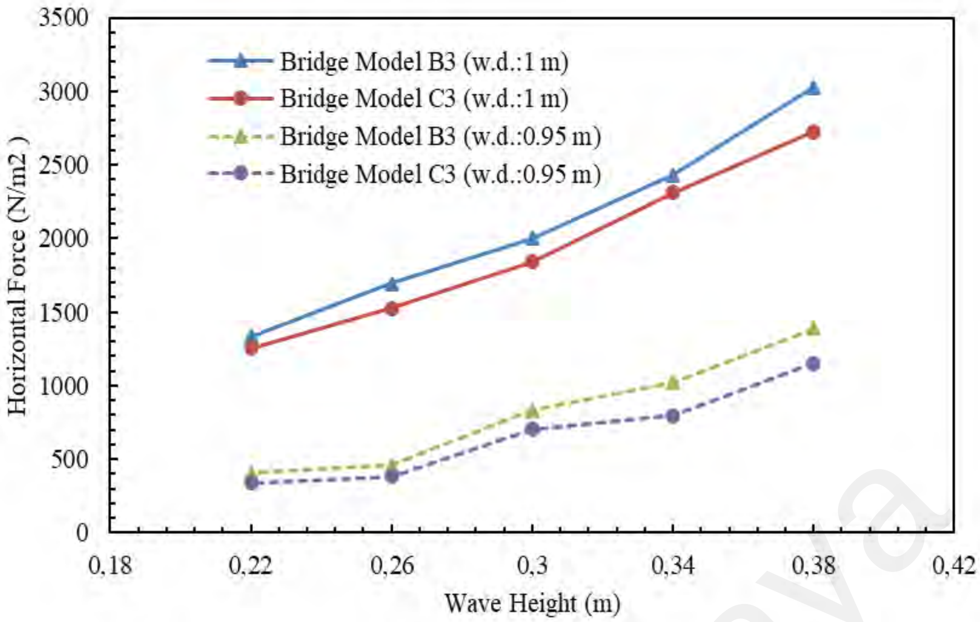

(a)

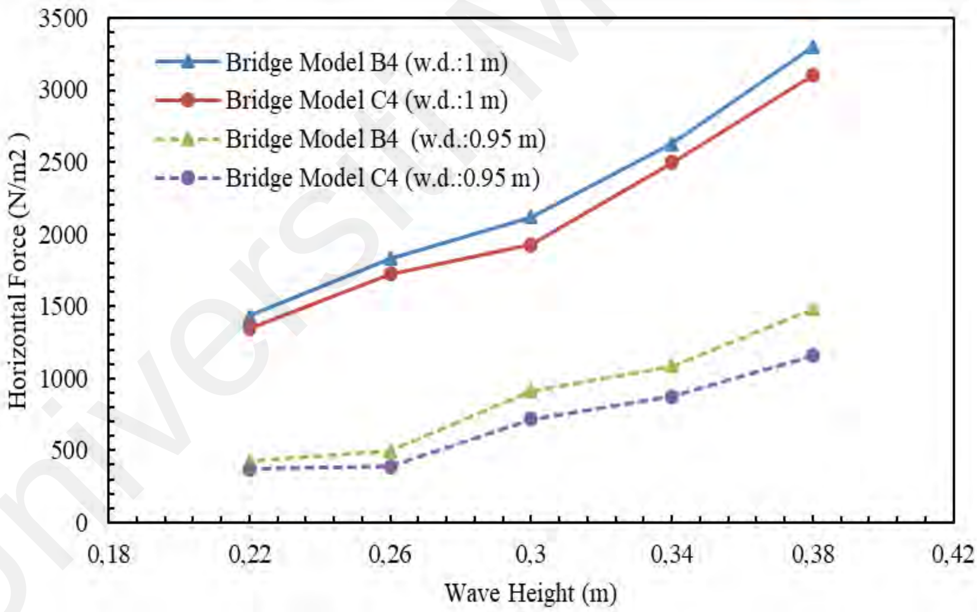

(b)

Figure 4.19: Comparison of horizontal force, number of girder and girder configuration due to various wave heights (a) Bridge models B3 and C3, (b) Bridge models B4 and C4, (c) Bridge models B5 and C5, (d) Bridge models B6 and C6

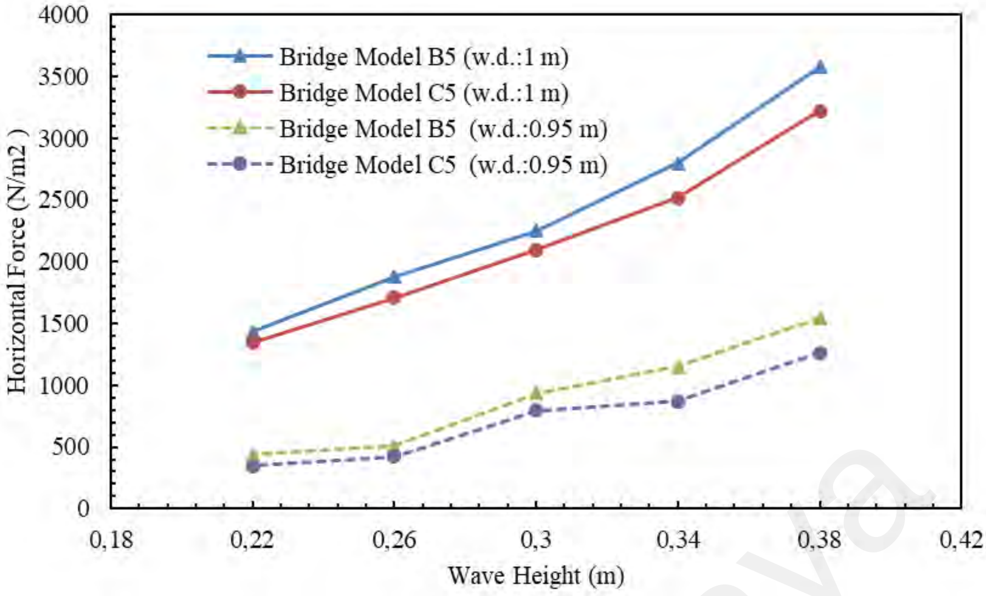

(c)

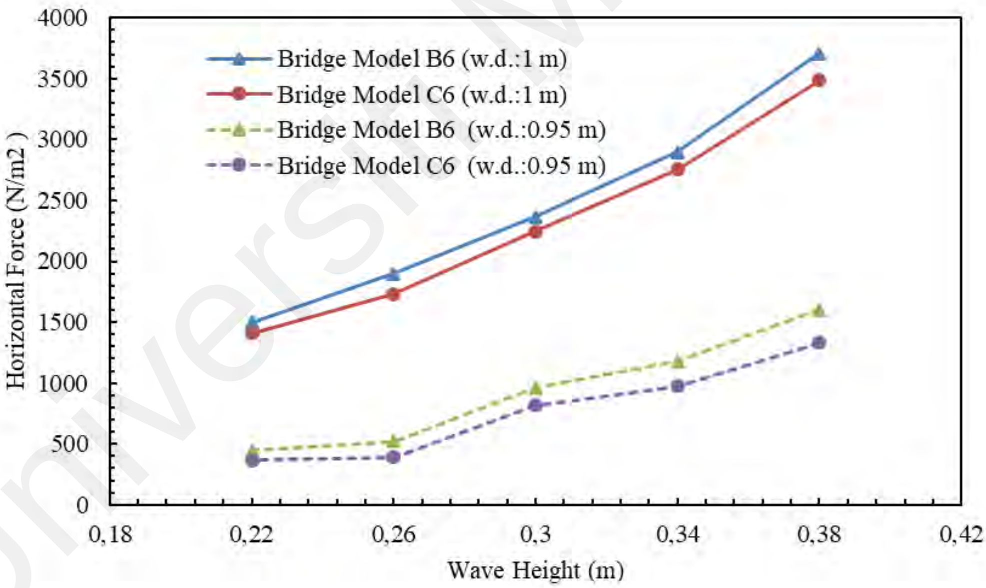

(d)

Figure 4.19 Comparison of horizontal force, number of girder and girder configuration due to various wave heights (a) Bridge models B3 and C3, (b) Bridge models B4 and C4, (c) Bridge models B5 and C5, (d) Bridge models B6 and C6 (continued)

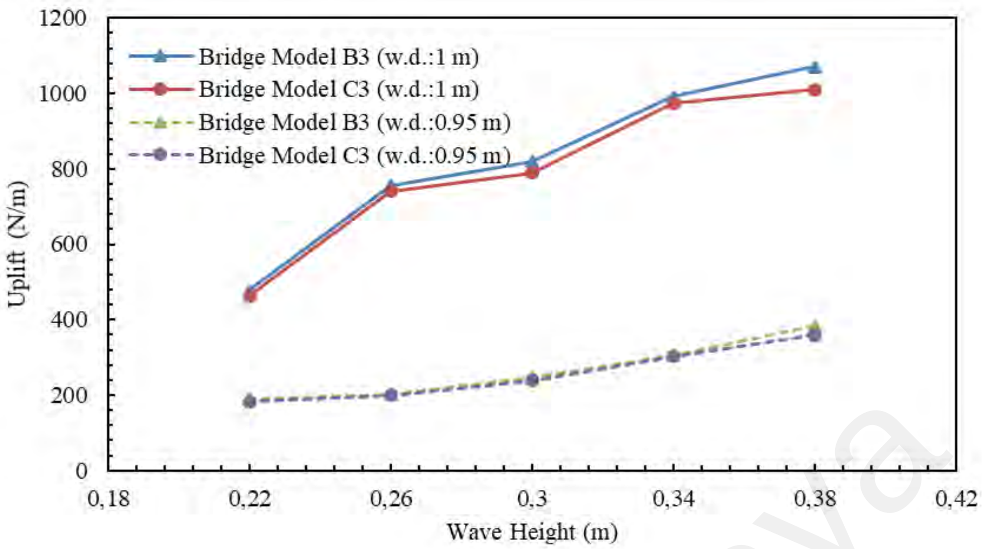

(a)

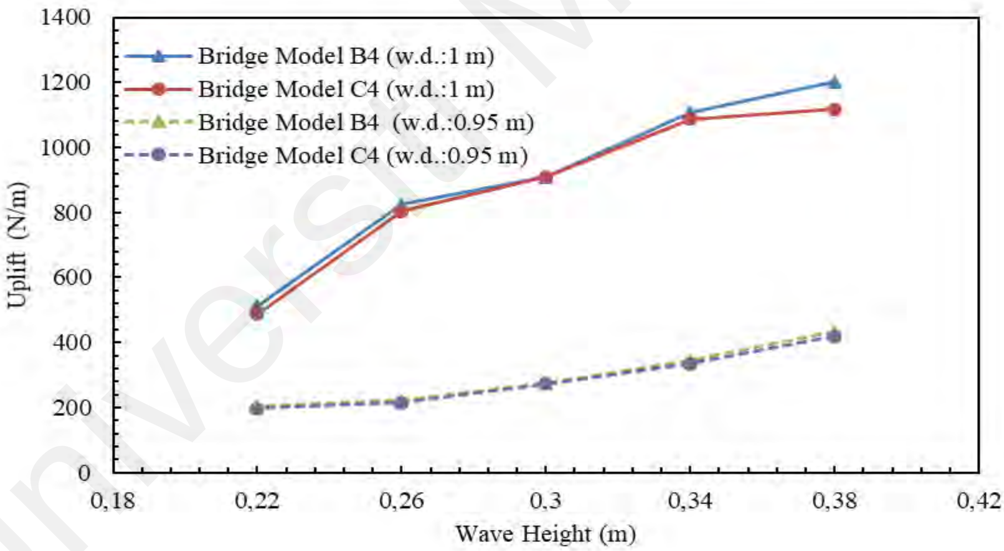

(b)

Figure 4.20: Comparison of uplift force, number of girder and girder configuration due to various wave heights (a) Bridge models B3 and C3, (b) Bridge models B4 and C4, (c) Bridge models B5 and C5, (d) Bridge models B6 and C6

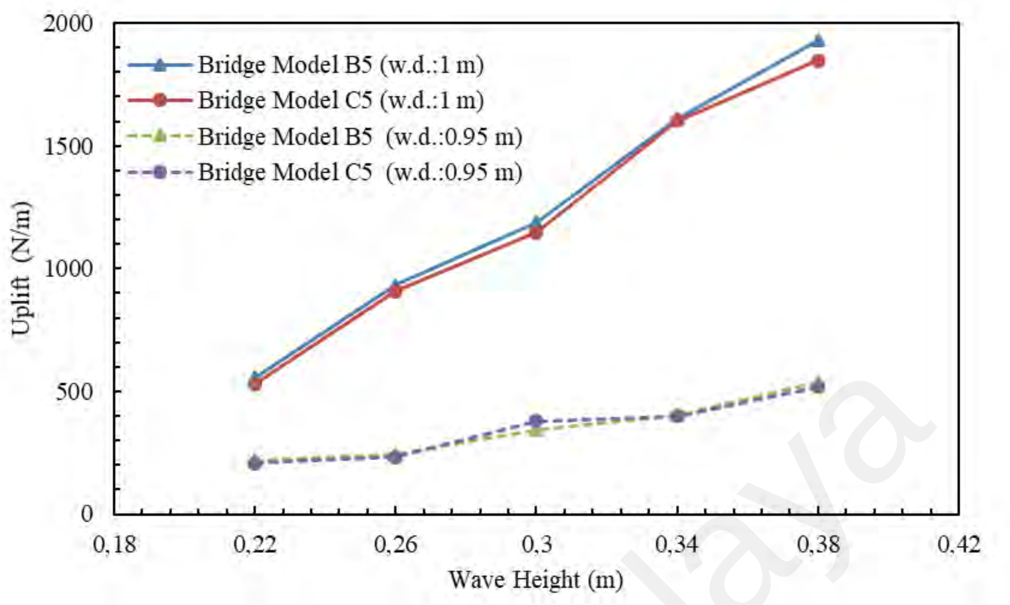

(c)

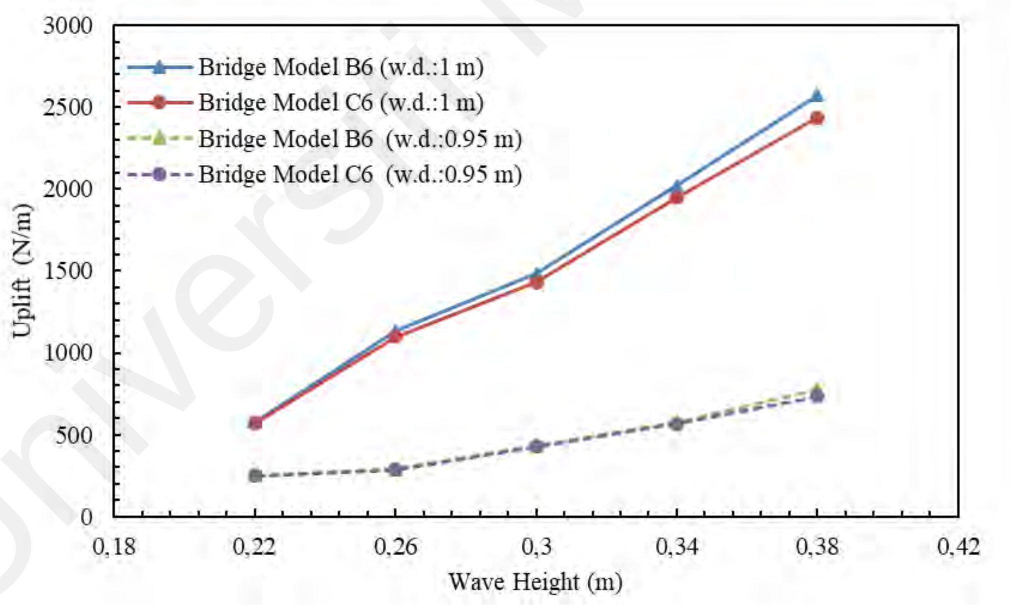

(d)

Figure 4.20: Comparison of uplift force, number of girder and girder configuration due to various wave heights (a) Bridge models B3 and C3, (b) Bridge models B4 and C4, (c) Bridge models B5 and C5, (d) Bridge models B6 and C6 (continued)

As shown in Figure 4.20, the uplift force appears to be dependent on water depth and wave height. In 0.95 m, the uplift force on Bridge Model C6 with raising weight height from 0.22 m to 0.38 m uplift is grown by 200 %. In this bridge model and higher shallow water (1 m), the variation of uplift significantly increased by 320 %.

The number of girders is notably influenced by uplift force. Increasing the number of girders on bridge models significantly increased uplift. However, this variation depended on wave conditions and shallow water.

In the case of 0.95 m and low wave height, raising the girder number only improved uplift by 35 %, but in higher wave height (for example, 0.38), increasing the girder to improve the uplift by 100 %.

The uplift in the case of 1.0 m with increasing the number of girders in the case of Bridge Model C improved up to 140 %, which is considerably higher than in the previous cases. Increasing the number of girders substantially increases the air trapped between girders. This led to a dramatic increase in the value of the uplift. This is similar to finding on wave load by Hayatdavoodi et al. (2014).

In addition, a comparison of the result of uplift on Bridge Model B and Bridge Model C proved that the uplift is almost independent of the girder configuration.

The flange part of I girder in Bridge Model B is equal with the bottom part of the box girder in Bridge Model C. This may provide an equal surface on the contact of the water. Only in case of 0.38 m wave height and 1 m depth does the uplift slightly drop in Model C. This is because of the very extreme turbulence condition of the wave on higher wave height.

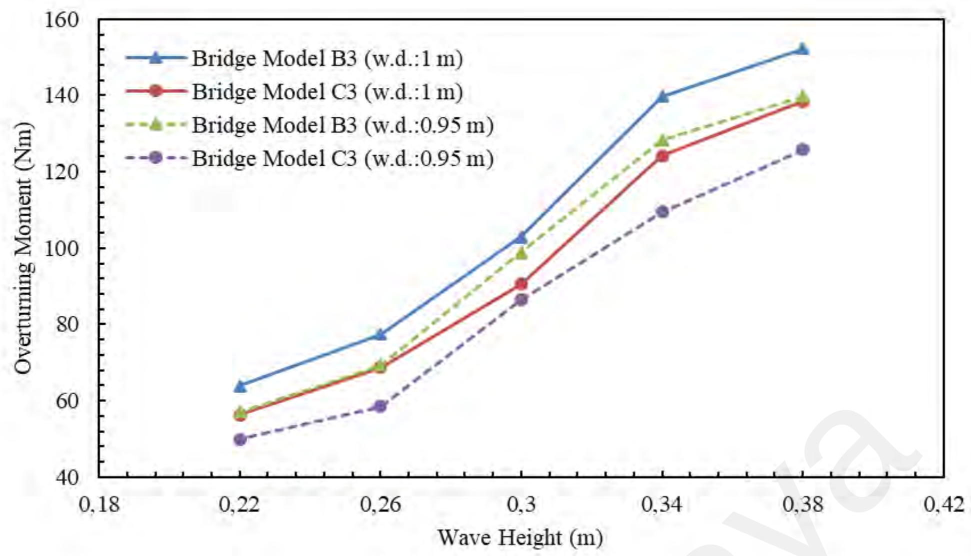

(a)

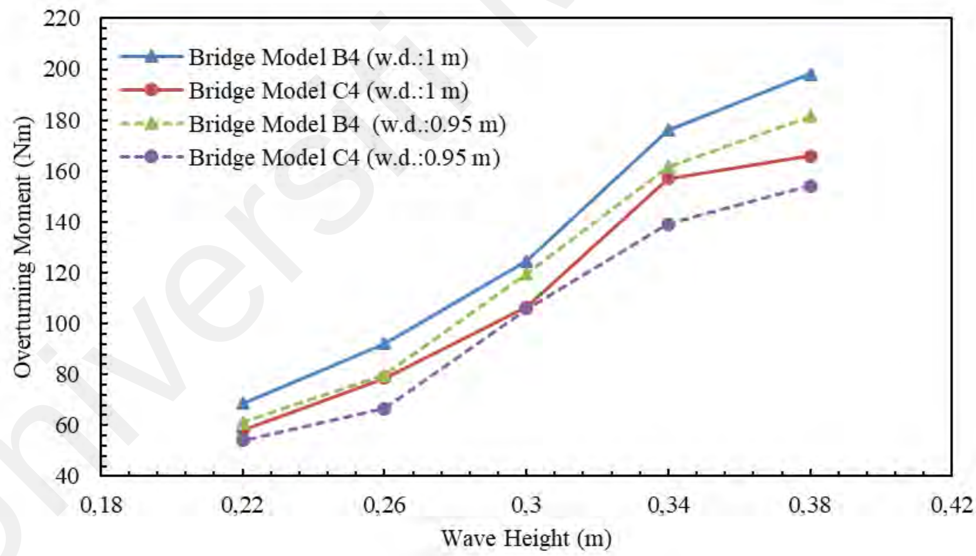

(b)

Figure 4.21: Comparison of the overturning moment, number of girder and girder configuration due to various wave heights (a) Bridge models B3 and C3, (b) Bridge models B4 and C4, (c) Bridge models B5 and C5, (d) Bridge models B6 and C6

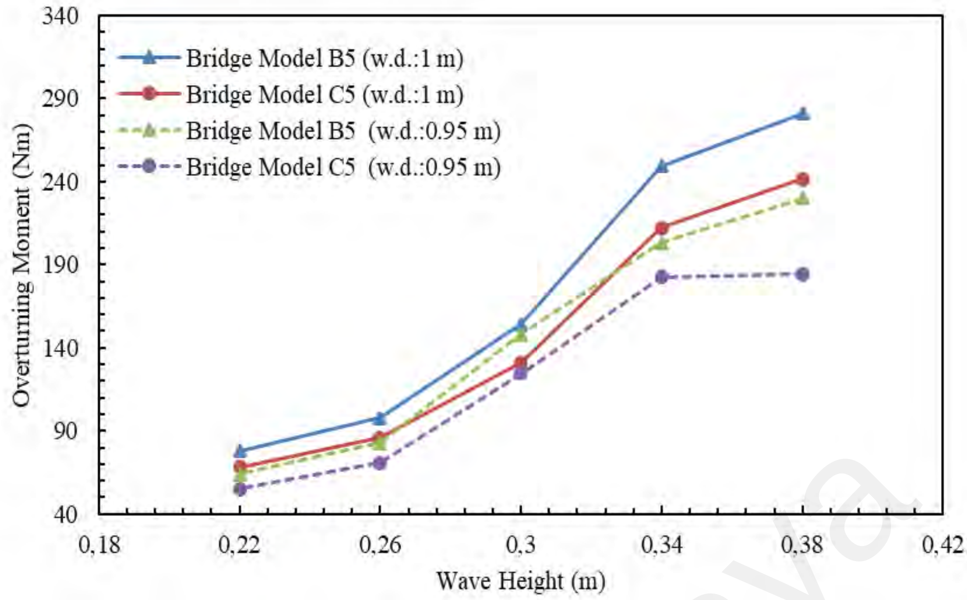

(c)

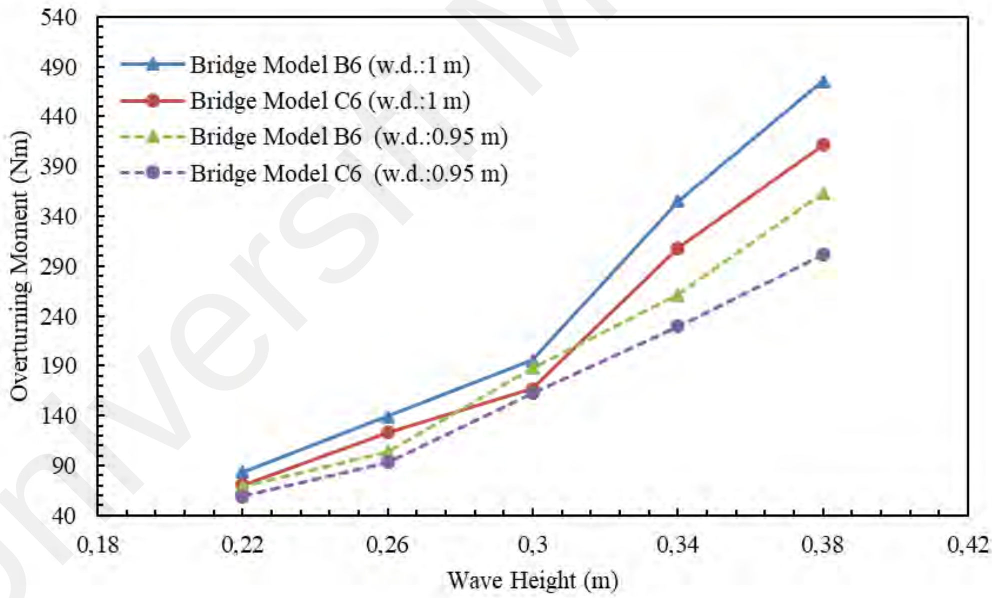

(d)

Figure 4.21: Comparison of the overturning moment, number of girder and girder configuration due to various wave heights (a) Bridge models B3 and C3, (b) Bridge models B4 and C4, (c) Bridge models B5 and C5, (d) Bridge models B6 and C6

In Figure 4.21 is displayed the relationship between overturning moment, number of girders, and shallow waters in Bridge Model B and C in wave height 0.22 to 0.38 with an interval of 0.04 m. Based on the figure, the overturning moment with respect to shallow water varies almost nonlinearly with the wave height. This fact is due to tsunami bore conditions and the presence of nonlinear diffraction of waves with the interaction of bridge models.

A comparison of the overturning moment in Bridge Model C shows that the wave height significantly influenced on uplift. This variation depended on the number of girders and shallow water.

The uplift in the case of 1 m water depth due to increasing wave height from 0.22 to 0.38 m is increased in Bridge Model C3 and Bridge Model C4 to 145 % and 185 %, respectively. This variation significantly increased with increasing the number of girders. Whereas, in Model C5 and Model C6, the difference of uplift in the lowest wave height to the highest wave height is very critical and boosted by 250 % and 480 %, respectively.

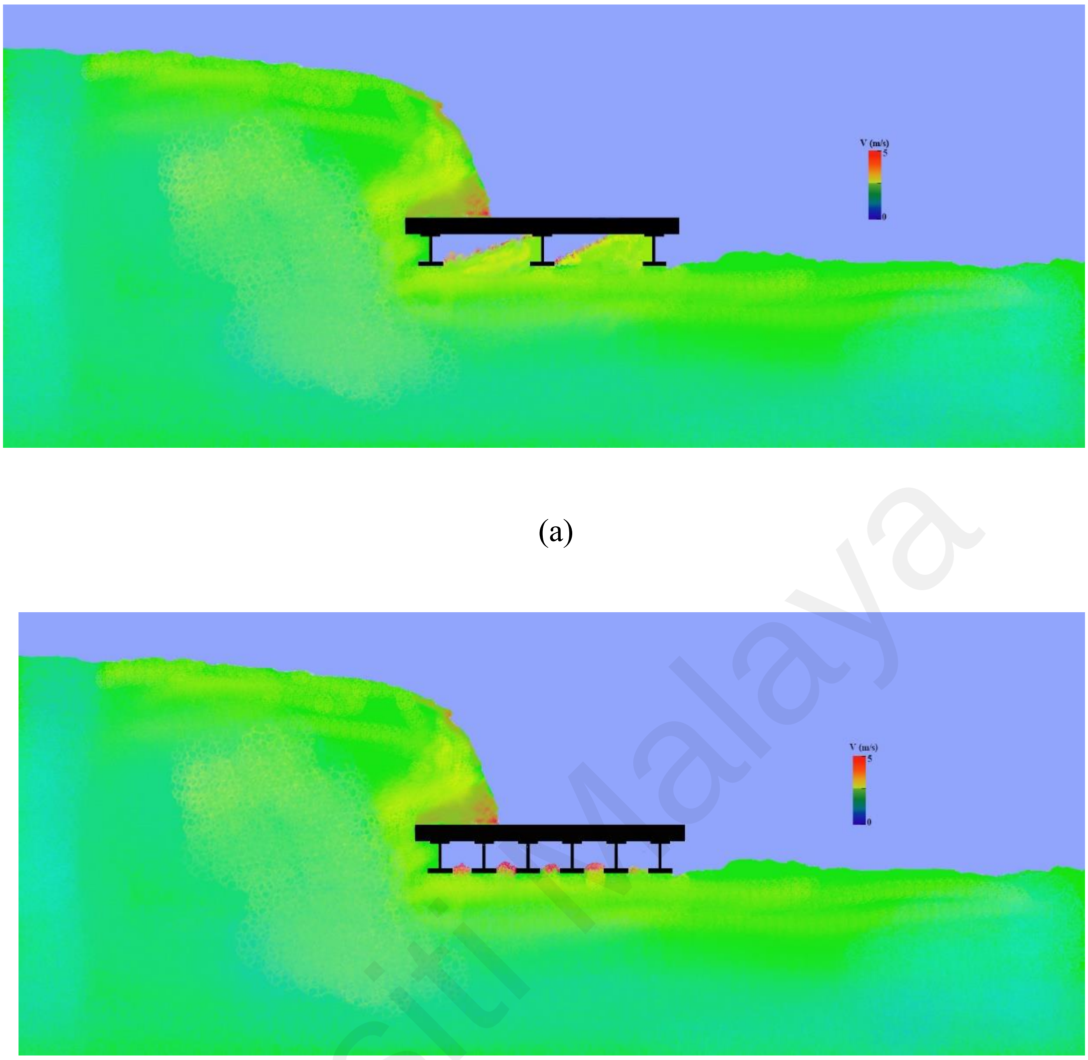

(a)

(b)

Figure 4.22:Velocity distribution in the initial stage of interaction of a tsunami bore 0.257 m and 1 m water depth, (a) the Bridge Model 3B with 3 girders (b) the Bridge Model 6B with 6 girders in the same time.

The computational results by LS-DYNA are utilized to evaluate the effect of bridge girders against the tsunami bore force and illustrated in Figure 4.22

The result in Figure 4.22 shows the initial moment of bore interaction with the bridge model. The maximum horizontal and vertical forces occur at about this time. As indicated in Figure 4.22 b, air remains in the space between the girders of Bridge Model 6B. This air trap is pushing deck and cased to increase the uplift, but it did not significantly affect the horizontal force.

In the wider space between girder, i.e., three girder that indicates in Figure 4.22 a, due to large space between girder the air can scape partially and then water has risen in the area between the girders. Hayatdavoodi et al. (2014) and Lau, (2009) applied this fact to reduce the wave load on coastal bridges.

Figure 4.23 is displayed the simulation with air and without air. In Figure 4.23 a, air pockets between the girders indicated and avoided water push the bridge deck. However, in Figure 4.23 b, due to the lack of air, the water filled the space between girders.

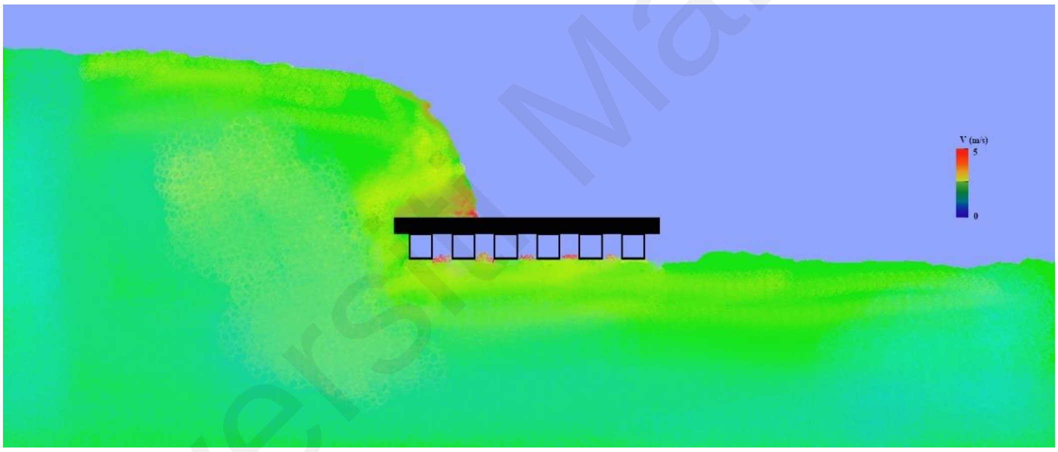

(a)

Figure 4.23: Velocity distribution in the initial stage of interaction of a tsunami bore 0.257 m and 1 m water depth, (a) with air (b) without air

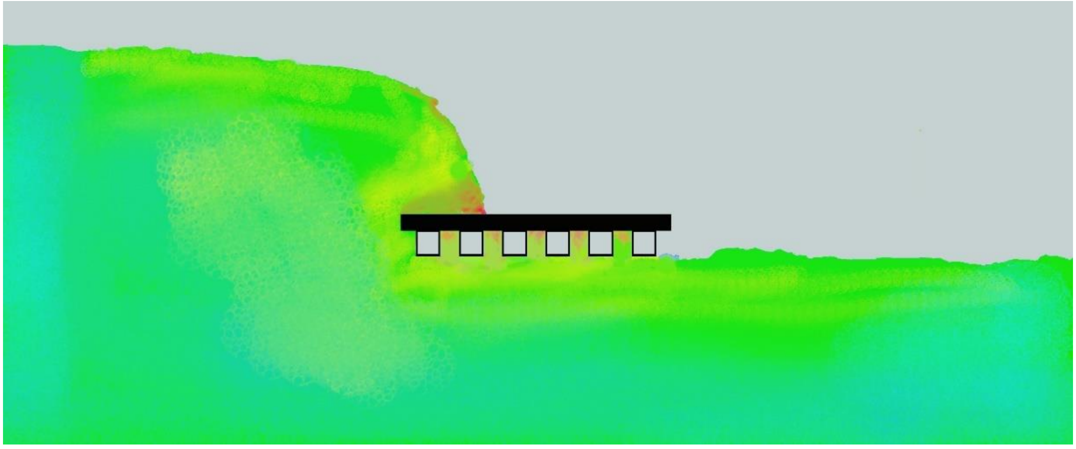

(b)

Figure 4.23:Velocity distribution in the initial stage of the interaction of a tsunami bore 0.257 m and 1 m water depth, (a) with air (b) without air (continue)

4.4.4 Bridge Model F and tsunami mitigation system

This section focuses on the effect of the baffle plate as a countermeasure device to mitigate the tsunami load on the coastal bridge. In this section, various baffle plate configurations were utilized on Bridge model A to evaluate the effect of this device and present an alternative device for mitigation tsunami force and protect bridges from collapse during a tsunami.

Figure 4. 24 and Figure 4. 25 presented the comparison between the variation of the horizontal force, uplift and overturning moment on Bridge model A and Bridge Model with various baffle plate (Model F1-F2) in two water depth (0.95 m and 1 m).

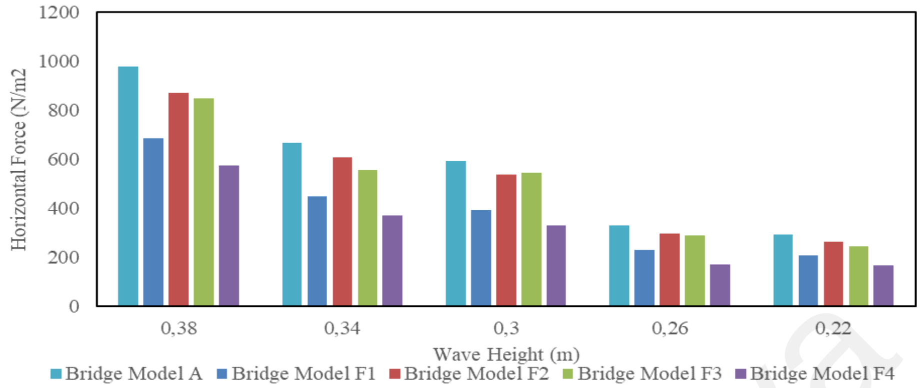

(a)

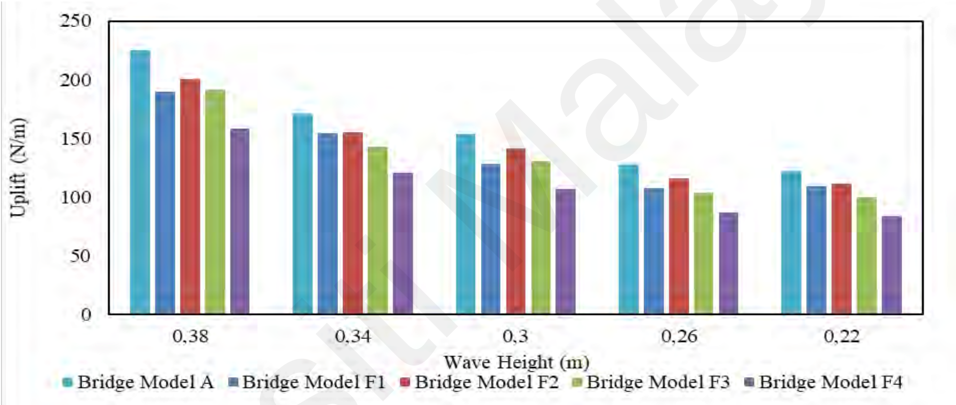

(b)

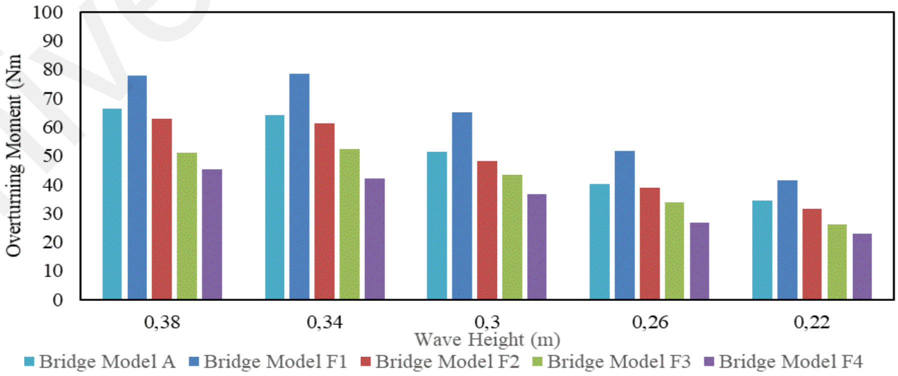

(c)

Figure 4. 24: Comparison of various baffle plate configurations on tsunami mitigation in 0.95 m water depth (a) Horizontal force, (b) uplift force, (c) overturning moment

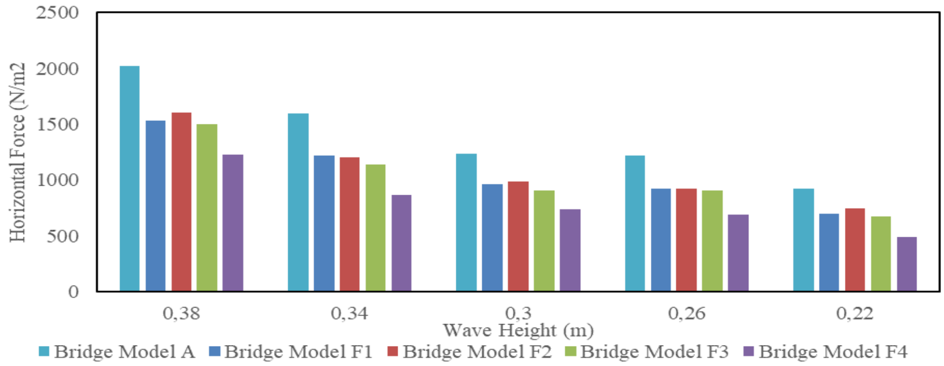

(a)

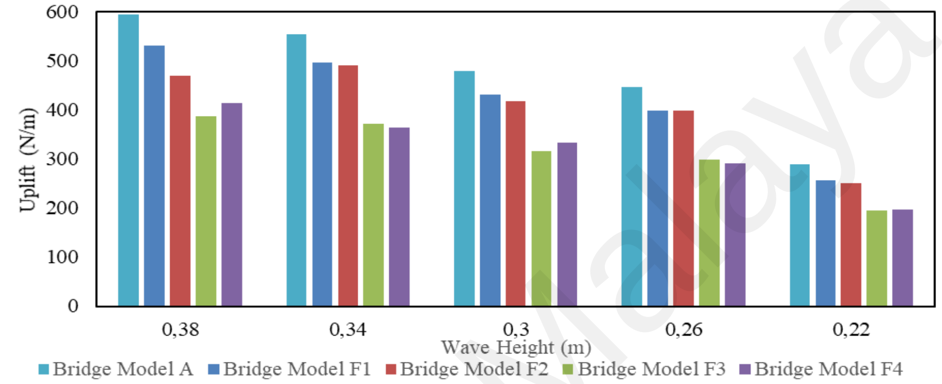

(b)

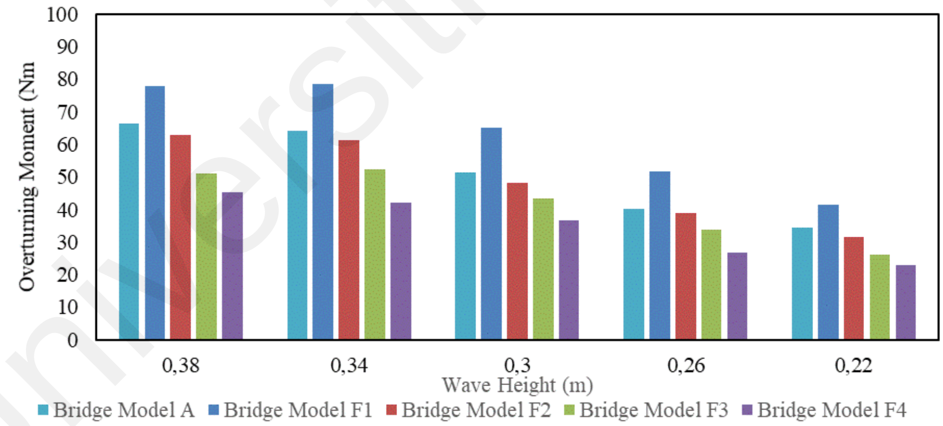

(c)

Figure 4. 25: Comparison of various baffle plate configurations on tsunami mitigation in 1 m water depth (a) horizontal force, (b) uplift force, (c) overturning moment

Result in Figure 4. 24 and Figure 4. 25 indicated that the full baffle plate (Bridge Model F4) significantly reduced the tsunami load on the bridge model. This system reduced up to 40 % horizontal force, and more than 35 % reduced uplift. Also, the mitigation system on Bridge Model F4 decreased the overturning moment by 30 %.

On side baffle (Bridge Model F1 and F2) could reduce only horizontal load, but there is no significant effect on uplift. Also, due to unbalanced stress distribution on the bridge deck, the overturning moment slightly increased.

Baffle plates only for bridge deck (Bridge Model F3) can be utilized in the case of higher shallow water. This is because a tsunami wave mostly influenced on deck, and is not critical for piers. However, in lower shallow water, both baffle plate on deck and piers notably reduced the tsunami loads.

This system presented an alternative to perforations on deck, where 60 % perforation on deck only reduced the horizontal force 17 % (Lau, 2009).

4.5 Comparison of Surface Elevation Between Experiment and Numerical Result

In this section, similar to experiments in the flume, the tsunami solitary wave and bore were simulated to validate and compare between experimental and numerical results. Five different wave heights, i.e. 0.38, 0.34, 0.30. 0.28 with two different water levels i.e. 1m and 0.95m were utilized. Computational modelling was carried out in all cases. Figure 4.26 and Figure 4.27 present the comparison of results for 0.38 wave height and bore height. A comparison between the surface elevations of solitary wave before the bridge is illustrated in Figure 4.26. In obtaining the real wave velocity in the simulation, the length of flume in all cases was assumed similar to experiments wave flume as 24m. The wave gauges H1-H3 (refer to Figure 3.16) measured solitary wave surface from a wave generator to the location before the platform. As illustrated in Figure 4.26, there is good agreement between free surface profile in the computational result and experiment result. There is a slight difference in the wave solitary surface between the experiment and computation after reaching the highest wave height, which may be due to viscous effect and friction between the fluid and the flume.

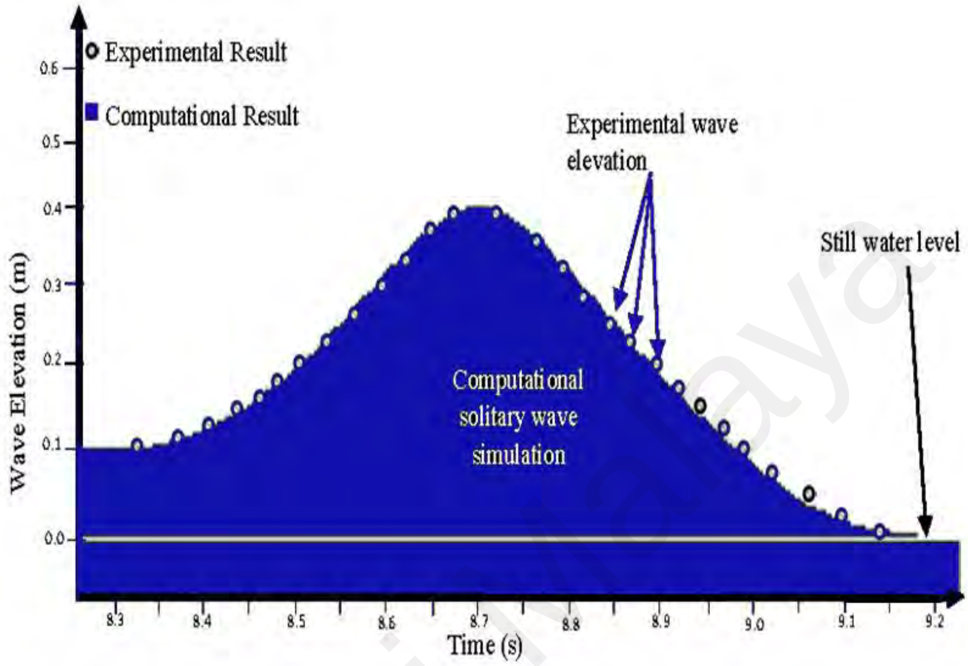

Figure 4.26: Comparison of the solitary wave surface between experiments and computational in 0.38 wave height and 1m water depth

Figure 4.27 indicates the elevation surface of the bore before hitting the bridge model. The result shows good agreement between the free surface elevation of the bore in numerical modelling and experiment. In this paper, the effect of breaking wave in the slope was ignored. More details of this challenging issue can be found in a study of a numerical modelling on breaking wave on slope and rigid structure by Sriram and Ma (2012) and research on breaking wave on a slope with LS-DYNA by Pelfrene (2011).

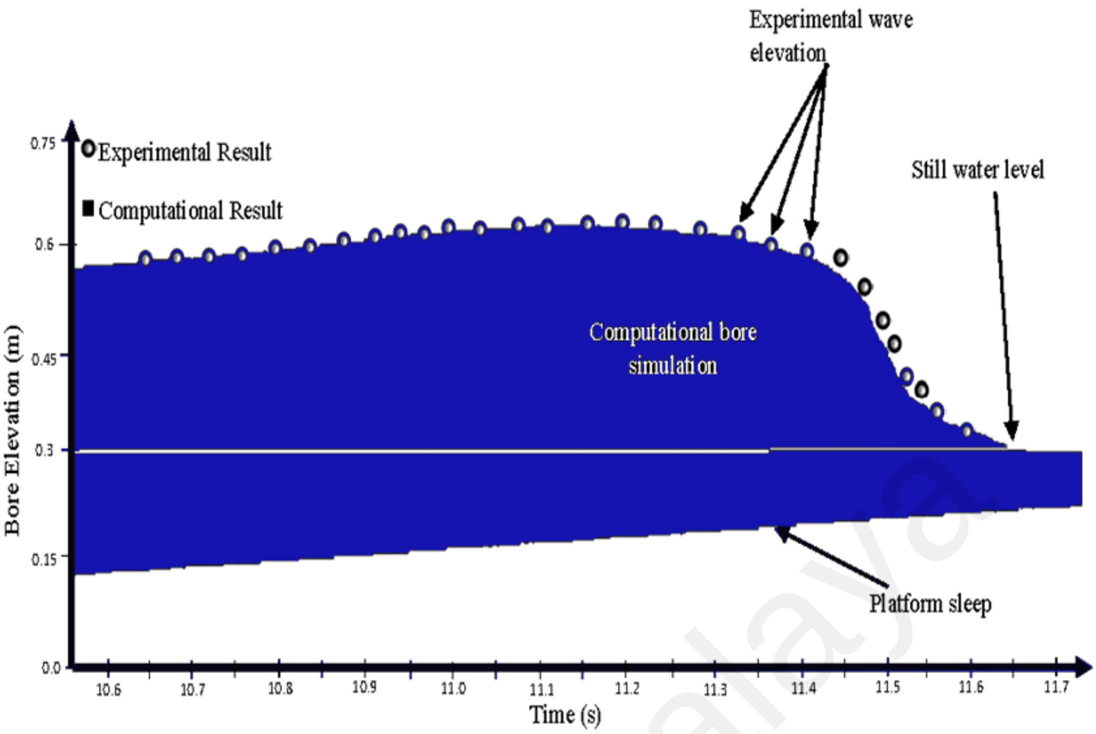

Figure 4.27: Comparison of the tsunami bore surface between experiments and computational in 0.38 wave height and 1m water depth

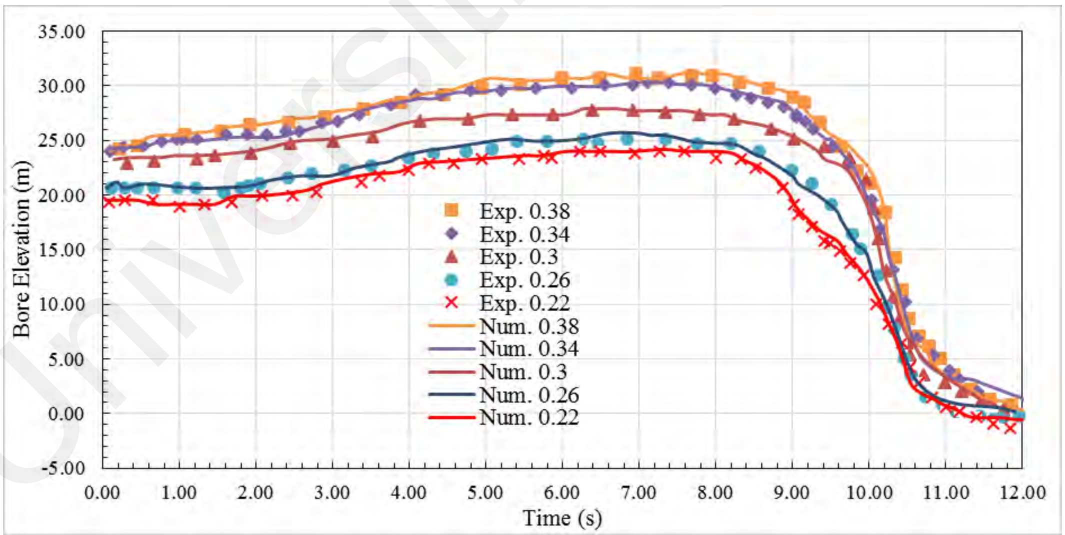

Figure 4.28: Comparison of the tsunami bore surface between experiments and computational in 0.38 m, 0.34 m, 0.30 m, 0.26 m, and 0.22 wave heights and 1m water depth

4.6 Comparison of Tsunami Loads Between Experiment and Numerical Results

Comparison of computational results by LS-DYNA and experiment results in 1m and 0.95 water depths in Bridge Model A is presented in Figure 4.29. Inflation technique is used to increase the density of the mesh in locations where the fluid behavior and properties of fluid is more critical, including the interfaces and wall-fluid interactions. The orthogonality of the mesh was further refined such that the maximum orthogonality of 0.96 to 0.98 and skewness of 0.0071 to 0.0004 were obtained. As described previously, the mesh depth was fixed at 0.05 m in all cases. To obtain the grid independency, four different mesh sizes were applied in this research. Note that d_y is mesh size in the horizontal direction and d_y is the mesh size in the vertical direction (Refer to section 3.2.3). The results show that overall there is good agreement between experimental results and results from computational simulation.

It can be observed from the results that in deeper shallow water, the agreement is better than smaller shallow water. The comparison between horizontal and uplift forces illustrated better determination of horizontal forces. It may be due to air bubbles entrapped in the fluid. Henry (2011) and Hayatdavoodi et al. (2014) studied the effect of entrapped air on bridge deck. Bullock et al. (2001) indicated the effect of air trapped on impact pressure. The results also indicated that with increased wave height, computational result is closer to the experimental result. In the results, overturning moment showed the least agreement in comparison to other forces. This occurrence might be reduced in 3D simulation as indicated in studies by Nimmala (2010) and Zhang (2009).

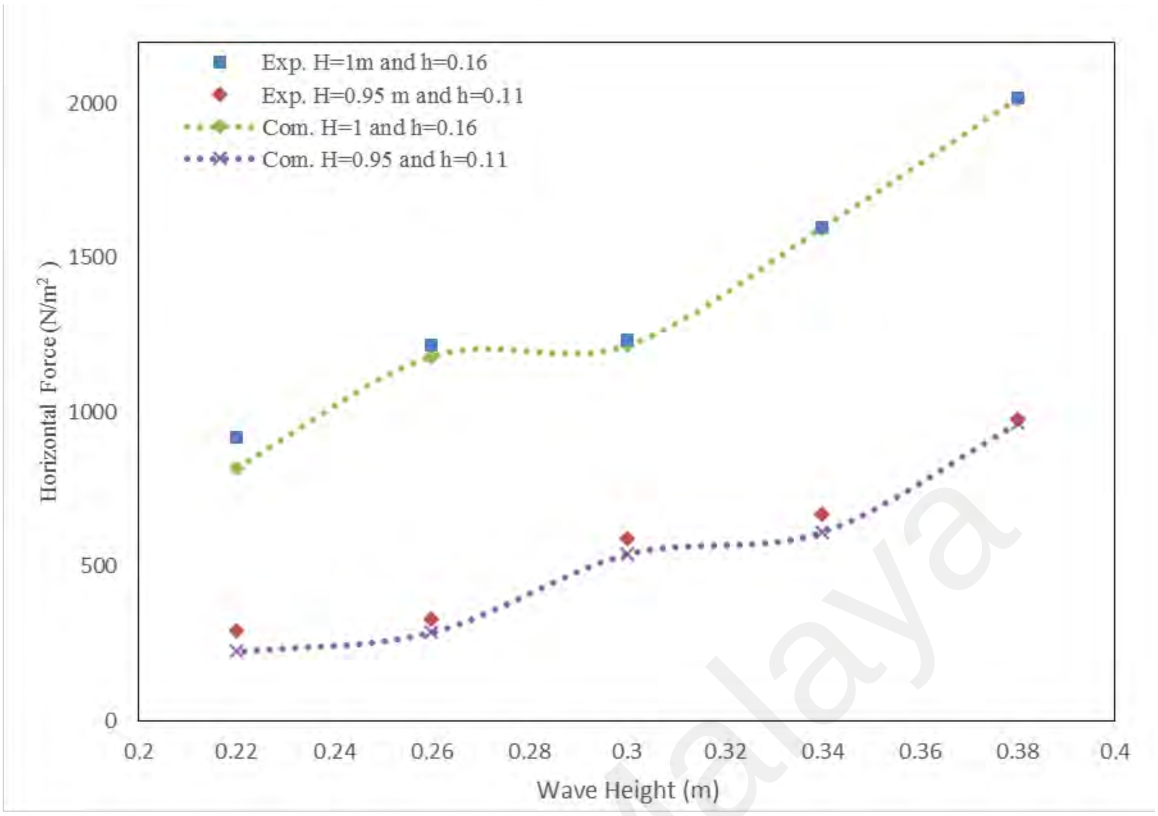

(a)

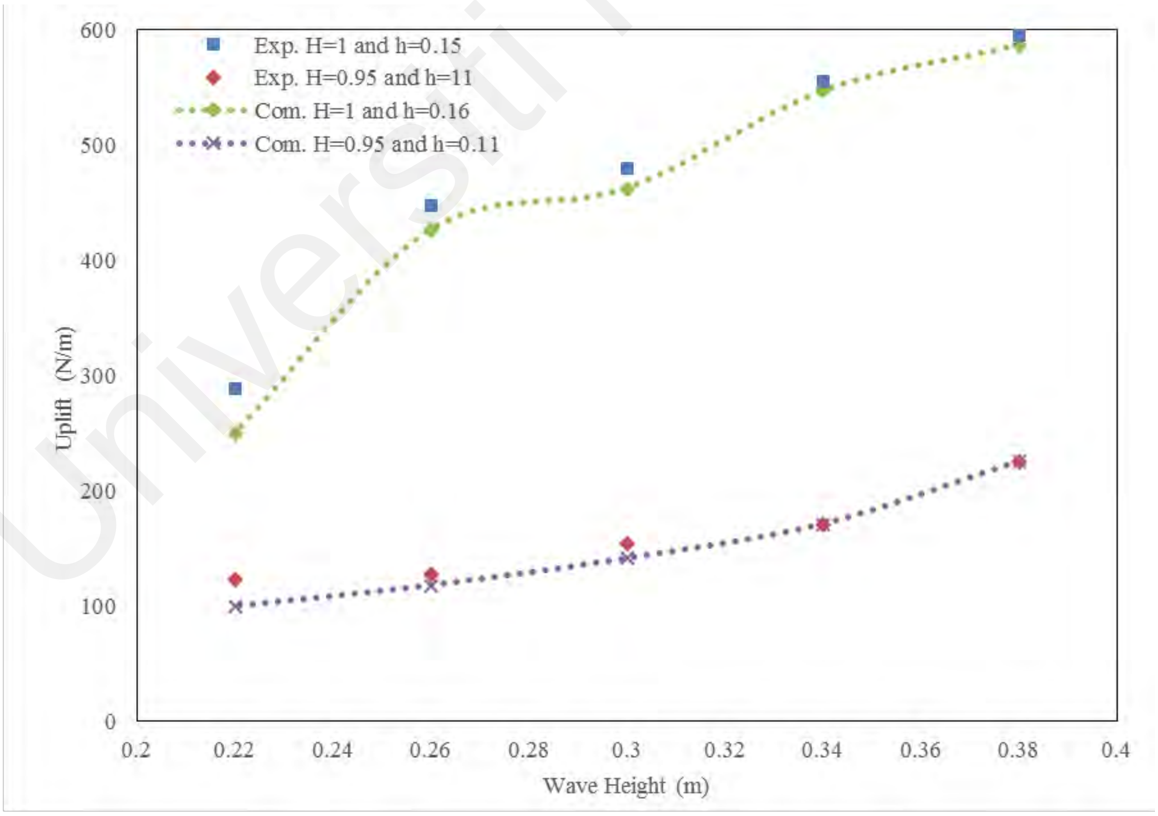

(b)

Figure 4.29: Comparison of computational and experiments result (a) horizontal force, (b) uplift force, (c) overturning moment

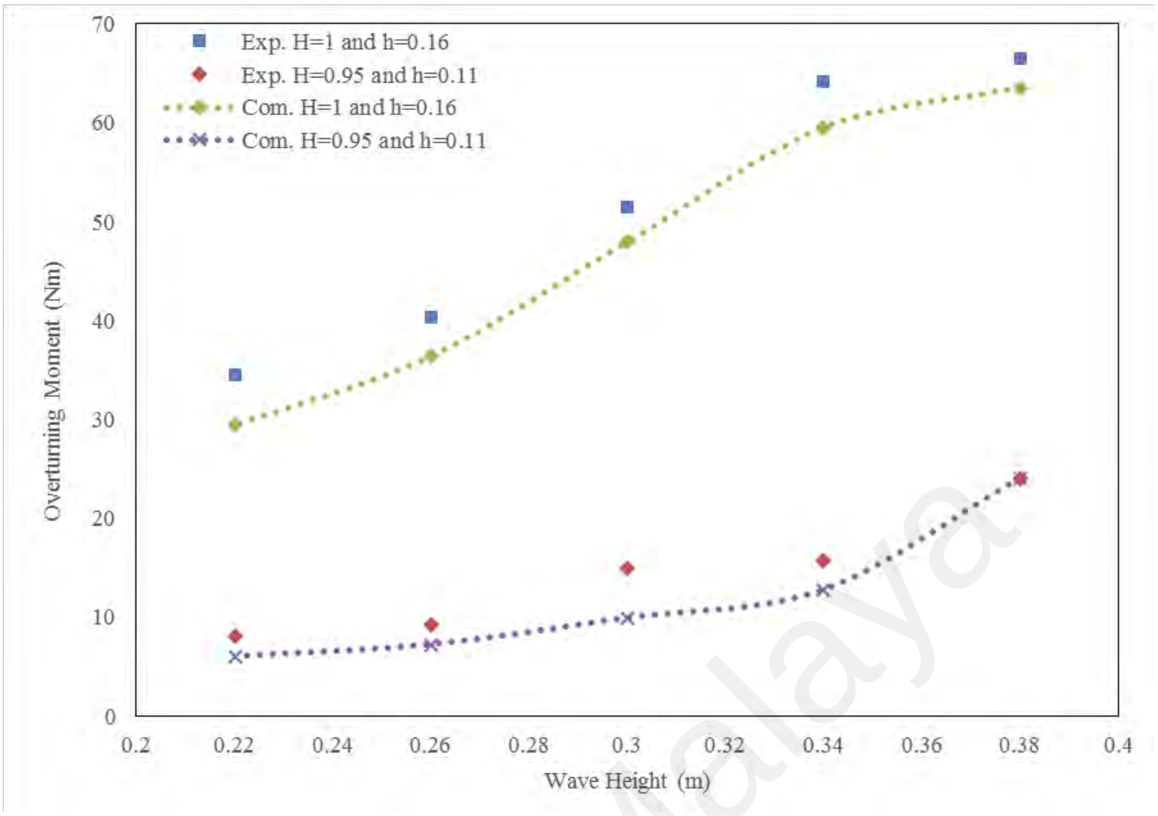

(c)

Figure 4.29: Comparison of computational and experiments result (a) horizontal force, (b) uplift force, (c) overturning moment (continue)

4.7 Evaluating accuracy of computational method with experimental result

In this section, performance of computational result of tsunami bore forces on coastal bridges by LS-DYNA are discussed. Figure 4.30 presents the accuracy of the fluid structure interaction (FSI) coupling algorithm combined with an Arbitrary Lagrangian-Eulerian (ALE) solver in the computational method to model tsunami bore forces on a coastal bridge. It can be seen that most of the points fall along the diagonal line for computational model. Consequently, it follows that prediction results are in very good agreement with the measured values for result on experiment. This observation can be confirmed with very high value for coefficient of determination. The number of either overestimated or underestimated values produced is limited. Consequently, it is obvious that the predicted values enjoy high level of precision.

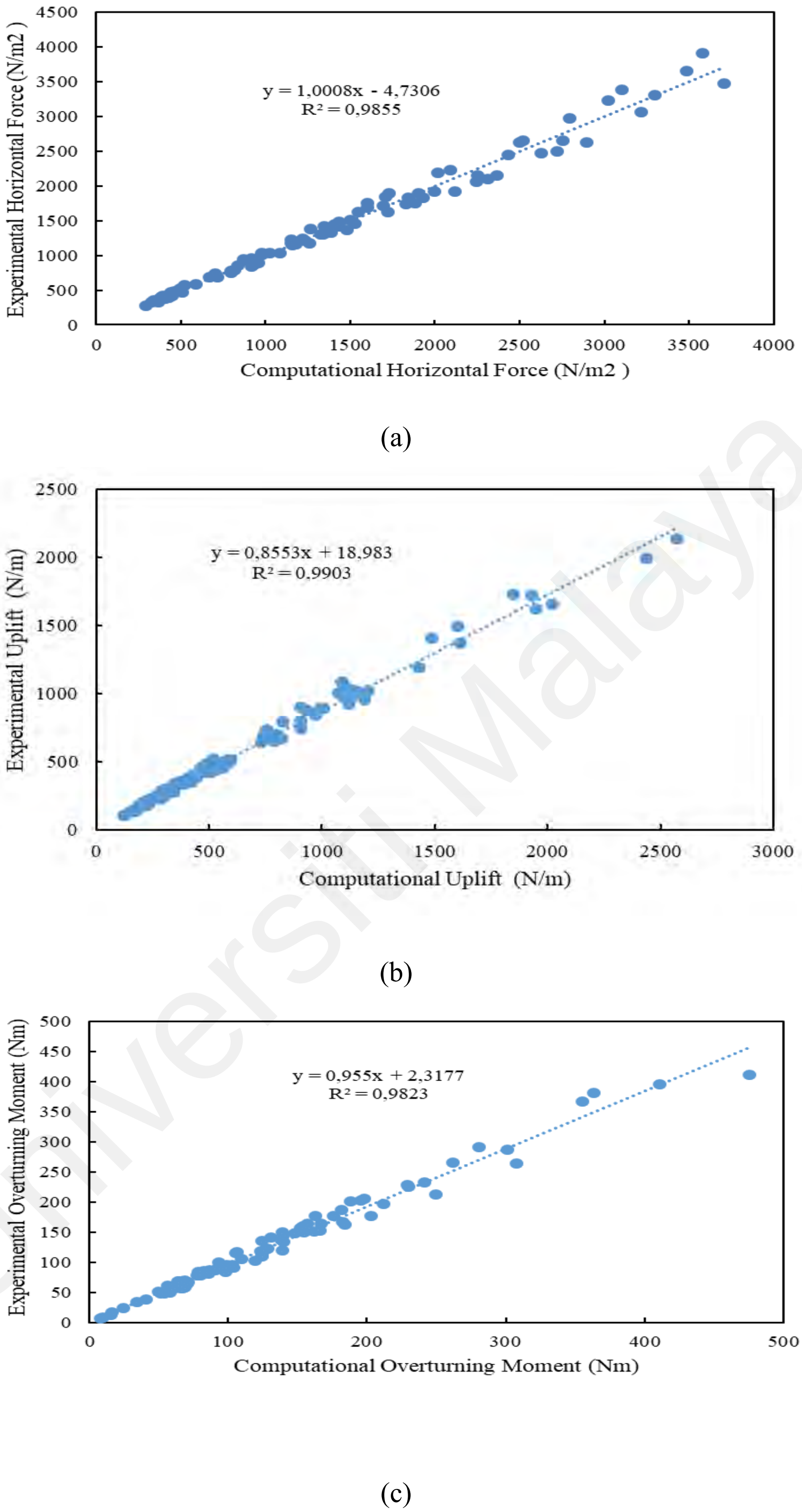

Figure 4.30: Scatter plots of computational and experimental result of tsunami bore force on a coastal bridge (a) Horizontal force, (b) Uplift (c) overturning moment.

In order to demonstrate the merits of the proposed computational method (ALE and FSI) by LS-DYNA software on a more definite and tangible basis, computational accuracy was compared with experiment results, which were used as a benchmark. Conventional error statistical indicators, RMSE, r, and R^2, were used for comparison. Table 4.2 summarizes the accuracy results for test data sets since training error is not credible indicator for prediction potential of particular model.

Table 4.2: Comparative performance statistics of the computational and experimental results in tsunami bore force on a coastal bridge.

Horizontal force			Uplift force			Overturning moment		
RMSE	R^2	r	RMSE	R^2	r	RMSE	R^2	r
107,01096	0.9855	0.9927	45,1522	0.9903	0.9951	11,37067	0.9823	0.9911

According to the result in Table 4.2 and based on RMSE analysis of computational results with the comparison with the experimental value, it could be concluded that the proposed computational model outperformed the results obtained with experimental measurement models.

CHAPTER 5: CONCLUSION

5.1 Introduction

This chapter concludes the study on experimental and computational studies of fluid structure interaction of tsunami bore on costal bridges to understand the potential effect of the tsunami forces on a coastal bridge. It will also put forward recommendations for future research.

5.2 Conclusion

Wave flume experiments and computational simulations were carried out to evaluate the forces acting on the deck and pier of the bridge exposed to tsunami bore. Computational simulation of tsunami impact on bridge structure was developed by using a finite-element code, LS-DYNA software, and ALE method. Experiments were performed in a 24m tsunami flume.

The solitary wave and bore surface elevation were in perfect agreement with numerical formulations and computational simulation. In this study, the horizontal, uplift forces, overturning moment, impact force on bridges in various shallow water depths, and wave heights were measured. The results indicated that the tsunami force on the bridge model, including horizontal, vertical forces, overturning moment, and impact load increase by increasing the wave height. However, this increase is not linear.

The increase in shallow water also plays a vital role in increasing the forces on the bridge model. In the case of lower shallow, with raising the wave height from lower height to highest height, the overturning moment increases more gradually than deeper shallow water. This behavior may relate to the fact that in the deeper shallow water, increasing the wave height leads to a more enhanced impact force due to splashing water on the bridge model.

The results show that the maximum impact load occurred in the location slightly higher than still water. The comparison of results between experiments and computational simulation with LS-DYNA showed good agreement.

Upon evaluating the effects of bore forces on the nine bridge models under varying tsunami conditions, it is observed that for many cases, maximal horizontal and vertical loads occur almost at the same time. The tsunami flow overtopped the bridge at this point, and the wave hit the seaward of bridge and then created a slamming load on it.

The wave height, as predicted, was the most significant determinant of tsunami forces. The relation of wave height and force seems to be a function of wave height. The correlation between force and the water level is more complicated because the water level was a variation of water depth and bridge clearance for this study. Consequently, it was complicated to determine the impact of water level on forces.

The time-history of the numerical and experimental results showed that, given identical tsunami conditions, the Box Girder Bridge type have lower horizontal forces compared to the I beam bridge bridges. Consequently, it would be more suitable to select the section of the Box Girder in the tsunami run-up zone rather than the I beam.

Addition in the number of girders on bridge models from 3 to 6 effected the measured force in the experiment. However, this variation was different in horizontal force, uplift and over turning moment. In the lower wave height and water level, measured forced did not significantly increase with addition of girder. However, in higher wave height, the measured forced in significantly increased.

The horizontal force also increased with addition of girder. This is due to the enhancement of impact surface of the bridge with addition of girder to induce horizontal component of the wave.

Increasing the number of girders substantially increases the air trapped between girders. This phenomenon led to a dramatic rise in the value of the uplift.

The baffle plate utilized in the study successfully reduced the measured force on bridge models. As result, the horizontal force measured on the bridge with a baffle plate on deck and pier was up to 40 % lower than the bridge without any mitigation system. Also, uplift is reduced by up to 35 %. Consequently, utilization of the baffle plate significantly decreased tsunami force and reduced the collapse risk on coastal bridges.

5.3 Future Work and Recommendations

Though there are numerous researches in the numerical and experimental modeling of tsunami on structures, it is necessary to conduct further research on various type of coastal bridges and mitigation system. Suggestions for future works can be summarized as follows:

- Conduct experimental and numerical modeling on larger scale or real scenario of wave height
- Conduct a study on different mitigation system on bridges or before coastal bridges
- Apply a machine learning method to predict loads on bridges
- Conduct a study on comparison of SPH and ALE method to better understand fluid structure interaction on bridges

REFERENCES

Aida I (1970) A numerical experiment for the tsunami accompanying the Kanto earthquake of 1923 Bull Res Inst Tokyo Univ 48:73-86

Aida I (1981) Numerical simulations of the off-Nankaido tsunami Bull Earthquake Res Inst 56:713-730

Allan JC, Komar PD, Ruggiero P, Witter R (2012) The March 2011 Tōhoku Tsunami and Its Impacts along the US West Coast Journal of Coastal Research 28:1142-1153

An C, Cai Y (2010) The effect of beach slope on the tsunami run-up induced by thrust fault earthquakes Procedia Computer Science 1:645-654

Aquelet N, Souli M, Olovsson L (2006) Euler–Lagrange coupling with damping effects: Application to slamming problems Computer methods in applied mechanics and engineering 195:110-132

Araki S, Deguchi I (2012) Prediction of Wave Force Acting on Horizontal Plate Coastal Engineering Proceedings 1:structures. 52

Araki S, Ishino K, Deguchi I Stability of Girder Bridge Against Tsunami Fluid Force. In: Proceedings of 32nd International Conference on Coastal Engineering (ICCE), Shanghai, China June 30-July 5 2010. p 2

Araki S, Itoh S, Deguchi I Experimental study on fluid force on bridge beam due to tsunami. In: Proceedings of the 18th International Offshore and Polar Engineering Conference, 2008. pp 586-591

Arikawa T, Ikebe M, Yamada F, Shimosako K, Imamura F (2005) Large model test of tsunami force on a revetment and on a land structure Journal of Coastal Engineering 52:746-750

Arikawa T, Nakano F, Ohtsubo D, Shimosako K, Ishikawa N (2007) Research on destruction and deformation of structures due to surge front tsunami Journal of Coastal Engineering 54:841-845

Arikawa T, Ohtsubo D, Nakano F, Shimosako K, Takahashi S, Imamura F, Matsutomi H (2006) Large model test on surge front tsunami force Journal of Coastal Engineering 53:796-800

Árnason H (2005) Interactions between an incident bore and a free-standing coastal structure. UMI Dissertation Services

Arneson L, Zevenbergen L, Lagasse P, Clopper P (2012) Evaluating Scour at Bridges.

Asakura R, Iwase K IT, TM, Kaneto T, Fujii N, M O (2000) An experimental study on wave force acting on on-shore structures due to overflowing tsunamis Proceedings of Coastal Engineering,Japan Society of Civil Engineers 47:911-915

Asakura R, Iwase K, Ikeya T, Takao M, Kaneto T, Fujii N, Omori M (2000) An experimental study on wave force acting on on-shore structures due to overflowing tsunamis Proceedings of Coastal Engineering:911-915

ASCE (1998) Minimum Design Loads for Buildings and Other Structures. American Society of Civil Engineers, Bandara K, Dias W (2012) Tsunami wave loading on buildings: a simplified approach Journal of the National Science Foundation of Sri Lanka 40:211-219

Benazir, Comfort, L.K., Luthfi, M, Supasri, A, Syamsidik. (2020). The 22 December 2018 Mount Anak Krakatau volcanogenic tsunami on Sunda Strait coasts,

Boon-intra S (2010) Development of a guideline for estimating tsunami forces on bridge superstructures

Bradner C, Schumacher T, Cox D, Higgins C (2010) Experimental setup for a large-scale bridge superstructure model subjected to waves Journal of waterway, port, coastal, and ocean engineering 137:3-11

Bricker JD, Kawashima K, Nakayama A CFD Analysis of Bridge Deck Failure Due To Tsunami. In: Proceedings of the International Symposium on Engineering Lessons Learned from the 2011 Great East Japan Earthquake, Tokyo, Japan, March 1-4 2012.

Bullock G, Crawford A, Hewson P, Walkden M, Bird P (2001) The influence of air and scale on wave impact pressures Coastal Engineering 42:291-312

CCH (2000) City and County of Honolulu Building Code. Department of Planning and Permitting of Honolulu Hawai'i Chapter 16 Article 11

CCH (2007) City and County of Honolulu Building Code. Department of Planning and Permitting of Honolulu Hawaii, Honolulu, Hawaii

Chakrabarti SK (1994) Modeling laws Offshore structure modeling, Advanced Series on Ocean Engineering, World Scientific:12-37

Chanson H, Aoki S-i, Maruyama M (2002) An experimental study of tsunami runup on dry and wet horizontal coastlines Science of Tsunami Hazards 20:278-293

Chen G, Emitt III C, Hoffman D, Luna R, Sevi A (2005) Analysis of the Interstate 10 Twin Bridge's Collapse During Hurricane Katrina Science and the Storms: the USGS Response to the Hurricanes of 2005:35-42

Chen Q, Wang L, Zhao H (2009) Hydrodynamic investigation of coastal bridge collapse during Hurricane Katrina Journal of Hydraulic Engineering 135:175-186

Chock G (2012) ASCE/JSCE Tohoku Tsunami Investigation of Structural Damage and Development of the ASCE 7 Tsunami Design Code for Buildings and Other Structures

Christensen ED, Deigaard R (2001) Large eddy simulation of breaking waves Coastal Engineering 42:53-86

Chung K, Liu C, Ko A (2003) Steel beams with large web openings of various shapes and sizes: an empirical design method using a generalised moment-shear interaction curve Journal of Constructional Steel Research 59:1177-1200

Cox DC, Mink JF (1963) The tsunami of 23 May 1960 in the Hawaiian Islands Bulletin of the Seismological Society of America 53:1191-1209

Cross RH (1966) Water surge forces on coastal structures. University of California, Hydraulic Engineering Laboratory, Wave Research Projects, Institute of Engineering Research, Cross RH (1967) Tsunami surge forces Journal of the Waterways and Harbors Division, Proceedings of the American Society of Civil Engineers 93:201-231

Cumberbatch E (1960) The impact of a water wedge on a wall J Fluid Mech 7:353-373

Cuomo G, Allsop W, Takahashi S (2010) Scaling wave impact pressures on vertical walls Coastal Engineering 57:604-609

Cuomo G, Shimosako K-i, Takahashi S (2009) Wave-in-deck loads on coastal bridges and the role of air Coastal Engineering 56:793-809

Dahdouh-Guebas F, Jayatissa LP, Di Nitto D, Bosire JO, Lo Seen D, Koedam N (2005) How effective were mangroves as a defence against the recent tsunami? Current biology 15:R443-R447

Donea J, Huerta A, Ponthot JP, Rodríguez-Ferran A (2004) Arbitrary lagrangian–eulerian methods Encyclopedia of computational mechanics

Douglass SL, Chen Q, Olsen J, Edge B, Brown D (2006) Wave forces on bridge decks Coastal Transportation Engineering Research and Education Center, Univ of South Alabama, Mobile, Ala

Fang, Q., Hong, R., Guo, A., & Li, H. (2019). Experimental investigation of wave forces on coastal bridge decks subjected to oblique wave attack. Journal of Bridge Engineering, 24(4), 04019011.

FEMA55 (2000) Manual Coastal Construction. FEMA 55. Federal Emergency Management Agency,

FEMA55 (2006) Chapter 11 Determining Site Specific Loads. Federal Emergency Management Agency, USA

FEMA646 (2008) The Federal Emergency Management Agency Coastal Construction Manual. FEMA,

Fine I, Rabinovich A, Bornhold B, Thomson R, Kulikov E (2005) The Grand Banks landslide-generated tsunami of November 18, 1929: preliminary analysis and numerical modeling Marine Geology 215:45-57

Fisher MA, Geist EL, Sliter R, Wong FL, Reiss C, Mann DM (2007) Preliminary analysis of the earthquake (Mw 8.1) and tsunami of April 1, 2007, in the Solomon Islands, Southwestern Pacific Ocean Science of Tsunami Hazards 26:3

Fuchs H, Hager WH (2012) Scale Effects of Impulse Wave Run-Up and Run-Over Journal of Waterway, Port, Coastal, and Ocean Engineering 138:303-311

Fujima K, Achmad F, Shigihara Y, Mizutani N (2009) Estimation of tsunami force acting on rectangular structures Journal of Disaster Research 4:404-409

Fukui Y, Nakamura M, Shiraishi H, Sasaki Y (1963) Hydraulic study on tsunami Coastal Engineering in Japan 6:67-82

Galvin CJ (1968) Breaker type classification on three laboratory beaches Journal of Geophysical Research 73:3651-3659

Ghobarah A, Saatcioglu M, Nistor I (2006) The impact of the 26 December 2004 earthquake and tsunami on structures and infrastructure Engineering structures 28:312-326

Ghouti L, Sheltami TR, Alutaibi KS (2013) Mobility prediction in mobile ad hoc networks using extreme learning machines Procedia Computer Science 19:305-312

Gladman B (2007) LS-DYNA® Keyword User's Manual–vol. I–Version 971. LSTC,

Goda Y New wave pressure formulae for composite breakwaters. In: Proceedings of 14th International Conference on Coastal Engineering Copenhagen, Denmark, 1974. vol 1. ASCE,, pp 1702–1720

Goff J et al. (2006) Sri Lanka field survey after the December 2004 Indian Ocean tsunami Earthquake Spectra 22:155-172

Goring DG (1978) Tsunamis--the propagation of long waves onto a shelf. California Institute of Technology

Grantz A, Plafker G, Kachadoorian R (1964) Alaska's Good Friday earthquake, March 27, 1964: A preliminary geologic evaluation. US Department of the Interior, Geological Survey,

Graumann A et al. (2006) Hurricane Katrina: a climatological perspective: preliminary report. US Department of Commerece, National Ocanic and Atmospheric Administration, National Environmental Satellite Data and Information Service, National Climatic Data Center,

H. Kasano, J. Oka, J. Sakurai, N. Kodama, T. Yoda (2012) Investigative Research on Bridges Subjected to Tsunami Disaster in 2011 off the Pacific Coast of Tohoku Earthquake. Paper presented at the Australian Structural Engineering Southbank, Victoria 3006, Australia

Hall Jr JV, Watts GM (1953) Laboratory investigation of the vertical rise of solitary waves on impermeable slopes. DTIC Document, Washington, D. C. Huang, Z., Y

Hammack J (1973) A note on tsunamis: their generation and propagation in an ocean of uniform depth. Cambridge Univ Press,

Hamzah M, Mase H, Takayama T Simulation and experiment of hydrodynamic pressure on a tsunami barrier. In: Coastal Engineering Conference, 2001. ASCE, pp 1501-1507

Hayatdavoodi M, Seiffert B, Ertekin RC (2014) Experiments and computations of solitary-wave forces on a coastal-bridge deck. Part II: Deck with girders Coastal Engineering 88:210-228

Heller V, Hager WH, Minor H-E (2008) Scale effects in subaerial landslide generated impulse waves Experiments in Fluids 44:691-703

Henry AM (2011) Wave Forces on Bridge Decks and Damping Techniques to Reduce Damages. Faculty of the Louisiana State University and Agricultural and Mechanical College in partial fulfillment of the requirements for the degree of Master of Science in Civil Engineering in The Department of Civil and Environmental Engineering By Aaron M. Henry BS, University of Tennessee

Huang G-B, Zhu Q-Y, Siew C-K Extreme learning machine: a new learning scheme of feedforward neural networks. In: Neural Networks, 2004. Proceedings. 2004 IEEE International Joint Conference on, 2004. IEEE, pp 985-990

Hughes SA (1993) Physical models and laboratory techniques in coastal engineering vol 7. World Scientific Publishing Company Incorporated,

IBC (2000) International Building Code Cengage Learning,

Iemura H, Pradono M, Yasuda T, Tada T (2007) Experiments of tsunami force acting on bridge models Journal of Earthquake Engineering 29:902-911

Iemura H, Pradono MH, Takahashi Y Report on the Tsunami Damage of Bridges in Banda Aceh and Some Possible Countermeasures. In: Proceedings of the 28th Earthquake Engineering Symposium, 2005. pp 22-24

Ikeno M, Mori N, Tanaka H (2001) Experimental study on tsunami force and impulsive force by a drifter under breaking bore like tsunamis Proceedings of Coastal Engineering:846-850

Ikeno M, Tanaka H (2003) Experimental study on impulsive force of drift body and tsunami running up to land Journal of Coastal Engineering 50:721-725

Jaffe BE, Gelfenbuam G (2007) A simple model for calculating tsunami flow speed from tsunami deposits Sedimentary Geology 200:347-361

Kaistrenko V, Sedaeva V (2001) 1952 North Kuril tsunami: New data from archives. In: Tsunami research at the end of a critical decade. Springer, pp 91-102

Kataoka S, Kusakabe T, Nagaya K Wave forces acting on bridge girders struck by tsunami. In: Proceedings of the 12th Japan Earthquake Engineering Symposium, , Tokyo, Japan, 2006. Japan Society of Civil Engineers, pp 154-157

Kathiresan K, Rajendran N (2005) Coastal mangrove forests mitigated tsunami Estuarine, Coastal and Shelf Science 65:601-606

Kawashima K et al. Damage of Bridges during 2011 Great East Japan Earthquake. In: Proceedings of 43rd Joint Meeting, US-Japan Panel on Wind and Seismic Effects, UJNR, Tsukuba Science City, Japan, 2011.

Kenji Kosa, Shinichi Nii, Kenta Miyahara, Shoji M (2010) Experimental Study For Estimating Tsunami Forces Acting on Bridge Girders. Paper presented at the 26th US - Japan Bridge Engineering Workshop, AGENDA, September 20-22

Kim J-H, Shin H-C (2008) Application of the ALE technique for underwater explosion analysis of a submarine liquefied oxygen tank Ocean Engineering 35:812-822

Klenzendorf JB (2007) Hydraulic performance of bridge rails based on rating curves and submergence effects. University of Texas at Austin

Klenzendorf JB, Barrett ME, Charbeneau RJ (2010) Impact of Bridge Rail Geometry on Floodplain Analysis Journal of Hydrologic Engineering 15:1016-1022

Kosa K (2012) Damage analysis of bridges affected by tsunami due to Great East Japan Earthquake Proc International Sym on Engineering Lessons Learned from the 2011 Great East Japan Earthquake:1386-1397

Koshimura S, Oie T, Yanagisawa H, Imamura F (2009) Developing fragility functions for tsunami damage estimation using numerical model and post-tsunami data from Banda Aceh, Indonesia Coastal Engineering Journal 51:243-273

Latief H, Harada K, Imamura F (1999) Experimental and numerical study on the effect of mangrove to reduce tsunami Tohoku Journal of Natural Disaster Science 35:127-132

Latter J (1981) Tsunamis of volcanic origin: summary of causes, with particular reference to Krakatoa, 1883 Bulletin volcanologique 44:467-490

Lau TL (2009) Tsunami force estimation on inland bridges considering complete pier-deck configurations. PhD, Chulalongkorn University

Lau TL, Lukkunaprasit P, Ruangrassamee A, Ohmachi T (2010) Performance of Bridges with Solid and Perforated Parapets in Resisting Tsunami Attacks Journal of Earthquake and Tsunami 4:95-104

Lavigne F et al. (2007) Field observations of the 17 July 2006 Tsunami in Java Natural Hazards and Earth System Science 7:177-183

Liu PL-F, Cho Y-S, Yoon S, Seo S (1995) Numerical simulations of the 1960 Chilean tsunami propagation and inundation at Hilo, Hawaii. In: Tsunami: Progress in prediction, disaster prevention and warning. Springer, pp 99-115

Liu T, Chung K (2003) Steel beams with large web openings of various shapes and sizes: finite element investigation Journal of Constructional Steel Research 59:1159-1176

López AM, Okal EA (2006) A seismological reassessment of the source of the 1946 Aleutian 'tsunami'earthquake Geophysical Journal International 165:835-849

LS-DYNA Keyword User's Manual (2007) Version 971 vol Volume, I. Livermore Software Technology Corporation.

Lukkunaprasit P, Lau T, Ruangrassamee A, Ohmachi T Tsunami Wave Loading on a Bridge Deck with Perforations. In: The 14th World Conference on Earthquake Engineering, 2008. pp 12-17

Lukkunaprasit P, Lau TL (2011) Influence of bridge deck on tsunami loading on inland bridge piers The IES Journal Part A: Civil & Structural Engineering 4:115-121

MANAWASEKARA CD (2013a) Tsunami Impact on a Coastal Building and Effect of Spatial Configuration of the Building on Acting Tsunami Force

Manawasekara CD (2013b) Tsunami Impact on a Coastal Building and Effect of Spatial Configuration of the Building on Acting Tsunami Force. Nagoya University

Matsutomi H, Shuto N (1994) Relation between building damage and inundation depth and velocity of tsunami Ann J Coast Eng 41:246-250

Mayer S, Garapon A, Soerensen LS (1998) A fractional step method for unsteady free-surface flow with applications to non-linear wave dynamics International journal for numerical methods in fluids 28:293-315

Mimura N, Yasuhara K, Kawagoe S, Yokoki H, Kazama S (2011) Damage from the Great East Japan Earthquake and Tsunami-A quick report Mitigation and adaptation strategies for global change 16:803-818

Moideen, R., Ranjan Behera, M., Kamath, A., & Bihs, H. (2019). Effect of girder spacing and depth on the solitary wave impact on coastal bridge deck for different airgaps. Journal of Marine Science and Engineering, 7(5), 140.

Murakami K, Sakamoto Y, Nonaka T (2012) Analytical Investigation Of Slab Bridge Damages Caused By Tsunami Flow Coastal Engineering Proceedings 1:structures. 42

Nakamura S, Tsuchiya Y (1973) On the Shock Pressure of Surge on a Wall Bulletin of the Disaster Prevention Research Institute 23:47-58

Nakao H, Nozaka K, Izuno K, Kobayashi H Tsunami Hydrodynamic Force on Various Bridge Sections. In: 15th World Conference on Earthquake Engineering, Lisbon, Portuguese, 2012.

Nakao M (2009) The Great Meiji Sanriku Tsunami June 15, 1896 at the Sanriku coast of the Tohoku region. Retrieved 2009-10-18,

Nian R, He B, Zheng B, Van Heeswijk M, Yu Q, Miche Y, Lendasse A (2014) Extreme learning machine towards dynamic model hypothesis in fish ethology research Neurocomputing 128:273-284

Nimmala SB (2010) An efficient high-performance computing based three-dimensional numerical wave basin model for the design of fluid-structure interaction experiments

Nistor I, Palermo D, Cornett A, Al-Faesly T Experimental And Numerical Modeling Of Tsunami Loading On Structures. In: Proceedings of the International Conference on Coastal Engineering, 2011. vol 32. p currents. 2

Nistor I, Saatcioglu M, Ghobarah A The 26 December 2004 Earthquake and Tsunami-Hydrodynamic forces on physical infrastructure in Thailand and Indonesia. In: Proceedings 2005 Canadian Coastal Engineering Conference, 2005. pp 1-15

Noarayanan L, Murali K, Sundar V (2012) Role of Vegetation on Beach Run-up due to Regular and Cnoidal Waves Journal of Coastal Research 28:123-130

Nott J (2003) Waves, coastal boulder deposits and the importance of the pre-transport setting Earth and Planetary Science Letters 210:269-276

Nouri Y (2008) The impact of hydraulic bores and debris on free standing structures. University of Ottawa,

Nouri Y, Nistor I, Palermo D, Cornett A (2010) Experimental investigation of tsunami impact on free standing structures Coastal Engineering Journal 52:43-70

Mazinani, I., Sarafraz, M. M., Ismail, Z., Hashim, A. M., Safaei, M. R., & Wongwises, S. (2021). Fluid-structure interaction computational analysis and experiments of tsunami bore forces on coastal bridges. *International Journal of Numerical Methods for Heat & Fluid Flow*.

Okal EA et al. (2010) Field survey of the Samoa tsunami of 29 September 2009 Seismological Research Letters 81:577-591

Ozdemir Z, Souli M, Fahjan Y (2010) Application of nonlinear fluid–structure interaction methods to seismic analysis of anchored and unanchored tanks Engineering structures 32:409-423

Pacheco KH (2005) Evaluation of tsunami loads and their effect on reinforced concrete buildings.

Padgett J, DesRoches R, Nielson B, Yashinsky M, Kwon O-S, Burdette N, Tavera E (2008) Bridge damage and repair costs from Hurricane Katrina Journal of Bridge Engineering 13:6-14

Parvin A, Ma Z (2001) The use of helical spring and fluid damper isolation systems for bridge structures subjected to vertical ground acceleration Electronic Journal of Structural Engineering 1:98-110

Patil S, Kostic M, Majumdar P Computational Fluid Dynamics Simulation of Open-Channel Flows Over Bridge-Decks Under Various Flooding Conditions. In: Proceedings of the 6th WSEAS International Conference on Fluid Mechanics (FLUIDS'09), 2009. pp 114-120

Payne G (2008) Guidance for the experimental tank testing of wave energy converters SuperGen Marine, Dec

Pelfrene J (2011) Study of the SPH method for simulation of regular and breaking waves Gent: Universiteit Gent

Pelinovsky E, Ivashenko A, Simov K May 26, 1983 tsunami in the Sea of Japan. In: Tsunamis: Their Science and Hazard Mitigation, Proceedings of the International Tsunami Symposium, 1985. p 234

Peregrine D (1995) Water wave impact on walls and the associated hydrodynamic pressure field Wave Forces on Inclined and Vertical Wall Structures:259-281

Petel OE (2011) Response of Shear Thickening Materials to Uniaxial Shock Compression. McGill University Libraries

Piro DJ (2013) A Hydroelastic Method for the Analysis of Global Ship Response Due to Slamming Events. The University of Michigan

Pradono M, Iemura H, Yasuda T (2008) Tsunami force on bridge models and force reductions by mangrove models. Paper presented at the The 14th World Conference on Earthquake Engineering, Beijing, China, October 12-17

Ramsden JD (1996) Forces on a vertical wall due to long waves, bores, and dry-bed surges Journal of waterway, port, coastal, and ocean engineering 122:134-141

Richardson E, Davis S (2001) Evaluating Scour at Bridges . Federal Highway Administration, Hydraulic Engineering Circular No. 18 Publication FHWA NHI:01-001

Robertson I, Riggs H, Mohamed A Experimental results of tsunami bore forces on structures. In: ASME 2008 27th International Conference on Offshore Mechanics and Arctic Engineering, 2008. American Society of Mechanical Engineers, pp 509-517

Salem, H., Mohssen, S., Nishikiori, Y., & Hosoda, A. (2016). Numerical collapse analysis of Tsuyagawa bridge damaged by Tohoku tsunami. *Journal of Performance of Constructed Facilities*, *30*(6), 04016065.

Santo J, Robertson IN (2011) lateral loading on vertical structural elements due to a tsunami bore Universtity of Hawaii, Sarpkaya T, Isaacson M, Isaacson MdSQ, Isaacson MdSQ (1981) Mechanics of wave forces on offshore structures vol 96. Van Nostrand Reinhold Company New York,

Sato H, Murakami H, Kozuki Y, Yamamoto N (2003) Study on a simplified method of tsunami risk assessment Natural Hazards 29:325-340

Schumacher T, Higgins C, Bradner C, Cox D, Yim SC Large-scale wave flume experiments on highway bridge superstructures exposed to hurricane wave forces. In: Sixth National Seismic Conference on Bridges and Highways, 2008.

Seiffert B, Hayatdavoodi M, Ertekin RC (2014) Experiments and computations of solitary-wave forces on a coastal-bridge deck. Part I: Flat Plate Coastal Engineering 88:194-209

Shoji G, Hiraki Y, Ezura Y (2012) Evaluation of Tsunami Fluid Force Acting on The Bridge Deck Damaged By The 2011 Off The Pacific Coast of Tohoku Earthquake Tsunami. Paper presented at the 9th International Conference on Urban Earthquake Engineering/ 4th Asia Conference on Earthquake Engineering March 6-8,,

Shoji G, Hiraki Y, Fujima K, Shigihara Y (2011) Evaluation of Tsunami Fluid Force Acting on a Bridge Deck Subjected to Breaker Bores Procedia Engineering 14:1079-1088

Shoji G, Mori Y Damage of road structures in Sri Lanka due to the 2004 Giant Tsunami in the Indian Ocean. In: Proceedings of the 9th Symposium on Ductility Design Method for Bridges, JSCE, 2006a. pp 221-224

Shoji G, Mori Y (2006b) Hydraulic model experiment to simulate the damage of a bridge deck subjected to tsunamis Annual Journal of Coastal Engineering 53:801-805

Shoji G, Moriyama T (2007) Evaluation of the structural fragility of a bridge structure subjected to a tsunami wave load Journal of Natural Disaster Science 29:73-81

Shoji G, Moriyama T (2008) Evaluation Of A Tsunami Wave Load Acting To A Deck of A Road Bridge

Shuto N (1987) The effectiveness and limit of tsunami control forests Coast Eng Jpn 30:143-153

Shuto N (1993) Tsunami intensity and disasters. In: Tsunamis in the World. Springer, pp 197-216

Shuto N, Matsutomi H (1995) Field survey of the 1993 Hokkaido Nansei-Oki earthquake tsunami. In: Tsunamis: 1992–1994. Springer, pp 649-663

Simons M et al. (2011) The 2011 magnitude 9.0 Tohoku-Oki earthquake: Mosaicking the megathrust from seconds to centuries science 332:1421-1425

Soloviev S, Kim K (1997) Catalog of tsunamis in the Pacific, 1969-1982. DIANE Publishing,

Souli M, Ouahsine A, Lewin L (2000) ALE formulation for fluid–structure interaction problems Computer methods in applied mechanics and engineering 190:659-675

Souli Mh, Benson DJ (2013) Arbitrary Lagrangian Eulerian and Fluid-Structure Interaction: Numerical Simulation. John Wiley & Sons, Sriram V, Ma Q (2012) Improved MLPG_R method for simulating 2D interaction between violent waves and elastic structures Journal of Computational Physics 231:7650-7670

Sugimoto T, Unjoh S Hydraulic Model Tests on the Bridge Structures Damaged by Tsunami and Tidal Wave. In: Proceedings of the 23th US-Japan Bridge Engineering Workshop, 2007. Tsukuba, Japan: Public Works Research Institute., pp 1-10

Takahashi S, Tanimoto K, Miyanaga S (1985) Uplift wave forces due to compression of enclosed air layer and their similitude low Costal Engineering 28, 191–206

Takahashi S et al. (2011) Urgent survey for 2011 Great East Japan earthquake and tsunami disaster in ports and coasts Technical note of the port and airport research institute:157

Tanaka N, Sasaki Y, Mowjood M, Jinadasa K, Homchuen S (2007) Coastal vegetation structures and their functions in tsunami protection: experience of the recent Indian Ocean tsunami Landscape and Ecological Engineering 3:33-45

Tanimoto K On the hydraulic aspects of tsunami breakwaters in Japan. In: Proceedings of the International Tsunami Symposium 1981, 1983. pp 423-435

Tanimoto K et al. (1983) Field and laboratory investigations of the tsunami caused by 1983 Nihonkai Chubu Earthquake Technical Note of the Port and Harbor Research Institute:1-299

Tanimoto K, Tsuruya K, Nakano S Tsunami Force of Nihonkai-Chubu Earthquake in 1983 and Cause of Revetment Damage. In: Proceeding of the 31st Japanese Conference on Coastal Engineering, 1984.

Tanioka Y, Satake K (2001) Detailed coseismic slip distribution of the 1944 Tonankai earthquake estimated from tsunami waveforms Geophysical Research Letters 28:1075-1078

Tappin DR, Watts P, McMurtry GM, Lafoy Y, Matsumoto T (2002) Prediction of slump generated tsunamis: the July 17th 1998 Papua New Guinea event Sci Tsunami Hazards 20:222-238

Thusyanthan I, Martinez E Model Study of Tsunami Wave Loading on Bridges. In: Eighteenth International Offshore and Polar Engineering Vancouver, BC Canada, 2008. pp 528-535

Tinti S, Giuliani D (1983) The Messina Straits tsunami of December 28, 1908: a critical review of experimental data and observations Il Nuovo Cimento C 6:429-442

Togashi H (1986) Wave force of tsunami bore on a vertical wall Science Tsunami Hazard 16:73-80

Tokura S, Ida T Simulation of Wave-Dissipating Mechanism on Submerged Structure using Fluid-Structure Coupling Capability in LS-DYNA. In: 5th European LS-DYNA Users Conference, Birmingham, England, 2005.

Triatmadja R, Nurhasanah A (2012) Tsunami Force on Buildings With Openings and Protection Journal of Earthquake and Tsunami 6

Tsutsumi A, Shimamoto T, Kawamoto E, Logan JM (2000) Nearshore flow velocity of Southwest Hokkaido earthquake tsunami Journal of waterway, port, coastal, and ocean engineering 126:136-143

TxDOT (2005) Bridge Railing Manual. Texas Department of Transportation, Texas

UBC (1997) Uniform building code.

Unjoh S Damage investigation of bridges affected by Tsunami during 2004 north Sumatra Earthquake, Indonesia. In: Proc. of 4th International Workshop on Seismic Design and Retrofit of Transportation Facilities, 2006.

Unjoh S, Endoh K (2006) Damage Investigation and the Preliminary Analyses of Bridge Damage caused by the 2004 Indian Ocean Tsunami Technical Memorandum of Public Works Research Institute:97

http://earthquake.usgs.gov/earthquakes/eqinthenews/2004/us2004slav/ (2007) Earthquake Center.

van de Lindt JW, Gupta R, Garcia RA, Wilson J (2009) Tsunami bore forces on a compliant residential building model Engineering Structures 31:2534-2539

Verdugo R, Konagai K, Okamura M, Tobita T, Torres A, Towhata I (2011) Geotechnical damage caused by the 2010 Maule, Chile earthquake

Wang DD, Wang R, Yan H (2014) Fast prediction of protein–protein interaction sites based on Extreme Learning Machines Neurocomputing 128:258-266

Wang X, Han M (2014) Online sequential extreme learning machine with kernels for nonstationary time series prediction Neurocomputing 145:90-97

Wemmenhove R, Gladsø R, Iwanowski B, Lefranc M Comparison of CFD Calculations and Experiment for the Dambreak Experiment with One Flexible Wall. In: The Twentieth International Offshore and Polar Engineering Conference, 2010. International Society of Offshore and Polar Engineers,

Wiegel R (1980) Tsunamis along west coast of Luzon, Philippines. Paper presented at the 17th Coastal Engineering Conference,

Winter, Andrew O., Michael R. Motley, and Marc O. Eberhard. "Tsunami-like wave loading of individual bridge components." *Journal of Bridge Engineering* 23.2 (2018): 04017137.

Wijatmiko I, Murakami K (2012) Study on the Interaction Between Tsunami Bore and Cylindrical Structure with Weir

Wong PK, Wong KI, Vong CM, Cheung CS (2015) Modeling and optimization of biodiesel engine performance using kernel-based extreme learning machine and cuckoo search Renewable Energy 74:640-647

Xiao H, Young YL, Prévost JH (2010) Parametric study of breaking solitary wave induced liquefaction of coastal sandyslopes Ocean Engineering 37:1546-1553

Xiao, S. C., & Guo, A. X. (2019). Effects of air relief openings on the mitigation of solitary wave forces on bridge decks. Journal of Hydrodynamics, 31(3), 594-602

Yeh HH (1991) Tsunami bore runup. In: Tsunami Hazard. Springer, pp 209-220

Yeh HH, Robertson I, Preuss J (2005) Development of design guidelines for structures that serve as tsunami vertical evacuation sites. Washington State Department of Natural Resources, Division of Geology and Earth Resources, Yeom G-S (2009) Behavior of a Container Drifted by Run-up Tsunami and Estimation Method of Its Collision Force. Nagoya University

Yim S, Yeh H, Cox D, Pancake C (2004) A Shared-Use Large-Scale Multidirectional Wave Basin For Remote Tsunami Research

Yim SC Modeling and simulation of tsunami and storm surge hydrodynamic loads on coastal bridge structures. In: Proceedings of the 21st US-Japan Bridge Engineering Workshop, Tsukuba Japan, 2005. pp 3-5

Yoshinori Shigihara, Fujima K Evaluation of tsunami force acted on the bridges of the vicinity of Banda Aceh by use of numerical simulation. In: Proceedings of the Indian Ocean Tsunami Modelling Symposium, Fremantle, Australia, 12-15 October 2010.

Yu Q, Miche Y, Séverin E, Lendasse A (2014) Bankruptcy prediction using extreme learning machine and financial expertise Neurocomputing 128:296-302

Zhang W (2009) An Experimental Study and a Three-Dimensional Numerical Wave Basin Model of Solitary Wave Impact on A Vertical Cylinder. Oregon State University

Zhu, M., Elkhetali, I., & Scott, M. H. (2018). Validation of OpenSees for tsunami loading on bridge superstructures. *Journal of Bridge Engineering*, *23*(4), 04018015.

Zienkiewicz O, Bettess P (1978) Fluid-structure dynamic interaction and wave forces. An introduction to numerical treatment International Journal for Numerical Methods in Engineering 13:1-16